TRENDS IN SCIENCES 2025; 22(9): 10308
https://doi.org/10.48048/tis.2025.10308
REVIEW ARTICLE

Paraffin-Based Phase Change Materials (PCM) with Enhanced Thermal Conductivity Through Particle Addition and Encapsulation Techniques for Thermal Energy Storage: A Critical Review of Materials Science

Muhammad Fauzi[1,2], Budhy Kurniawan[1,*], Amdy Fachredzy[1,2], Muhammad Alif Hamzah Nabawi[2] and Anggito Pringgo Tetuko[2]

[1]Department of Physics, Faculty of Mathematics and Natural Sciences, Universitas Indonesia, Jawa Barat 16424, Indonesia
[2]Research Center for Advanced Materials, National Research and Innovation Agency (BRIN), Jakarta 10340, Indonesia

([*]Corresponding author's e-mail: budhy.kurniawan@sci.ui.ac.id)

Received: 5 April 2025, Revised: 10 May 2025, Accepted: 17 May 2025, Published: 5 July 2025

Abstract

The rising global energy demand is contributing significantly to environmental degradation, energy scarcity, and increased carbon dioxide emissions, thereby intensifying the challenge of climate change. Notably, the building sector accounts for approximately 40% of total energy consumption, primarily driven by a 12 and 37% increase in heating and air conditioning usage, respectively. In response to this pressing issue, phase change materials (PCM) have emerged as a promising solution due to their outstanding thermal energy storage (TES) capabilities. PCM can be classified into organic, inorganic, and eutectic types, with paraffin-based PCM being the most extensively studied. However, the practical application of paraffin-based PCM is limited by their inherently low thermal conductivity. To address this limitation, various enhancement techniques, including particle incorporation and encapsulation methods, have been explored to improve thermal performance. This review presents a comprehensive analysis of these approaches aimed at enhancing the thermal conductivity of PCM. Furthermore, the feasibility of incorporating PCM directly into concrete for TES applications is critically evaluated. The review also discusses key PCM characteristics, including thermal properties, physical stability, and chemical stability. By offering an in-depth examination of PCM classifications, performance enhancement strategies, and practical applications, this review provides valuable insights into the potential of PCM for advancing sustainable energy systems.

Keywords: Phase change materials, Thermal energy storage, Concrete, Thermal conductivity enhancement, Thermal performance, Encapsulation, Materials science

Introduction

Energy is a crucial element in the evaluation of progress across various domains worldwide, such as technology, environmental protection, and economic development across the globe [1]. However, the growth in population and energy use has resulted in environmental deterioration, energy shortages, carbon dioxide emissions, and exacerbated climate change [2]. In addition, global energy use is projected to increase by 28% between 2015 and 2040 [3]. The energy consumption in the construction industry is significant, with the sector responsible for approximately 40% of the overall energy usage. This is primarily due to an increase in heating and air conditioning usage by 12 and 37%, respectively, in 2025 [4]. Tackling this worldwide challenge requires the adoption of sustainable energy alternatives and a reduction in air conditioning usage. However, the implementation of these solutions has been insufficient because of their instability and

inability to meet global energy requirements. Therefore, it is necessary to increase the energy efficiency of renewable energy storage systems [5]. Various techniques can be employed to store energy, including the mechanical, magnetic, electrochemical, and thermal approaches [6]. The most effective storage method for each type of energy depends on the efficiency. Thermal Energy Storage (TES) is considered a suitable alternative solution for reducing the energy consumption in buildings because it can be utilized directly without the need for conversion into other forms of energy [7].

TES is a method of capturing and utilizing heat energy in materials when required. Heat energy can be stored in 2 forms: Latent or sensible. In Latent Heat Storage (LHS) systems, the application of latent heat typically involves the use of LHS materials, specifically Phase Change Materials (PCM). These PCM undergo transitions between physical states in order to store thermal energy at a steady temperature. PCM have several phase transformations, such as solid-liquid, solid-gas, solid-solid, liquid-solid, liquid-gas, gas-solid, and gas-liquid, where each phase change provides high efficiency at the minimum temperature change and greater heat storage density [8-10]. However, LHS utilizing sensible heat is achieved through the temperature increase of the material and thus has less potential for TES applications [11]. Processes involving gas-solid and gas-liquid phase transitions are characterized by substantial changes in volume, making them unsuitable for use in large-scale applications. Solid-solid phase change materials (PCM) typically have a lower latent heat compared to their solid-liquid counterparts, making solid-liquid PCM a relevant heat storage medium, in addition to exhibiting the characteristics of small volume change, good equilibrium, high density and temperature-controllable operation during phase change [12].

PCM can be utilized in a variety of applications such as thermal energy storage, solar energy storage systems, building cooling systems, and textile heat recovery systems [13]. In addition, PCM are a solution to TES for cooling in buildings. Furthermore, to maximize the efficiency of PCM utilization, it is necessary to know the material characteristics and the appropriate PCM phase for TES application in buildings. Solid-liquid PCM is a common phase that is widely used, and based on the type of material, it is classified into organic, inorganic, and eutectic PCM [14]. Organic PCM are the most widely used due to the characteristics of organic materials that are non-toxic, do not require supercooling systems, and are not phase separated [15]. There are 2 different types of organic PCM: paraffinic and nonparaffinic. The commercially available organic heat storage PCM is paraffin due to has the characteristics of a carbon number range of $18 \leq n \leq 50$, paraffin phase transition temperature between 40 and 59°C, paraffin specific heat capacity of approximately 2,100 J/kg.K, and latent heat of 180 - 230 kJ/kg [15,16]. However, paraffin as a PCM for TES has the disadvantage of low thermal conductivity (K) that affects longer heat absorption process. Therefore, it is necessary to increase the thermal conductivity of the PCM.

The thermal conductivity of PCM can be enhanced by adding material particles that have high thermal conductivity, such as carbon, metal oxides, and other types of materials. In addition, PCM encapsulation can be utilize to improve thermal conductivity, which has been investigated in previous studies [17-19]. A significantly large number of researchers have reported thermal enhancement achieved by dispersing nanoparticles in the PCM fraction. Singh *et al.* [20] conducted a study in 2022 investigation of the thermal energy properties and latent heat performance of paraffin-based PCM. Several materials with high thermal conductivities were added as fillers in the composites: SiO_2, Al_2O_3, and MgO. Nanomaterials of 0.1, 0.3 and 0.5% (v/v) were incorporated into paraffin synthesized using the homogenization method at temperature of 65°C for 1.5 h and then sanitized at 65°C for 2.5 h. However, these materials are not added to the composites. The authors proposed that the addition of nanomaterials with high thermal conductivity characteristics can significantly improve the thermophysical properties of PCM. Compared with pure paraffin, the viscosity dynamics of the MgO, Al_2O_3, and SiO_2 based PCM samples increased by 80, 83.3 and 90%, respectively. Similarly, the thermal conductivity increased by 10.71, 18.36 and 29.32% for MgO, Al_2O_3, and SiO_2, respectively. In a separate study, Prabhu *et al.* [3] analyzed paraffin-based PCM that has been added by Al_2O_3 nanoparticles with 7.5 and 10 wt.% using the

magnetic stirring homogenization method at 50°C for 4 h. The author obtained the latent heat phase change of 203.89 kJ/kg and 10% is 187.44 kJ/kg at sample of 7.5% PCM. Furthermore, the thermal conductivities obtained by 7.5 and 10% PCM showed improvement of 42 and 57%, respectively, compared to pristine paraffin.

Other additions to carbon-based materials have also been investigated. Hu *et al*. [21], the addition of carbon nanotubes (CNT) and styrene butadiene styrene with the addition of 2 wt.% CNT and SBS variations of 18, 13 and 8 wt.% into paraffin-based PCM. Mixing process was conducted at temperature 180°C for 3 h. The enthalpy during the melting (ΔHm) phase was 142.28, 147.63 and 157.70 kJ/kg. This shows a decrease compared to pristine paraffin of 200.01 kJ/kg. Thus, the addition of CNTs to PCM is a promising solution for TES applications. The authors also proposed that PCM composites have good morphological structures and mechanical properties. In a separate study, Sharshir *et al.* 2021 [22] investigated the effects of adding copper oxide (CuO) and cobalt oxide (Co_3O_4) to paraffin. PCM synthesis was performed by magnetic stirring at temperature of 60°C, followed by sonication method for 0.5 h to ensure continuous dispersion of nanoparticles in the paraffin. The results show that the added nanoparticles were evenly distributed in the paraffin layer. Based on differential scanning calorimetry (DSC) analysis, the melting enthalpy of paraffin was reduced by 11, 20 and 19.7% by the addition of CuO, Co_3O_4, and CuO@Co_3O_4, respectively. Therefore, the authors suggested that the treatment method of adding carbon-based materials can overcome the drawbacks of pure paraffin PCM as TES.

He *et al.* [23] and He *et al.* [24], investigated the thermomagnetic properties of paraffin wax (PW)-Fe_3O_4 composites. This study focused on the effects of different concentrations of Fe_3O_4 on energy storage, which were analyzed using both experimental and numerical methods. The experiments were conducted using a thermostat at 90 - 100°C for 30 min, followed by sanitization at temperature of 80 - 90°C for 30 min. The results showed that the thermal conductivity of the samples increased with the addition of Fe_3O_4:0.251, 0.298, 0.315 and 0.331 (W/mK) for pristine PW, Fe_3O_4-PW (1 wt.%), Fe_3O_4-PW (2 wt.%), and Fe_3O_4-PW (3 wt.%), respectively. Furthermore, the latent heat values also decreased with the addition of Fe_3O_4, from 208.0, 204.6, 200.3, and 197.8 (kJ/kg) for the pristine PW, Fe_3O_4-PW (1 wt.%), Fe_3O_4-PW (2 wt.%), and Fe_3O_4-PW (3 wt.%) samples, respectively. These results suggest that the PCM is effective for storing energy. The utilization of encapsulation can also enhance the thermal performance of the PCM.

Al-Yasiri and Szabó [25], examined the use of aluminum encapsulation on PCM in concrete to assess its impact on thermal properties. Researchers discovered that PCM significantly improved the thermal performance of concrete at maximum outdoor temperatures. Furthermore, a larger encapsulation area increased the heat transfer in the PCM and improved the filling and discharging rates. Consequently, a larger encapsulation area led to a higher temperature and heat transfer reduction, as well as longer heat retention times. On the other hand, in the research by Tetuko *et.al.* [26], the thermal efficiency of PCM was improved by adding magnetite (Fe_3O_4) and PCM encapsulation in concrete with copper tubes for thermal energy storage application. The thermal analysis results showed that the addition of 50% mass of magnetite particles into paraffin increased the thermal conductivity value of 0.53 (W/m°C) compared to pristine paraffin of 0.32 (W/m°C). Furthermore, the authors proposed the temperature distribution results that PCM encapsulated in concrete is effective to store the thermal energy and stable during the heating and cooling processes. The copper tube as an encapsulated medium in concrete, also affects the stability of the PCM shape and increases the rate of endothermic processes. Therefore, the addition of particles with high thermal conductivity to the PCM, as well as the encapsulation method, can be novel finding to the application of PCM as TES.

Based on the current state of research, it is evident that existing studies lack a comprehensive evaluation PCM characterization, in-depth thermal analysis, and simulation-based assessments of PCM in TES applications. In response, this review synthesizes and integrates findings from previous research to address these gaps. The literature was selected based on its relevance to PCM fundamentals, TES implementation, and the identification of research limitations or unexplored areas. Priority was given to recent publications from the 2020 - 2025 period to ensure the

inclusion of the most current advancements. This critical review focuses on passive and sustainable strategies to reduce energy consumption in buildings by integrating paraffin-based PCMs encapsulated in concrete, alongside the incorporation of materials with enhanced thermal conductivity. In addition, the review presents detailed material characterization analyses, including surface morphology, thermal properties, physical and chemical stability, and simulation studies. It further explores the principles of PCM integration into concrete systems to improve storage efficiency, thereby contributing to the development of future energy-efficient building technologies.

Phase change materials (PCM)

Phase Change Materials (PCM) are utilized for thermal storage. **Figure 1** illustrates the classification of PCM as TES, which is distinguished by its chemical and physical properties [27]. In this process, the PCM undergoes phase transition changes between solid and solid, solid-liquid, gas-solid, and gas-liquid [28,29]. However, PCM are generally applied as thermal energy storage in concrete/buildings with materials that have a solid-liquid phase. This is because PCM that undergo phase transition changes between liquids and solids can occur isothermally (constant temperature) at the time of melting (heat storage) or solidification (crystallization), as well as in the temperature range after its application [28].

The PCM used in the TES system undergoes a transformation from solid to liquid. During this process, the PCM absorbs thermal energy as latent heat via an endothermic reaction. This absorbed energy increases the molecular or atomic energy within the material, intensifying the vibrations between the atoms and weakening the chemical bonds as the PCM reaches its melting point. This results in the transition of the material from the solid to the liquid state. Conversely, when the PCM cools to its freezing temperature, it exothermically releases energy through a process known as solidification. This process regenerates chemical bonds and releases energy, causing the PCM to transition from liquid back to solid. This cycle of heat absorption (charging) and release (discharging) can be repeated multiple times, allowing the PCM to function as an energy storage system [17,28,30,31]. This process is illustrated in **Figure 2** [29,32-34]. The phase change characteristics are described by 2 aspects: The phase change temperature and phase change enthalpy, which determine the actual application and storage capacity of thermal energy [35]. In addition, PCM that have phases other than liquid-solid can also be used in other alternative applications [36]. The PCM in other phases can also be used depending on the application and desired PCM property variables. The properties of PCM for its effective use, especially as a TES, are shown in **Figure 3** [37-39].

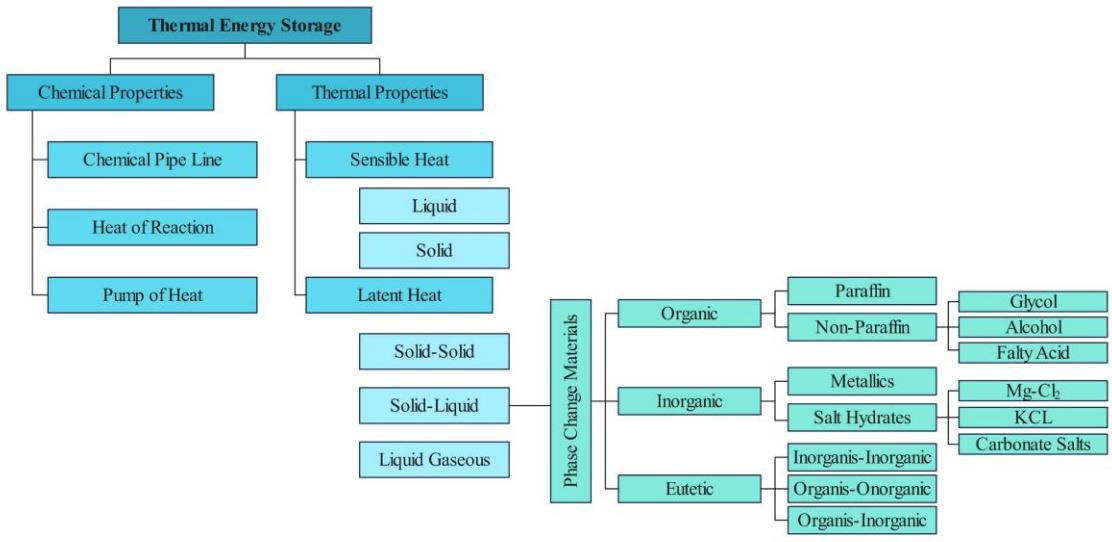

Figure 1 Classification of PCM as thermal energy storage.

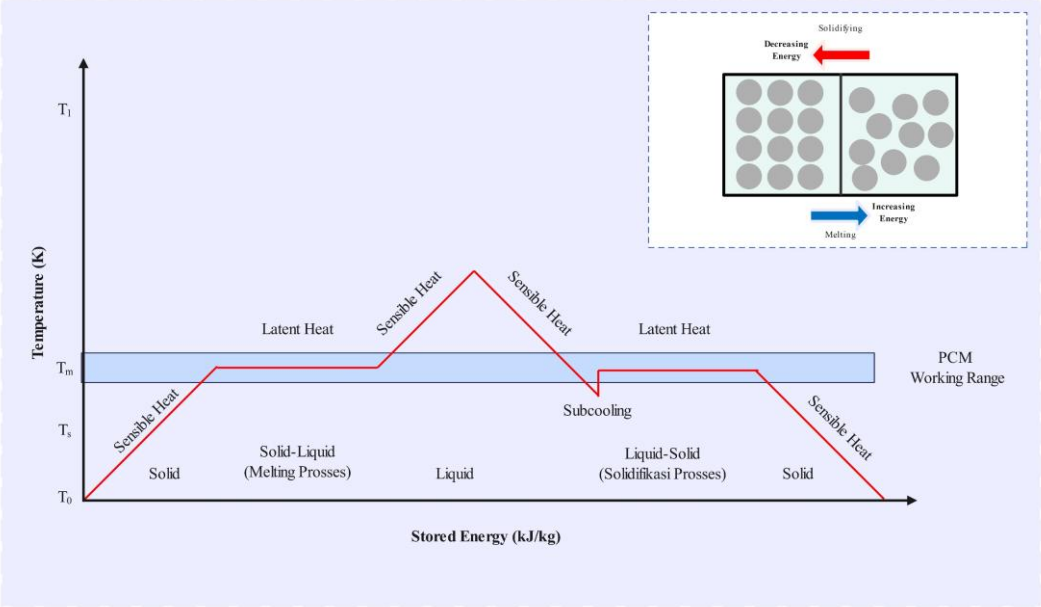

Figure 2 Phase change transition of solid-liquid PCM.

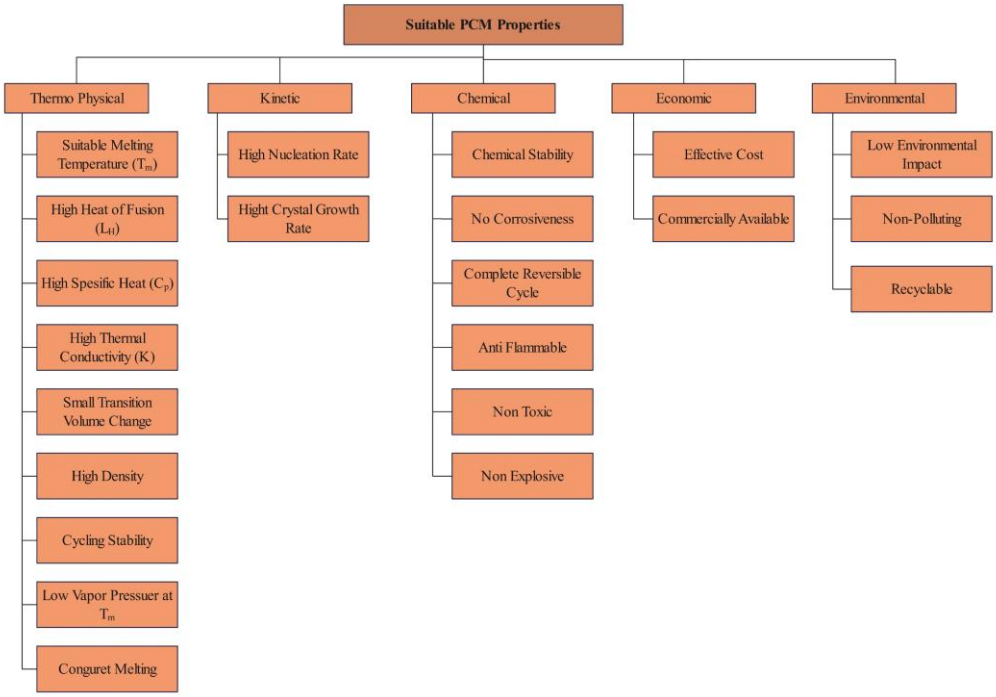

Figure 3 Characteristics of suitable PCM.

The selection of PCM to be used as a thermal energy storage (TES) material is very important for the efficiency and effectiveness of its application. Therefore, it is necessary to consider certain important properties that must be studied [40]. The subsequent descriptions of the anticipated properties related to thermophysics, kinetics, chemistry, technology, and economics are enumerated [38,41-44].

Thermal characteristics: In addition to meeting the required temperature range for intended use, the phase change material (PCM) should exhibit a substantial latent heat of fusion, which determines the amount of heat exchanged between the PCM and its surroundings. Moreover, PCM should possess a high specific heat (enhancing sensible heat storage capacity), superior thermal conductivity (potentially shortening

charging and discharging times), considerable density, minimal volume change during phase transition (limited expansion), cyclic durability, and reduced vapor pressure at operational and melting points.

Kinetic attributes: Rapid nucleation rate (to prevent supercooling of the liquid state) and rapid crystal growth rate (to ensure optimal energy recovery from the storage system).

Chemical qualities: Fully reversible cycle, chemical stability without significant degradation after multiple freeze/melt cycles, chemical compatibility with construction and encapsulation materials, non-corrosive nature, non-toxic composition, non-explosive properties, and non-flammability.

Economic factors: Cost-efficient and readily available for large-scale applications.

Environmental considerations: Minimal environmental impact, non-polluting throughout its service life, and potential for recycling.

Paraffin classification of PCM

Based on their structural composition, Phase Change Materials (PCM) are divided into 3 main groups: Organic, inorganic, and eutectic [45]. Organic PCM are the most commonly utilized, accounting for 81% of the total usage, as illustrated in **Figure 4** [46]. PCM in the organic category can be subdivided into paraffin and non-paraffin types. In addition, inorganic substances, including salt hydrates and metals, have been recognized as promising PCM for potential use. Eutectic materials, on the other hand, are classified into 3 distinct groups: Organic-organic eutectics, inorganic-inorganic eutectics, and combinations of organic and inorganic eutectic substances [47].

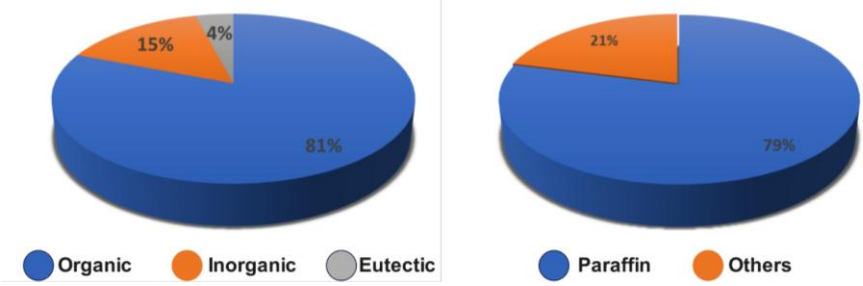

Figure 4 Research statistics of PCM usage types.

Organic PCM, particularly paraffins, are widely used due to their advantages, including a broad range of applications. **Figure 5** shows the changes in the melting enthalpy with respect to the melting temperature for several common PCM. By concurrently evaluating their thermal capacities, each type of PCM working range was assessed to meet the specified criteria. Paraffin exhibits an enthalpy range of 100 - 230 kJ/kg with a broad melting temperature range of -40 120°C. Consequently, paraffin was deemed suitable as a composite PCM matrix for TES applications. **Table 1** summarizes the advantages and disadvantages of each PCM category.

Organic PCM

Organic materials are generally referred to as natural materials or carbon-based compounds and can be categorized into 2 types: Paraffin and non-paraffin. Organic PCM are widely utilized owing to their lower cost compared to inorganic PCM. Additionally, organic PCM possess minimal latent heat, chemical stability, and corrosion resistance. Furthermore, organic PCM are repeatable use with good stability and small volume degradation, do not require a supercooling phase, and exhibit a high latent heat of fusion. Therefore, making the organics PCM compatible with a wide range of temperatures (15 - 45°C) [49-51]. Organic PCM are compatible with various materials and can be further divided into 2 subcategories: Paraffin and non-paraffin [52]. Non-paraffin PCM include fatty acids, alcohols, esters, and glycols. Their thermophysical characteristics are similar with those of paraffinic organic PCM. The thermophysical properties of some organic PCM are listed in **Table 2**.

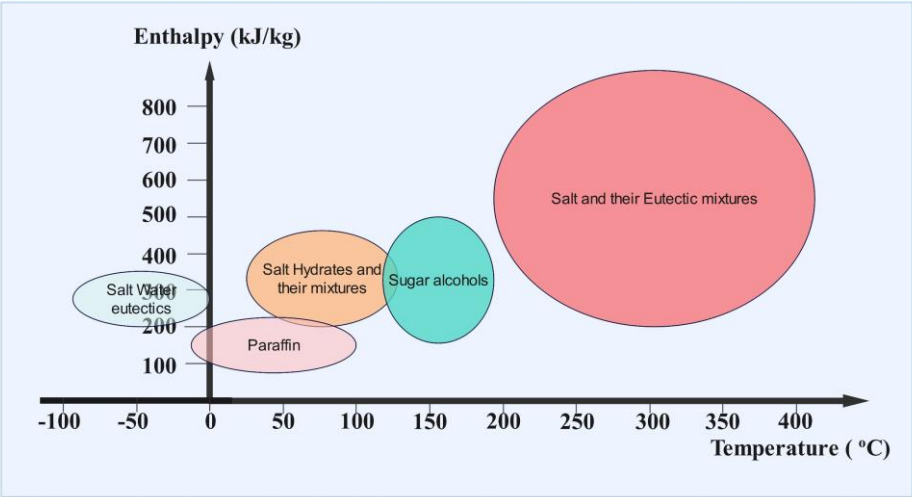

Figure 5 Relationship between fusion enthalpy and fusion temperature for various categories of PCM [30].

Table 1 Summary of advantages and disadvantages of the PCM category [14,30,47,48].

PCM Catagory	Advantages	Disadvantages
Organic • Paraffin • Alkanes • Fatty Acids • Glycols • Alcohols • Etc	• Have a larger temperature scale in phase change • Chemically inert (self-nucleating) and stable especially in closed containers • No phase separation • High heat of fusion • Does not require supercooling • Compatible with other materials • Recyclable, non-toxic, easy to handle, non-reactive, and rational operational costs	• Low thermal conductivity • Flammable • Low volumetric latent heat storage capacity • More volatile
Inorganic • Alkali • Alkali Metals • Halides • Salts • Etc	• High volumetric latent heat storage capacity • Easily available • Less expensive • Higher thermal conductivity • Thermal fusion of these PCM is very high • Low volume change • These PCM are non-flammable • Easily modified to surfaces with different functional groups	• High degree of cooling • Corrosive • Long-term stability is low • Brittle • Easy to break leading to leakage • Phase separation • Congruent melting • High volume change
Eutectics • Eutectic hydrates • Eutectic Paraffins • Eutectic Salts	• The melting point of these PCM is very sharp • High volumetric thermal storage density • Properties can be customized to fit specific needs • Adjustable phase change temperature high thermal conductivity	• Less thermophysical property data available for many combinations • High cost • Low latent heat • Low heat capacity

Table 2 Thermal properties of organic PCM.

Organic PCM	Latent Heat H_f (kJ/kg)	Melting Temperature T_m (°C)	Thermal Conductivity K (W/m.K)	Density ρ (kg/m^3)	Ref.
Acetamide	260	82	0.4	1160	[46]
Acetic acid	192	17	0.26	1214	[53]
Adipic acid	213 - 260	151 - 154	1.15	1360	[54]
Palmitic acid	163	55	0.21	989	[55]
Formic acid	150 - 250	7.8	0.3	1227	[56]
Steara acid	199 - 203	69.2 - 69.4	0.29	940	[57]
Erythritol	373.91	118.78	0.73	1450	[58]
Lauric acid	178-185.92	44.03 - 49	0.22	66	[57]
Octadecane	241	28	0.26	774	[46]
Paraffin	142	65	0.23	760	[59]
Paraffin RT70	260	69-71	0.2	770	[59]
Paraffin Wax	190	44	0.21	830	[60]
Paraffin Wax	184.48	54.32	0.15	833.6	[61]
Urea	250	134	0.8	1320	[46]

From **Table 2**, it is evident that organic PCM exhibit varying latent heat values, with paraffin demonstrating a range of 188 - 260 kJ/kg. Furthermore, when considering its application in thermal energy storage for concrete, paraffin also possesses a suitable melting point within the temperature range of 44 - 71°C.

Utilization of paraffin as PCM

Paraffin is a compound mixture of alkanes having a compound formula of CnH_{2n+2}, where n represents the number of carbon atoms and ranges from 1 to 17. At room temperature, alkanes with n values of 1 - 4 were gases, whereas those with n values between 5 and 17 were liquids. Solid waxy substances form when n exceeds 17. The melting point of paraffin increases as the carbon atom count increases, and it possesses high latent heat. Paraffin is composed of hydrocarbons and is classified as a polycrystalline substance featuring various molecular structures, including branched linear, cyclic, isoalkanes, and cycloalkanes [62].

Table 3 presents the advantages and disadvantages of paraffin, and **Table 4** displays the physical properties of paraffins based on their respective carbon atoms. Paraffin is considered an optimal PCM for energy storage owing to its broad range of melting temperatures. Moreover, paraffin exhibits chemical stability because of its lack of functional groups and free electrons. The comparable electronegativity values of carbon and hydrogen atoms coupled with their robust covalent bonding render paraffin unreactive with other substances [63]. On the other hand, the use of paraffin can also be adapted to the required application by looking at the characteristics of thermo-physical properties, the wide range of paraffin indicates that paraffin is a PCM compatible organic material used as a PCM composite matrix.

Paraffin is a PCM material that is stable and neutral at temperatures below 500°C, and it begins to degrade at temperatures between 150 and 300°C [63,67]. Paraffin is extensively utilized as a thermal energy storage material because of its numerous advantageous properties. These include a broad melting temperature range, non-corrosive nature, low vapor pressure, absence of a super-cooling phase requirement, high heat of fusion, and cost-effectiveness for commercial production. Despite these benefits, paraffin exhibits poor thermal conductivity, leading to prolonged heat absorption and incompatibility with plastic containers. However, various strategies can be implemented to enhance the performance of paraffin in thermal energy storage applications to address these limitations.

Table 3 Advantages and disadvantages of paraffin [1,64-66].

	Advantages	Disadvantages
Paraffin	• Has a larger temperature scale in phase change • Medium thermal storage density • Chemically inert and stable especially in closed containers • Robust and stable • Better storage density (with respect to mass) • Good resemblance to metals • Fewer constraints in terms of safety • Does not require supercooling process • Available at rational cost/operating cost • Higher heat of fusion • Safe and non-reactive	• Has water insoluble and water-resistant characteristics • No side reactions with chemical reagents • Can produce fire easily (burning) • Low enthalpy of phase change • Smaller amount for enthalpy of phase change, thermal conductivity, density, and melting point • Easy to burn • High volume change between solid and liquid states • Has an undefined melting temperature

Table 4 Physical properties of paraffin based on carbon atoms.

Paraffin with carbon atoms	Freezing point T_s (°C)	Latent Heat H_f (kJ/kg)	Density ρ (kg/m^3)	Spesific heat	Thermal Conductivity K (W/m.K)	Oil content (%)	Ref.
C_{13}-C_{24}	22 - 24	189	0.90	2.1	0.21	20	[68]
C_{18}	28	244	0.81	2.1	0.15	0	[69]
C_{16}-C_{28}	42 - 44	189	0.91	2.1	0.21	5	[69]
C_{20}-C_{33}	48 - 50	189	0.91	2.1	0.21	<0.5	[68]
C_{22}-C_{45}	58 - 60	189	0.92	2.1	0.21	4	[70]
C_{23}-C_{45}	62 - 64	189	0.92	2.1	0.21	<0.5	[68]
C_{21}-C_{50}	66 - 68	189	0.93	2.1	0.21	3	[70]

Researchers have extensively explored and devised novel experiments to evaluate the various organic phase transition types of paraffin for practical purposes. **Table 5** provides an overview of past studies conducted on paraffin PCM.

Table 5 Summary of paraffin utilization as PCM.

Samples of PCM	Melting temperature T_m (°C)	Latent heat H_f (kJ/kg)	Thermal conductivity K (W/m K)	Application	Ref.
• *Paraffin Wax* + 0.5 wt% SiO_2	• 62.7	• 189	• 0.24	Thermal storage	[71]
• *Paraffin Wax* + 0.5 wt% MWCNT	• 61.5	• 184.12	• 0.26		
• *Paraffin Wax* + 0.5 wt% SiO_2 + 0.5 wt% MWCNT	• 61.2	• 180.20	• 0.35		
• *Paraffin Wax* + 1 wt% SiO_2 + 1 wt% MWCNT	• 60.3	• 177.50	• 0.40		
	• 59.7	• 176.83	• 0.45		
• Paraffin+2 wt% Ti	• 50.8	• 163.55	• 1.3	Thermal management	[72]
• Paraffin+2 wt% Al	• 47.9	• 80.79	• 0.6		

Samples of PCM	Melting temperature T_m (°C)	Latent heat H_f (kJ/kg)	Thermal conductivity K (W/m K)	Application	Ref.
• Paraffin	• 56.64	• 203.56	• 0.92	Thermal energy storage	[73]
• Paraffin + 5 wt% Fe_3O_4	• 54,45	• 186.50	• 1.06		
• Paraffin	• 48.44	• 208	• 0.251	Convection of regulation	[74]
• Paraffin + 1 wt% Fe_3O_4	• 48.37	• 204.6	• 0.298		
• Paraffin + 2 wt% Fe_3O_4	• 47.35	• 200.3	• 0.315		
• Paraffin + 3 wt% Fe_3O_4	• 47.10	• 197.8	• 0.331		
• Busa nikel/paraffin berlapis graphene	• 38	• 99	• 4.6	Thermal management in battery	[75]
• Paraffin/aluminum	• 57	• 96.2	• 13.2	Cooling system in building	[76]
• Paraffin	• 56.63	• 203.56	• 0.26	Effect of magnetic field on the melting performance of PCM materials	[77]
• Paraffin 0.5 wt% Fe_3O_4	• 55.93	• 202.55	• 0.29		
• Paraffin 1 wt% Fe_3O_4	• 55.23	• 201.54	• 0.32		
• Paraffin 3 wt% Fe_3O_4	• 54.70	• 196.75	• 0.36		
• Paraffin	• 57.26	• 189.24	• 0.21	Thermal energy storage	[78]
• Paraffin	• 27.6	• 188.0	• 0.3	Thermal energy storage	[79]
• 0.02 wt% NGPCM	• 27.61	• 171.1	• 0.36		
• 0.06 wt% NGPCM	• 27.34	• 171.7	• 0.37		
• 0.10 wt% NGPCM	• 27.71	• 148.4	• 0.34		
• 0.02 wt% NCPCM	• 27.75	• 170.6	• 0.32		
• 0.06 wt% NCPCM	• 27.57	• 167.3	• 0.33		
• 0.10 wt% NCPCM	• 27.84	• 150.8	• 0.34		
• Paraffin@copper foam	• 53.3	• 132.5	• 4.9	Thermal energy storage	[80]
• paraffin@nickelfoam	• 52.7	• 144.4	• 1.3		

Utilization of non-paraffin as PCM

Non-paraffin organic Phase Change Materials (PCM) comprise the most extensive group of PCM with a diverse range of properties. Each type of non-paraffin organic PCM possesses its own unique set of characteristics in contrast to paraffins, which exhibit similar properties. The chemical formula $C_mH_nO_2$ was used to designate a particular non-paraffin PCM. Non-paraffin organic PCM possess a high latent heat capacity, which distinguishes them from paraffins. However, like paraffins, they are generally flammable and exhibit lower resistance to oxidation [81]. In addition, non-paraffin PCM are characterized by their low thermal conductivities and combustion temperatures. These materials also possess varying degrees of toxicity, necessitating additional safety measures and increasing the handling costs. Pusphendra and Shailendra conducted a comprehensive study on organic materials and identified several esters, fatty acids, alcohols, and glycols as suitable candidates for energy storage applications [82]. The primary advantage of non-paraffin PCM lies in their ability to combine with other non-paraffin PCM, resulting in an enhanced latent heat fusion capacity. When mixed with other non-paraffin PCM, these materials can maintain desirable properties, such as high deformation stability, resistance to phase separation after repeated cycling, and crystallization without supercooling. As a result, this method provides the best PCM to be used, however it causes significant production costs owing to the expense of exploring suitable combinations and concentrations [83-86]. **Table 3** summarizes the thermal properties

reported in previous studies using nonparaffin PCM, indicating their widespread use [87].

Peng *et al.* [87] investigated the potential use of erythritol as a PCM. Research findings indicate that erythritol exhibits extensive phase transition properties, with a transition temperature of approximately 118°C and latent heat of approximately 314 kJ/kg. Its high energy-storage density and non-corrosive nature make it a popular choice for medium-temperature energy-storage applications. However, the widespread use of erythritol is hindered by its substantial supercooling requirements and relatively poor thermal conductivity during phase transitions. The primary factor influencing the latent heat and thermal conductivity of erythritol during phase transitions is the alteration of the hydrogen bonds within its structure. Modifying the quantity and intensity of these hydrogen bonds can potentially enhance the latent heat and address the issue of low thermal conductivity. Furthermore, Jianhui et al. 2023 explored a single modification technique to overcome erythritol's (ET) constraints as PCM [88]. The application of multiple modification methods to enhance PCM efficiency for energy storage shows great potential. The combined effect of multiple approaches surpasses traditional single-modification techniques, boosting thermal conductivity, minimizing supercooling, and offering a comprehensive answer. The researchers suggest using graphene oxide (GO) nanosheet-modified melamine foam (MF) and polyaniline (PANI) to develop an innovative ET-based PCM through blending and adsorption modification of porous substances. PANI functions as a nucleation site, expediting crystallization and decreasing supercooling in the PCM.

The GO@MF foam acts as a porous framework for ET encapsulation and improves heat conduction, substantially enhancing heat storage and release rates. As a result, the supercooling of the GO@MF/PANI@ET (GMPET) composite PCM decreased from 91.2 for pure ET to 57.9, and its thermal conductivity (1.58 W/mK) was roughly triple that of pure ET (0.57 W/m K). After being subjected to 140 °C for 2 h, the GMPET composite PCM displayed minimal ET leakage with a mass loss ratio under 0.75%. It also exhibited a high melting enthalpy of about 259 kJ/kg and an initial mass-loss temperature around 198°C. The phase transition temperature and latent heat storage capacity of the GMPET PCM remained stable even after 200 cycles. Fatty acids, another widely used non-paraffin PCM with the formula $CH_3(CH_2)2nCOOH$, are recognized for their reusability, high heat of fusion, adjustable phase-change temperature, and lack of supercooling [84,89]. However, fatty acids are prone to instability when heated, have low thermal conductivity, corrosiveness, and relatively expensive [89].

According to **Table 6**, the thermal properties of fatty acids indicate that these materials can be utilized as PCM in various applications. This is also supported by the research conducted by Guihua Fang and Maosen Zhao, 2022 [91], in this study, the thermal characteristics of the fatty acids were investigated. Modified graphite (MEG) was synthesized using ultrasonic techniques in a myristic acid-ethanol solution, employing it as a heat conduction enhancer. They then created a fatty acid composite phase change material (PCM) with a superior overall thermal performance using MEG. Thermal conductivity measurements and differential scanning calorimetry revealed that the thermal conductivity of the composite PCM increased by 139.3% with the addition of 2 wt.% MEG. Notably, after 200 cycles of heat storage and release, the synthesized composites exhibited latent heat values of 182.6 and 187.1 kJ/kg, comparable to the eutectic cycling of pure fatty acids. The thermal cycling, thermogravimetric analysis, and thermal conductivity changes of the PCM composite demonstrated its excellent dispersion and thermal cycling stability. Additionally, the composite exhibited high performance and improved energy storage efficiency.

Table 6 Summary of paraffin utilization as PCM [90].

Materials	Melting Temperature (°C)	Latent Heat (kJ/kg)
Acetamide	81	241
Acetic acid	16.7	184
Capric acid	36	152
Eladic acid	47	218
LA Lauric acid	43.93	178.11
Lauric acid	49	178
MA Myristic acid	54.28	191.27
Methyl fumarate	102	242
Myristic acid	58	199
PA, palmitic acid	62.73	206.16
Palmatic acid	55	163
Pentadecanoic acid	52.5	178
Polyethylene glycol 600	20–25	146
SA stearic acid	69.62	217.62
Stearic acid	69.4	199
Tristearin	56	191

Inorganic PCM

Inorganic PCM are typically classified into 2 subcategories: Salt hydrates and metals. PCM are readily available, economically viable, and exhibit unique characteristics. Unlike organic compounds, inorganic PCM have latent heat per mass and volume of more than 220 kJ/kg and a melting temperature range of 5 - 130°C [92]. Inorganic PCM are cost-effective, inexpensive, and nonflammable. However, suboptimal cooling and release processes and insufficient long-term stability limit their usefulness as latent heat storage systems. Several significant challenges hinder the development of these materials as PCM, including their limited thermal cycling durability, reactivity with containment materials, vulnerability to contamination, and toxicity of certain components. However, it is feasible to formulate inorganic compound mixtures that undergo uniform melting and solidification without phase separation [93]. For instance, the combination of Na_2CO_3 and NaCl not only maintains a substantial thermal energy capacity of 283.3 kJ/kg but also enhances the exceptional thermal and chemical stability of the material in CO_2-rich environments at elevated temperatures of approximately 700°C [94].

Utilization of salt hydrate as PCM

Salt hydrates form when anhydrous salts form solid crystal structures in the presence of water. Certain salts exist in an anhydrous state; however, upon the introduction of water, they absorb it at a specific molar ratio during ionization, resulting in general modification of their ionic structure [95]. Although numerous salt hydrates can be synthesized [92], only a limited number of them are thermodynamically stable and capable of releasing the requisite energy, rendering them suitable as PCM [96]. The energy released during the hydration process of anhydrous salts can be utilized as a sustainable energy source with the potential for long-term commercialization [97]. Salt hydrates typically melt to form structures that contain fewer water molecules [98,99].

Upon reaching their melting point, hydrate crystals decompose into anhydrous salts and water, or into lower hydrates and water. A significant challenge associated with numerous salt hydrates is that the melting process is frequently problematic because of insufficient water release to dissolve all solid phases present. This phenomenon occurs because of density differences, causing the lower hydrate (or anhydrous salt) to descend to the bottom of the container. Moreover, salt hydrates generally exhibit poor

nucleation characteristics, resulting in liquid supercooling before the initiation of crystallization. To address this issue, a nucleating agent may be introduced to initiate crystal formation or maintain a portion of the crystals in a small cold region to serve as nucleation sites [98,99]. He *et al.* [99], emphasized the importance of latent heat storage (LHS) using phase change materials (PCM) to address the discrepancy between the thermal energy supply and demand in buildings. Despite its potential, hydrated salt, a promising PCM, faces challenges, such as significant supercooling, phase separation, and poor thermal conductivity, hindering its progress. This study aimed to enhance $Ba(OH)_2{\cdot}8H_2O$ by introducing nucleating and thickening agents to mitigate supercooling and improve thermal properties, while incorporating expanded graphite (EG) to increase the thermal conductivity. **Table 7** provides an overview of previous studies on the use of hydrated salts as PCM.

Table 7 PCM salt hydrate summary.

Types of PCM	Supports	Nucleating agent	Tm (°C)	ΔHm (kJ/kg)	Supercooling degree (°C)	Ref.
$CH_3COONa{\cdot}3H_2O$	Expanded Graphite	$Na_2HPO_4{\cdot}12H_2O$	57.8	218.6	7.1	[100]
$Na_2CO_3{\cdot}10H_2O$ $Na2HPO_4{\cdot}12H_2O$	Expanded Perlite	-	26.81	151.73	6.3	[101]
$MgCl_2{\cdot}6H_2O$	Modified EG	TX-100	116.24	116.7	1.3	[101]
$CH3COONa{\cdot}3H_2O$	expanded vermiculite	$Na_2B4O_7{\cdot}10H_2O$	57.6	270.6	-	[102]
$CaCl_2{\cdot}6H_2O$	Expanded Perlite	$SrC_{l2}{\cdot}6H_2O$	27.38	87.44	-	[103]
$Na_2HPO_4{\cdot}12H_2O$	Cellulose sponge	Paraffin	35.2	227.3	19.5	[104]
$Na_2SO_4{\cdot}10H_2O$- $Na_2HPO_4{\cdot}12H_2O$	Fly ash	$Na_2B_4O_7{\cdot}10H_2O$	25.3	106.9	5.6	[105]
$Na_2SO_4{\cdot}10H_2O$ $Na_2CO_3{\cdot}10H_2O$	expanded vermiculite	$Na_2B_4O_7{\cdot}10H_2O$	23.98	110.3	0.64	[106]

Table 7 presents the findings from previous studies utilizing salt hydrates as phase change materials (PCM). In one such study, Fu *et al.* [103], Expanded Perlite (EP) was employed as a supporting medium to encapsulate $CaCl_2{\cdot}6H_2O$ salt hydrate via vacuum impregnation at 88.1 kPa. The researchers examined 4 different ratios of $CaCl_2{\cdot}6H_2O$ within the EP to determine the maximum PCM loading without leakage using a diffusion-oozing loop test. The composite maintained excellent shape stability and thermal cycling reliability with 55 wt.% $CaCl_2{\cdot}6H_2O$ content. X-ray diffraction (XRD) and Fourier transform infrared (FT-IR) analyses confirmed the absence of chemical reactions between the components after impregnation and minimal latent heat loss following 1,000 melting-freezing cycles. EP, typically produced by heating pearlite to 1,000 - 1,300°C, expands 4 - 30 times its original volume, creating numerous pores that enhance the thermal stability and render it suitable for adsorbing and impregnating hydrated salt PCM. Expanded vermiculite (EV), which possesses a layered pore structure, is another porous support material that is frequently utilized for stable hydrated salt PCM. For instance, Xie *et al.* [106], employed a binary eutectic hydrated salt (EHS, $Na_2SO_4{\cdot}10H_2ONa_2CO_3{\cdot}10H_2O$ with a 1:1 mass ratio, phase change temperature of 25.04°C, and melting enthalpy of 198.6 kJ/kg) to enhance indoor thermal comfort.

Despite extensive research on salt hydrate as a phase-change material (PCM), its practical application remains a significant challenge. The primary issue is the absence of a suitable melting point for thermal storage in salt-hydrate PCM. This problem arises because n moles of hydration water cannot dissolve one mole of

salt, which results in a saturated solution at the melting temperature. Consequently, excess salt solids precipitate at the bottom of the container, becoming unavailable for recombination with water during solidification, which impedes the reverse process in the filling-discharging cycle. Another prevalent issue associated with salt hydrates is supercooling. The nucleation rate is typically low at fusion temperatures, necessitating the supercooling of the solution. This led to energy dissipation at significantly lower fusion temperatures. Furthermore, salt hydrates tend to undergo spontaneous nucleation with fewer water molecules during exothermic processes. To mitigate this issue, chemicals have been introduced to selectively enhance the solubility of lower salt hydrates compared with pure salt hydrates with a higher number of water moles [107].

Utilization of metals as PCM

The categories of low-melting-point and eutectic metals have not been extensively explored for PCM technology, owing to significant barriers. However, these metals demonstrate potential in terms of volume given their high heat of fusion per unit volume. Their high thermal conductivities obviate the need for additional weight increasing fillers. Metal PCM, similar to other materials utilized for comparable purposes, can transfer heat from critical devices, effectively regulating the temperature of the device during periods of temporary high-power operation [108]. These materials can store this heat by utilizing the latent heat of fusion, absorbing energy from one material and releasing it to another as required [97]. For instance, the thermal conductivity of Cu is recorded as 180.4 W/mK at 1,600°C [109]. Consequently, metallic PCM may exhibit superior thermal properties compared to those of salt hydrates and organic PCM.

Metallic phase-change materials (PCM) are extensively utilized in diverse applications, including electric vehicle production and high-temperature management. Their widespread adoption is attributed to the inadequacy of organic PCM and salt compounds. Metal PCM not only address the requirement for enhanced thermal conductivity but also exhibit superior mechanical properties, with the Young's modulus of aluminum reaching 70 GPa [110]. However, the primary limitation of metal PCM is their high cost [109,111]. Compared to salts, metal PCM are more expensive owing to the extraction process and specific implementation requirements [109]. Notwithstanding this constraint, numerous studies have been conducted to investigate the potential of metal PCM. Al-Jethelah *et al.* [112], investigated the utilization of metal as a phase change material (PCM). An experimental study was conducted to examine the melting process of a nano-PCM within a metal foam enclosure under constant heat-flux conditions. Visualization experiments were performed using a bio-based nano-PCM comprising copper oxide (CuO) nanoparticles dispersed in coconut oil PCM within an open-cell metal foam. Their findings demonstrated that the incorporation of nanoparticles and metal foam enhanced both the melting rate and the energy storage capacity. For low-porosity (88%) porous media, uniform melting was observed, which was primarily attributed to conduction-based heat transfer. Conversely, high-porosity (96%) porous media exhibited non-uniform melting, with greater melting occurring at the top than at the bottom, as heat transfer occurred through convection at the top and conduction at the bottom. These results have potential applications in latent heat energy storage systems, thermal management of prismatic batteries in rechargeable hybrid electric vehicles, and cooling systems for electronics in remote locations. The addition of nanoparticles to the PCM resulted in a 1.2% enhancement in the melting process, whereas embedding metal foam in pure PCM led to a more substantial improvement of 41.2% at 1814 W/m^2 and 2160 s. The energy storage rate was accelerated by 2.61% with the addition of nanoparticles and by 28.81% with the use of metal foam, compared with pure PCM, at 2835 W/m^2 and 2,280 s, respectively.

Promsen *et al.* [113], investigated a novel approach to incorporate metal phase-change materials (mPCM) into solid oxide fuel cell (SOFC) stacks, with the objective of improving thermal conditions and enhancing SOFC operational flexibility. The study utilized 3-dimensional computational fluid dynamics modeling, employing electrochemical and melting/solidification solvers to simulate various mPCM-SOFC stack operating scenarios, including extreme load fluctuations, such as rapid start-ups and shutdowns. Researchers have evaluated pure aluminum and copper-silicon-manganese eutectic alloys as potential mPCM candidates. Their findings indicated

that mPCM can improve the SOFC stack temperature distribution and facilitate the utilization of an exceptionally high air utilization rate of 85%, potentially reducing the parasitic air blower requirements. Moreover, mPCM demonstrated the capacity to mitigate stack temperature variations during significant load changes. The liquefaction of the PCM was observed to extend the peak load operation by absorbing substantial heat, whereas PCM compaction contributed to maintaining steady-state stack temperatures. Furthermore, the mPCM exhibited potential as an inlet gas preheater, enabling direct fuel and room-temperature air input into the stack, thereby enhancing cooling performance.

Eutectic PCM

A eutectic mixture is one that comprises soluble organic and inorganic compounds at a specific atomic ratio that solidifies and melts concurrently to form a crystalline mixture of components during crystallization. By combining 2 organic PCM, it is possible to create a new PCM with improved properties, such as latent heat and supercooling values. This would fall under the category of organic-organic PCM [114,115]. Occasionally, 2 inorganic PCM can be combined to create an inorganic-organic PCM, which frequently demonstrates superior characteristics compared with its individual inorganic components [116]. Furthermore, organic and inorganic PCM can be combined to form organic-inorganic PCM [117]. These combinations are referred to as eutectic mixtures (EMs). The properties, advantages, disadvantages, and applications of these mixtures are determined by their constituent materials [118]. However, these mixtures are meticulously engineered to enhance the positive attributes of the resulting PCM, thereby improving its usability and reliability for intended purposes. It is essential to recognize that, in the production of eutectics, combinations that offer cost-effective solutions are highly desirable for commercial applications. A notable characteristic of most eutectics is their resilience under repeated thermal cycling, rendering them well suited for use in low-temperature refrigeration systems [118].

Although there has been limited research into the use of eutectic mixtures in TES applications in buildings due to the temperature range, eutectic PCM have been widely studied. **Table 8** provides an overview of the use of eutectic PCM and their thermal properties [45,116,118].

Table 8 Summarizes previous research on eutectic PCM.

Materials	Composition (wt%)	Latent heat (kJ/kg)	Melting temperature (°C)
Trietiloletan + air + urea	38.5 + 31.5 + 30	160	13.4
$C_{14}H_{28}O_2 + C_{10}H_{20}O$	34 + 66	147.7	24
$LiNO_3 + NH_4NO_3 + NaNO_3$	25 + 65 + 10	80.5	80.5
$LiNO_3 + NH_4NO_3 + KNO_3$	26.4 + 58.7 + 14.9	81.5	81.6

Fan *et al.* [119], examined the thermal properties, durability, and reliability of lauric acid-based binary eutectic mixtures, with a specific focus on their potential applications in improving building energy efficiency. A gradual cooling curve experiment confirmed the eutectic point of the lauric acid-based binary eutectic blend, revealing eutectic compositions of 4LA = 70%, 4LA = 79%, and 4LA = 82% with corresponding melting temperatures of 35.10, 37.15, and 39.29°C. The latent heat of melting was determined to be ΔHm = 166.18, 183.07, and 189.50 kJ/kg for LA-MA, LA-PA, and LA-SA binary eutectic PCM, respectively. Schroder's formula was utilized to calculate the melting temperature, eutectic point, and melting enthalpy of the LA-MA, LA-PA, and LA-SA binary PCM, and the theoretical calculations demonstrated close agreement with the experimental results. FT-IR and XRD analyses indicated no chemical reactions during the preparation of the LA-MA, LA-PA, and LA-SA eutectic PCM, suggesting good compatibility between the PCM eutectic mixture and its components. TG and cycle tests demonstrated the exceptional thermal stability and reliability of the LA-MA eutectic PCM, LA-PA eutectic PCM, and LA-SA eutectic PCM below 126.51, 135.7 and 110.08 °C, respectively. The research concluded that lauric acid-based binary eutectic PCM exhibit

potential as effective insulation materials for building energy conservation.

Krishna *et al.* [89], investigated the synthesis of a fatty acid/metal ion composite PCM by incorporating sodium ions into lauric acid, with the objective of enhancing its thermophysical properties for thermal energy storage applications. These composites were formulated by introducing 0.2, 0.5, or 1 wt.% sodium metal into lauric acid. Compared to pure lauric acid, the composites exhibited increases in the enthalpy of fusion and phase change by 5.3, 7.9, and 10.6%, respectively. The composite also exhibited a slight decrease in the melting point as the sodium metal content increased. FTIR spectroscopy revealed no interaction between lauric acid and sodium metal, suggesting an enhanced composite stability. Thermogravimetric analysis indicated a 30% increase in the decomposition temperature of the composite with the addition of sodium metal, rendering it suitable for thermal energy storage applications [89]. In a separate investigation, Lu *et al.* [116], examined an alternative type of eutectic PCM by combining a wax-like PCM consisting of 2 fatty acids with mesoporous carbon nanoparticles. The authors reported that the resulting structure exhibited exceptional properties, with mesoporous carbon nanoparticles demonstrating a high drug-loading efficiency of 14.2% and photothermal conversion efficiency of 24%.

Thermal conductivity enhancement of PCM

Thermal energy transmission through solid materials can occur through a variety of mechanisms, including electric carriers (such as electrons or holes), phonons (lattice waves), electromagnetic waves, spin waves, and other forms of excitation. In metallic materials, electric carriers are primarily responsible for the heat transfer, whereas lattice waves tend to be the dominant heat conductors in insulators. The total thermal conductivity (K) of a material can be expressed as the sum of its individual components, each corresponding to a distinct excitation mechanism [120], as shown by Eq. (1):

$$K = \Sigma_{\alpha} K_{\alpha} \quad (1)$$

The symbol represents the excitation, and the thermal conductivity of solid materials varies depending on the intensity and temperature, which are specific to the materials in question. These variations can be explained by differences in the crystal size for individual specimens or grain dimensions in polycrystalline samples, imperfections or defects in the lattice structure, dislocations, non-harmonic lattice forces, concentration of carriers, interactions between carriers, lattice vibrations, and the interplay between magnetic ions and lattice waves. Consequently, investigating thermal conductivity using both experimental and theoretical approaches present an intriguing field of research [120].

A significant focus of research pertains to the efficacy of PCM applications, which is strongly correlated with the thermal conductivity as a critical parameter. Upon examination of the micro-mechanisms and material structure, the thermal conductivity of the phonons in the PCM was observed to be relatively low. Enhancing the thermal conductivity of PCM remains a crucial area of investigation [121,122]. The thermal conductivity of PCM composite materials is influenced by various factors, with phonon scattering being the primary mechanism limiting their heat conduction capabilities. More specifically, phonon scattering plays a substantial role in determining the thermal conductivities of PCM composite materials. The study of phonons provides the most fundamental understanding of heat conduction at a microscopic scale.

Furthermore, phonons play a crucial role in facilitating the heat transfer across materials. Research aimed at enhancing the thermal conductivity of composite materials primarily focuses on the efficient transmission of phonons along the microscopic axis. This approach is considered the most effective method for phonon transmission because these heat carriers can propagate randomly without obstacles, potentially achieving the desired thermal conductivity in composites. The transmission of phonons in composite materials is primarily governed by 3 factors: The phonon velocity, specific heat capacity, and mean free path. However, the thermal transfer in composite phase change materials (PCM) and phonon interfaces is not solely determined by these factors. Additional parameters such as temperature, atomic weight, density, and binding energy also influence this process.

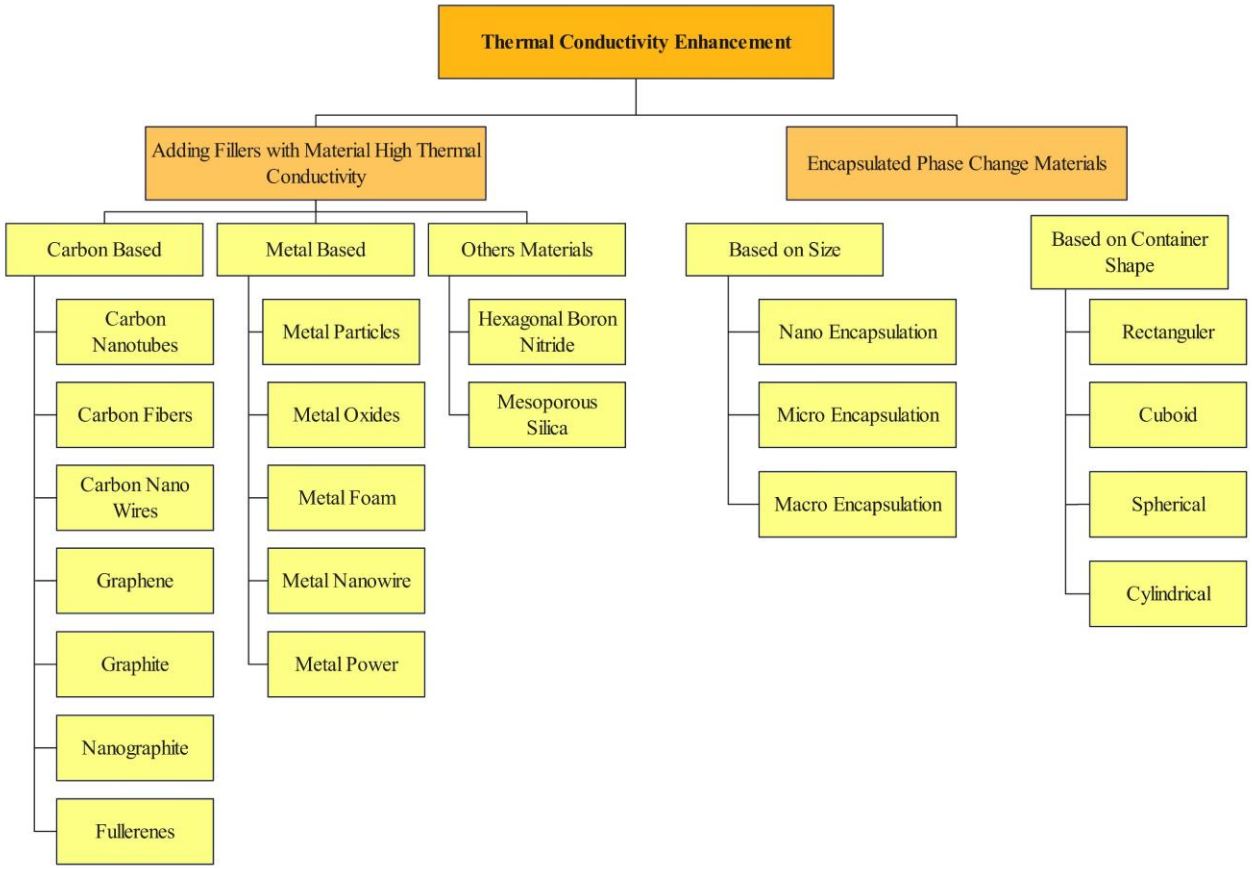

Figure 6 Thermal Conductivity enhancement method on PCM.

According to the elucidation of the essential mechanism of thermal conductivity in materials, it can be deduced that the thermal conductivity of PCM can be enhanced through 2 primary methods, as depicted in **Figure 6(a)** incorporating substances with exceptional/elevated thermal conductivity and (b) the encapsulation method.

Particle addition

Previous research has extensively explored methods to enhance the low thermal conductivity of PCM, particularly through the incorporation of particle additives with high thermal conductivity. Additives include carbon-based materials and metal-based substances. Additionally, researchers have developed other types of materials, such as hexagonal boron and mesoporous silica, to address this issue.

Carbon-based materials

PCM that incorporate carbon-based materials, such as graphite expansion, carbon fibers, carbon nanotubes, and graphene, have been studied and analyzed. These materials generally have high thermal conductivities and low densities, making them suitable for use in PCM, particularly paraffin. Owing to its unique characteristics of corrosion resistance, softness, and plasticity, graphene has been added to carbon-based thermal conductivity. Furthermore, studies have been conducted to improve the thermal conductivity of PCM [123]. Graphene, as a multifunctional material, is highly effective due to its high surface area, very high thermal conductivity, high charge carrier mobility, and optical transmittance. Their suitability for applications in nanoelectronics, supercapacitors, sensors, and energy storage are demonstrated by these properties. The 2-dimensional honeycomb lattice of carbon atoms in graphene allows it to function in light-to-heat conversion by capturing photons and storing them in the lattice [124-126].

In contrast to previous studies, Cui *et al.* [127], the investigation examined the thermal properties of paraffin wax PCM enhanced with graphene. Results demonstrated a reduction in mass loss ratio to below 0.34%, an enhancement in thermal conductivity to 0.33 W/m·K, and a solar heat storage efficiency of 75.68%.

Furthermore, higher concentrations of graphite nanoparticles were observed to have a positive effect on the thermal conductivity. According to *Jiang et al.* [128], the primary factors used to evaluate the heat transfer improvement effect of composite phase change materials are the thermal conductivity, thermal conductivity enhancement, and thermal conductivity enhancement per filler volume fraction. However, the simultaneous modulation of all 3 parameters for PCM composites remains a challenge. To address this issue, graphite fibers were incorporated through in-plane bonding as a thermal conductivity enhancer for PCM. In-plane bonding allows graphite planes to be dispersed in the interface region of the PCM, thereby facilitating the enhancement of phonon vibrations and reducing the interfacial thermal resistance. The optimized PCM composite exhibited a high thermal conductivity of 36.49 W/mK at 20.7 vol% carbon fiber.

This type of carbon-based material addition can also be employed with carbon nanotubes (CNTs) because only a small volume fraction is required to increase the thermal conductivity and density of the PCM [129,130]. In the research of Die *et al.* [67], the addition of 2 wt.% CNTs resulted in a thermal conductivity of 0.39 W/mK for the PW-SBS/CNT-85 composite at 25°C, which is approximately 1.5 times higher than that of pure Paraffin Wax. **Table 9** summarizes previous studies on the addition of carbon-based materials to PCM. The enhancement of thermal conductivity of PCM by adding carbon material shows the value of thermal conductivity is successfully improved. CNT became the most stable and high enhancement material with the addition of 0.5, 1, 2 and 20 wt.% of 0.35, 0.97, 0.4 and 0.2 W/m.K, respectively.

Table 9 Summary of carbon-based material addition to PCM.

Samples of PCM	Carbon based additives	Mass fraction of additives	Thermal conductivity K (W/m.K)	Ref.
Paraffin Wax	MWCNT	0.5 wt%	0.35	[71]
Paraffin Wax	SiO_2@MWCNT	0.5 wt%	0.40	[71]
Paraffin Wax	SiO_2@MWCNT	1 wt%	0.45	[71]
Paraffin Wax	Graphite Fiber	1 vol%	1.66	[131]
Paraffin Wax	CNT	2 wt%	0.39	[129]
Paraffin Wax	Graphene	0.1 wt%	0.59	[132]
Paraffin Wax	Graphene Oxide	1 wt%	0.67	[127]
Paraffin	Graphene oxide	1.7 wt%	0.9	[133]
Paraffin	Expanded Graphite-700	1 wt%	0.92	[134]
Paraffin	Expanded Graphite	30 wt%	0.51	[135]
Paraffin	Carbon Fiber	-	0.51	[136]
Paraffin	Carbon Fiber	8 wt%	0.4	[137]
Paraffin	Carbon Fiber	8.3 wt%	2.04	[136]
Paraffin	Carbon Nanotube (CNT)	1 wt%	0.97	[138]
Paraffin	Carbon Nanotube (CNT)	20 wt%	0.2	[139]
Paraffin	Carbon Nanotube (CNT)	2 wt%	0.4	[140]

Metal-based materials

Metal-based substances exhibit superior thermal conductivity owing to their enhanced heat transfer capabilities and effective mixing characteristics compared to the original material. Consequently, numerous researchers have focused on utilizing various metals as additives to enhance the thermal conductivity of PCM. **Table 10** lists the thermophysical properties of metal-based materials.

Table 10 Summary of carbon-based material additions to PCM.

Metal Based	Density (Kg/m^3)	Thermal Conductivity K (W/m.K)	Specific Heat (KJ/kg.K)	Ref.
Al_2O_3	3,890	20 - 30	0.78	[20]
MgO	3,580	61.9	0.721	[20]
SiO_2	2,650	11.715	0.536	[20]
Fe_3O_4	7,874	9.7	-	[74]
TiO_2	3,900	11.8	697	[141]
CuO	6,300	37	550.5	[141]
Fe_3O_4	6,300	15	-	[142]
Al_2O_3	3,260	36	-	[143]
ZnO	5,600	29	514	[144]
Zn	7,140	121	388	[145]

Table 11 Summary of metal material addition to PCM.

Samples of PCM	Metal based additives	Mass fraction of additives	Thermal conductivity K (W/m.K)	Ref.
Paraffin	SiO_2	0.5 wt%	0.26	[71]
Paraffin	Al	50 wt%	1.27	[146]
Paraffin	Copper foam	-	3.0	[147]
Paraffin	Ag	9.14 wt%	1.2	[147]
Paraffin	Al_2O_3	7.5 wt%	0.24	[148]
Paraffin	Al_2O_3	10 wt%	0.25	[148]
Paraffin	Fe_3O_4	50 wt%	0.53	[26]
Paraffin	TiO_2	0.1 wt%	0.26	[149]
Paraffin	TiO_2	0.5 wt%	0.33	[149]
Paraffin	TiO_2	1 wt%	0.36	[149]
Paraffin	TiO_2	2 wt%	0.28	[149]
Paraffin	Fe_3O_4	10 wt%	0.37	[150]
Paraffin	Fe_3O_4	20 wt%	0.40	[150]
Paraffin	ZnO	2 wt%	0.26	[151]
Paraffin	ZnO	4 wt%	0.30	[150]
Paraffin	ZnO	6 wt%	0.32	[150]
Paraffin	ZnO	10 wt%	0.35	[150]

Based on the data in **Table 10**, it can be concluded that the thermophysical properties of metals that can be added to PCM provide a solution to the weakness of thermophysical properties in PCM materials, particularly in organic PCM. Several studies have been conducted, as reported by Singh *et al.* [20]. In their investigation the authors added SiO_2, Al_2O_3 and MgO nanoparticles to paraffin PCM. The authors conducted a thermal performance analysis and found that the addition of SiO_2 to PCM resulted in a greater increase in the thermal conductivity compared to Al_2O_3 and MgO. This is attributed to the smaller particle size and low density of SiO_2, which allows for greater interaction with pure paraffin and improved thermal conductivity. Additionally, the low density of nanoparticles allows the paraffin to hold more nanoparticles, resulting in an increased heat transfer rate and Brownian motion, leading to a higher filling level. The thermal conductivity values for 0.1 vol% addition of SiO_2, Al_2O_3, and MgO particles at 50°C were 0.255, 0.225, and 0.215 W/mK, respectively. On the other hand, He *et al.* [74]. Added Fe_3O_4 magnetite particles to PCM paraffin wax and found that the thermal conductivity value increased with the addition of Fe_3O_4, with the pristine PW, Fe_3O_4-PW (1 wt.%), Fe_3O_4-PW (2 wt.%), and Fe_3O_4-PW (3 wt.%) having thermal conductivity

values of 0.251, 0.298, 0.315, and 0.331 W/mK, respectively. Furthermore, **Table 11** provides a summary of previous research on the addition of metal materials to PCM.

According to the outcomes, it has been discovered that the thermal conductivity of PCM composites made with various metal-based materials can be improved. The relevant thermal conductivity data for the PCM composites are presented in **Table 11**. When metals are used as thermal conductivity additives, they exhibit poor structural stability. This issue arises because some metals are prone to oxidation, whereas others are susceptible to corrosion by acidic and alkaline substances. Additionally, metals with high densities can cause the precipitation of metal particles within the PCM composite [152].

The thermal properties of PCM with additive combinations have been summarized, leading to the conclusion that this method results in excellent thermal stability and can be applied across various environments. To effectively utilize the technique of incorporating additives with high thermal conductivity, several investigations must be conducted: (1) Numerous experiments have been conducted to enhance the thermal conductivity of PCM, yet most employ a single additive. Therefore, the combination of 2 types of additives with mutual enhancement (such as carbon fiber and graphene, or metal oxide and carbon nanotubes) may be applicable to PCM. (2) The incorporation of additives may result in a reduction of the latent heat of PCM; thus, the mass fraction of additives should be adjusted to achieve an appropriate latent heat value while still enhancing the thermal conductivity of PCM composites. Some studies have reported that a decrease in latent heat is typical due to increased thermal conductivity; however, the latent heat must exceed 100 kJ/kg for use as thermal energy storage (TES). This can be addressed by ensuring the mass fraction of additives remains below 15 wt%. (3) The long-term stability of PCM can be improved by incorporating surfactants into PCM composites, which facilitates more uniform particle distribution and extends the life cycle of PCM. Several studies have proposed the use of surfactants in PCM composites.

Alrobei *et al.* [153] conducted a study aimed at enhancing the thermal conductivity of paraffin wax through the application of surfactants. The surfactants employed as thermal conductivity enhancers (TCE) included cetyltrimethyl ammonium bromide (CTAB), dioctyl sodium sulfosuccinate (AOT), and sodium dodecyl sulfate (SDS). The self-aggregation of surfactants into micelles serves as a conductive medium within the paraffin wax, thereby improving thermal conductivity. The highest heat transfer rate, with a peak temperature of 71°C, was observed in the AOT micellar paraffin wax. The addition of SDS, CTAB, and AOT surfactants resulted in an increase in the highest temperature by 4, 8.4 and 18.33%, respectively, compared to pure PCM [153]. Conversely, Pantea et al. focused on the production of nanoemulsions with commercial RT42 paraffin fine droplets, stabilized using the anionic surfactant SDS via a sonication method [154]. The study investigated the impact of PCM nanoemulsion formulation on thermophysical and rheological characterization. The findings indicated a reduction in the supercooling rate from 12.8 to 8.6°C as the volume fraction of PCM was varied from 10 to 45 vol%. This reduction is attributed to the enlargement of the PCM droplet size from 110 to 164 nm while maintaining a constant PCM-to-surfactant ratio of 10:1. The incorporation of Fe_3O_4 nanoparticles as a nucleating agent at concentrations of 1 and 4% resulted in a decrease in the supercooling degree from 10.2 to 8.2°C with the addition of 4% Fe_3O_4 nanoparticles. The samples demonstrated remarkable stability over a one-year storage period and under dynamic conditions, including 50 freeze-thaw cycles. An investigation into the rheology and gelation mechanism, through the estimation of attraction and repulsion interaction forces among the droplets, revealed that the nanoemulsion with a volume fraction ≥30% transitioned from a fluid-like state to a viscoelastic gel due to the thinning attraction caused by SDS micelles in the continuous phase. These findings contribute to a deeper understanding of the factors influencing the gel formation of viscoelastic PCM nanoemulsions and their potential applications in various fields.

Leong *et al.* [155] investigated the properties of efficient phase change materials (PCM), emphasizing the necessity for both high latent heat and thermal conductivity. This study examined the influence of multi-walled carbon nanotube (MWCNT) weight percentage (0 - 0.08 wt%) and various surfactants,

including gum arabic (GA), polyvinylpyrrolidone (PVP), sodium doxylbenzene sulfonate (SDBS), and sodium dodecyl sulfate (SDS), on the thermal conductivity, melting temperature, latent heat of melting, and thermal stability of paraffin wax. The findings revealed that paraffin wax with 0.06 wt% MWCNTs, without surfactant, exhibited the highest thermal conductivity improvement (48%) compared to pure paraffin wax. Additionally, paraffin wax with 0.08 wt% MWCNTs combined with PVP, SDBS, and SDS demonstrated higher thermal conductivity than samples with GA. Thermogravimetric analysis (TGA) indicated that all samples exhibited one-step decomposition characteristics.

Sheikh *et al.* [156] conducted an experimental investigation into the effects of incorporating graphite with various surfactants into a biobased PCM on its cooling performance. The graphite-based PCM (GraPCM) was prepared by stirring and sonicating graphite with surfactants such as Sodium Stearoyl Lactylate, SDBS, and SDS in a liquid biobased PCM. The experiments showed that the thermal conductivity of the bio-based PCM increased with graphite-SDS at a mass fraction of 5% graphite. A graphite ratio of 1:3 resulted in a 240% increase to 0.748 W/m K and a 218% increase to 0.70 W/m K when mixed with graphite-SDBS and surfactant at a 5% mass fraction of graphite. This resulted in the longest time for GraPCM-SDBS and GraPCM-SDS to reach the reference temperature of 43 °C, with delays of 185 and 175 s, respectively. It was observed that increasing the surfactant concentration further delayed reaching the reference temperature in the case of GraPCM-SDS. These results align with existing literature, which suggests that surfactants and graphite enhance the thermal conductivity of PCM. Several other studies have successfully reported improvements in the long-term stability of PCM and addressed the negative impacts of additive methods. For instance, Zaimi *et al.* [157] evaluated the role of Sodium Dodecylbenzene Sulfonate as a surfactant in enhancing the thermophysical properties of paraffin/graphene nanoplatelet PCM. Zhou *et al.* [158] examined the effects of SDBS and BS-12 on the functional groups and wettability of multicomponent acidified lignite.

Encapsulation

Barrett K. Green pioneered the PCM encapsulation technique as early as 1940. This method involves encapsulating the PCM material with an appropriate coating substance to isolate it from its environment. Encapsulated phase change materials are categorized based on the material design area, core-shell phase change, and PCM shape stability [159]. Core-phase change materials comprise PCM particles at the center, surrounded by a shell composed of different materials. Various manufacturing techniques for PCM encapsulation exist, including emulsion polymerization [160], interfacial polycondensation [161], miniemulsion polymerization, in situ polymerization, sol-gel [159], and alternative methods [162]. The classification of PCM encapsulation is determined by the particle size:

(i) nano encapsulation (between 1 and 1,000 nm)
(ii) micro encapsulation (between 0 and 1,000 μm)
(iii) macro encapsulation (above 1 mm)

PCM encapsulation is typically categorized according to the type of container used, such as spherical, cylindrical, tubular, or cubical containers, as depicted in **Figure 7**. Additionally, encapsulation processes are generally classified into 3 types based on their formation mechanism: physical, physical-chemical, and chemical methods, as shown in **Table 12** [163,164].

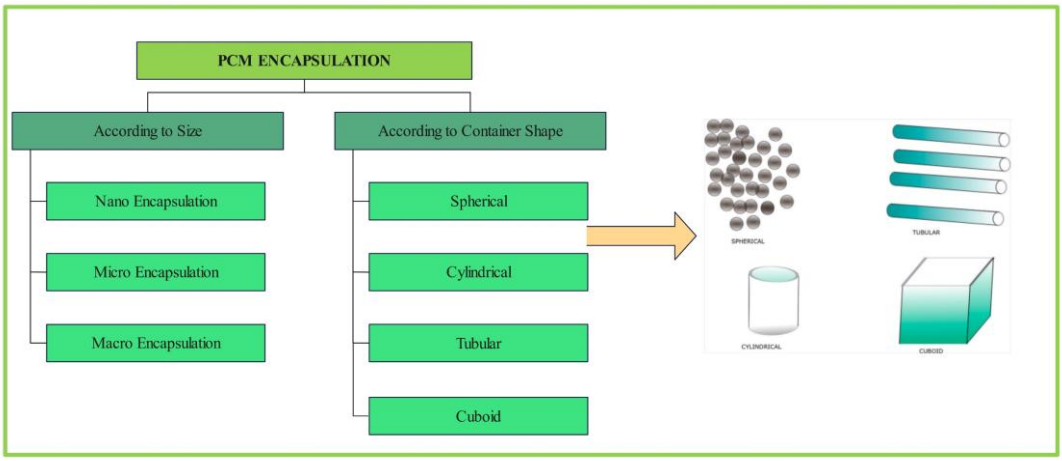

Figure 7 PCM encapsulation classification.

Table 12 PCM encapsulation method [165].

Category	Category
Physical Methods	Suspension-based pan coating, centrifugal extrusion methods, drying through spray processes, nozzle vibration technology, evaporation or extraction of solvents, impregnation using vacuum, and bonding through electrostatic means.
Chemical Methods	Emulsion polymerization, interfacial polymerization, suspension polymerization, in situ polymerization,.
Physics-Chemical Method	Complex coacervation, ionic gelation, sol gel.

In accordance with the data presented in **Table 12** on PCM encapsulation methods, each category was further divided into sub-methods, as depicted in **Figure 13** [14,132].

Nano encapsulation

A relatively recent technique for PCM encapsulation is nano-encapsulation, which seeks to address issues such as leakage protection, improved thermal physical strength, enhanced heat transfer, increased reliability, and stable charging and discharging cycles. Nano-encapsulation is a coating technology that involves nanoparticles, referred to as the core or active material, coated with a secondary material known as the matrix or shell to create nanocapsules. The core contains the active ingredient, whereas the shell protects the core from the environment. This shield can be temporary or permanent, and the core is typically released through diffusion or in response to triggers such as pH or shear, allowing for timely and directed movement to the intended site. Extensive research efforts have explored the application of nano-encapsulation in phase change materials (PCM) to enhance their thermophysical characteristics and durability. In one such investigation, Marske *et al.* [166], investigated shape-stabilized phase change materials (ss-PCM) using the sol-gel method and demonstrated their capacity to store thermal energy at levels up to 5 times higher than that of conventional composite PCM. Recent investigations have focused on developing ss-PCM with enhanced mechanical stability through a porogen-assisted sol-gel process. The researchers examined the Effects of sodium dodecyl sulfate (SDS) and poly (vinyl alcohol) (PVA) porogens on the properties of in situ formed ss-PCM. During gelation, silica frameworks were constructed around the PCM droplets coated with SDS in an oil-in-water emulsion. Irrespective of the quantity of porogen utilized in the synthesis, all the ss-PCM exhibited high shape stability (~100%), exceptional long-term performance (>2,000 thermal cycles), and strong chemical stability. Increasing the PVA content resulted

in the separation of the emulsion into large hydrophilic and small hydrophobic regions, expanding the silica macropore width in the ss-PCM from 1,007 to 8,801 nm due to silica fragmentation during drying. This fragmentation reduced the compressive strength (1.2 MPa) and thermal conductivity (0.37 W/mK) of ss-PCM by 50 and 17% (10°C), respectively. Conversely, insufficient SDS failed to stabilize all the PCM droplets in the emulsion, resulting in partial silica phase fragmentation. Excessive SDS concentrations decreased the emulsion viscosity and stability, causing silica macropores to collapse during drying. This collapse diminished the compressive strength (10.2 MPa) and thermal conductivity (0.37 W/mK) of the ss-PCM by 63% and 25% (10°C), respectively.

Micro encapsulation

Microcapsules are produced by coating phase change materials (PCM) with film-forming materials to create particles on the micron or nano scale. The methods for creating microcapsules can be divided into 3 categories based on their synthesis mechanism: Physical, chemical, and physico-chemical. A significant amount of research has been conducted on the microencapsulation of PCM, as shown in **Table 14**.

Table 13 PCM nano encapsulation summary.

Core	Shell	Method	Melting temperature T_m (°C)	Latent heat H_f (kJ/kg)	Ref.
Paraffin	Magnetic Nanoparticles	Interfacial Polymerization	55.85	87.40	[167]
Paraffin	PMMA-SiO_2	Interfacial Polymerization	26.80	69.90	[168]
Paraffin	PS-co-EA	Emulsion Polymerization	42.39	49.03	[169]
Paraffin	St-co-MMA	Miniemulsion polymerization	61.50	140.30	[170]
Paraffin	PS	Sol-Gel	27.10	110.05	[171]
Paraffin Wax	Gelatin/Acacia	Spary Drying	60	145	[172]
Paraffin Wax	Gelatin/Acacia	Coacervation	60	213	[172]
Paraffin Wax	SiO_2	Sol-Gel	27.1	110.1	[173]

Table 14 PCM micro encapsulation summary.

Core	Shell	Method	Melting temperature T_m (°C)	Latent heat H_f (kJ/kg)	Ref.
Paraffin	MF/GO	In-situ Polymerization	44.2	202.8	[18]
Paraffin	MF/Graphene	In-situ Polymerization	82.8	108.9	[174]
Paraffin	Methy methacrylate	Emulsion Polymerization	21.5	136.9	[175]
Paraffin	$CaCO_3$	Self-assembly	47.5	115.2	[176]
Paraffin	Polyurea	Interfacial Polymerization	27.5	92.5	[177]

Complementing the results presented in **Table 14**, Do *et al.* [16], investigated microencapsulation methods that utilize interfacial polycondensation reactions. Their objective was to prevent PCM liquid leakage at temperatures exceeding the melting point, and to develop a novel PCM with enhanced thermal

conductivity and energy storage capacity. In this study, stable phase-change microcapsules comprising a silica shell and Fe_3O_4 were combined with n-eicosane. Cu metal nanoparticles were incorporated into the outer wall of the capsule to enhance thermal conductivity for efficient heat transfer. This study demonstrated that n-eicosane-Fe_3O_4@SiO_2@Cu microcapsules exhibited exceptional heat transfer properties owing to their high thermal conductivity and effective thermal energy storage release performance by inhibiting supercooling. These microcapsules achieved an encapsulation efficiency of 61.48%, an energy storage efficiency of 61.47%, and a thermal storage capacity of 99.99%. Furthermore, multiple cycles of differential scanning calorimetry demonstrated outstanding thermal reliability and shape stability even during repeated melting and cooling processes. This indicates that the Fe_3O_4@SiO_2@Cu n-eicosane microcapsules have potential as PCM suitable for industrial applications.

Khan *et al.* [178], emphasized the critical importance of microencapsulation in preventing phase change materials (PCM) from escaping into their surrounding environment. The optimal microcapsules should facilitate the storage and release of latent heat from the PCM without inducing any physicochemical alterations in the core (PCM) or shell material (polymer). The properties of the shell material determine the characteristics of the PCM capsules, including heat transfer efficiency, thermal conductivity, water dispersibility, and durability. The investigators in this study employed a random copolymer, poly(methyl methacrylate-co-2-hydroxyethyl methacrylate) (poly(MMA-co-HEMA)), with an optimal ratio of 75/25 (methyl methacrylate (MMA)/2-hydroxyethyl methacrylate (HEMA)) as the encapsulating shell for Paraffin Wax (PCM). Microcapsules approximately 5 μm in diameter, with a shell thickness of approximately 0.8 μm, were synthesized using the emulsion solvent evaporation technique, achieving a high encapsulation efficiency (~92.34%) and thermal storage capability (99.85%). The water-absorbable PHEMA (poly(2-hydroxyethyl methacrylate)) shell not only exhibited excellent water dispersibility but also demonstrated an increase in thermal conductivity from 0.1 to 0.49 W/(mK) at 25°C when wet compared to its dry state. The capsules exhibited good longevity and maintained their thermal properties and water dispersibility even after 500 heating/cooling cycles. To assess the practicality of this water-dispersible microencapsulated PCM, it was incorporated into natural rubber latex in various proportions, resulting in rubber composites with exceptional thermoregulatory properties and enhanced mechanical strengths.

Macro encapsulation

Macroencapsulation of PCM enhance heat transfer rates by increasing surface area and thermal conductivity. This process is typically applied to PCM in thermal building systems. Macroencapsulation prevents direct contact between PCM and building materials or the surrounding environment, thereby ensuring PCM stability. The macroencapsulation process involves encapsulating the PCM in a shell material larger than 5 mm in size, with the shape of the encapsulated shell varying (tube, cylinder, bag, cube, etc.). This design allows for the easy incorporation of macro-encapsulated PCM into building envelopes of diverse dimensions and shapes. The different container types used for the macro-encapsulated PCM are illustrated in **Figure 11**. The geometry of a container depends on the dimensions of the parent building material to be incorporated. Ideally, the container should be made of metallic or plastic. If high heat transfer is a priority, a metal container is preferred [179].

Qudama and Marta [25], conducted an experiment to evaluate the thermal efficiency of concrete bricks containing PCM. They produced 4 concrete bricks, with 3 incorporating macroencapsulated PCM and one serving as a control. The thermal performances of the bricks were assessed under high-temperature conditions. This study investigated the effect of PCM encapsulation on the thermal properties of bricks while maintaining a constant PCM quantity. The bricks featured 3 distinct PCM capsule configurations: a single large capsule (Brick-B, 4×4×10 cm^3), 2 capsules (Brick-C,4×4×5 cm^3), and 5 capsules (Brick-D, 4×4×2 cm^3). The researchers calculated the peak temperature reduction (PTR), conductive heat transfer reduction (HTRc), and delay time (TD) by comparing the inner and outer surface temperatures of the PCM-infused bricks to the reference brick. The findings indicate that incorporating PCM into concrete bricks significantly enhances their thermal performance, even at extreme outdoor temperatures. Notably, Brick-D exhibited the most

favorable thermal characteristics, with PTR, HTRc, and TD improvements of 156.5, 61 and 133%, respectively, compared to the control brick under maximum outdoor temperature conditions.

Andrzejczyk *et al.* [186] examined the variation in macro patterns of PCM encapsulation in concrete, as illustrated in **Figure 8(a)**. Their findings demonstrated that Cuboid_2 blocks containing 1.5 kg PCM required approximately 1 h longer to fully melt compared to Cuboid_1 blocks with 1 kg PCM. This discrepancy was attributed to the larger PCM mass, which required more energy for melting. Moreover, increasing the PCM content results in lower maximum block temperatures. Concrete blocks without PCM reached 67.8°C, while those with 1 kg and 1.5 kg PCM attained 47.2 and 30.8°C, respectively. The study concluded that the PCM mass should be optimized for local conditions to achieve maximum effectiveness because excess PCM may not fully melt.

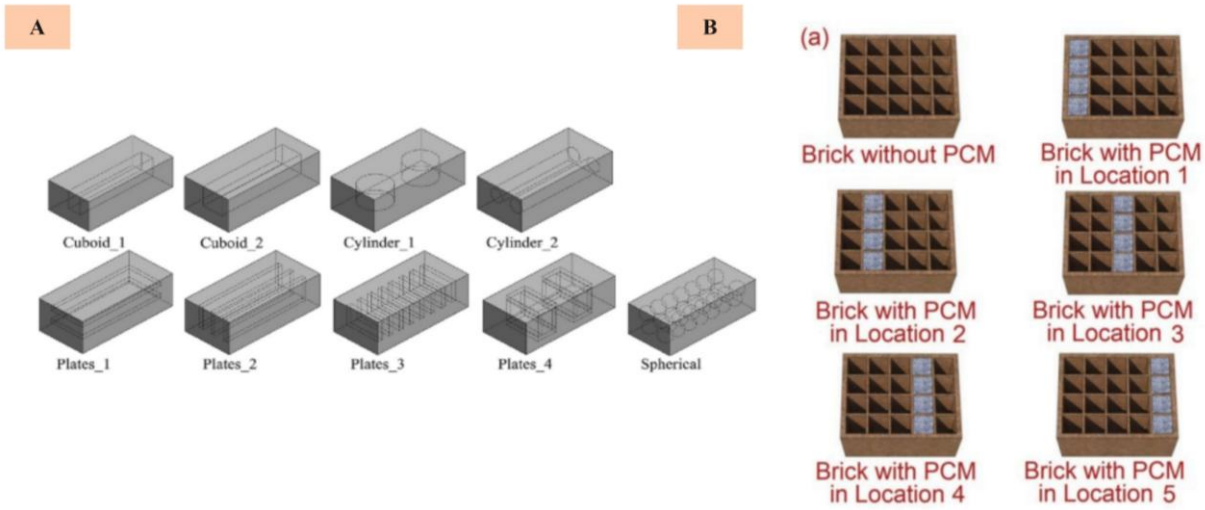

Figure 8 Schematic of Variation of PCM Macroencapsulation Method in Concrete, (a) reprinted with permission from Elsevier [180], (b) reprinted with permission from Elsevier [181].

Figure 8 illustrates various macroencapsulation techniques employed in phase change material (PCM) for thermal energy storage applications in concrete. The widespread utilization of macroencapsulation methods has been demonstrated in previous research. For instance,

On other hand, Gao et al, 2020 [182], investigated the heat-related characteristics of PCM-filled hollow bricks, as illustrated **Figure 8(b)**. The researchers selected a standard hollow brick with 20 cavities and considered 5 locations for PCM placement utilizing a 20% filling ratio. To simulate real-world applications, a typical wall was constructed. All wall components were assumed to be uniform and isotropic with constant physical properties. The study documented the thermal properties of the wall material, and the PCM employed had a phase-change temperature range of 18 - 23°C. According to Vérez *et al.* [183], the utilization of latent heat energy storage can significantly enhance the energy system efficiency owing to its superior energy density compared to sensible heat storage methods. The researchers emphasized that the design of the storage material encapsulation is a critical factor that substantially influences the heat transfer during the charging and discharging processes of the storage system. Consequently, they determined that macro-encapsulation represents a widely adopted and efficacious approach in thermal energy storage (TES) systems, primarily because of its manufacturing feasibility and cost-effectiveness.

PCM application

PCM can be used in various applications, such as thermal storage, thermal management of electronic equipment, heat pipes, batteries, construction, building cooling, solar energy, and solar stills. **Table 16** is a summary of previous research on PCM applications.

Table 15 Summary of PCM applications.

PCM Type	Method	PCM application	Ref.
Paraffin-copper foam	Experimentation and Simulation	Thermal energy storage	[184]
Paraffin/beeswax/plaster	Experimentation	Applications in buildings	[185]
biodegradable PCM	Experimentation and Numerical	Battery	[186]
Paraffin and oil	Experimentation	Energy storage in solar stills	[187]
Composite PCM foam	Experimentation	Heat pipe-assisted thermal and thermoelectric storage	[188]
Paraffin and nanoparticles	Numerical simulation	Heat pipe solar system	[189]

Thermal energy storage (TES)

Energy storage systems employ 4 primary methodologies: mechanical, electrical, thermochemical, and thermal. Thermal energy storage is frequently utilized in buildings, as shown in **Table 16**. This methodology involves the storage of excess thermal energy in materials for subsequent use in heating and cooling applications [190]. Thermal energy storage (TES) enhances the thermal energy efficiency by reconciling the discrepancies between energy consumption and production in terms of timing, temperature, location, and power [190]. The TES process comprises of 3 phases: Charging, storage, and discharging. Charging occurs when an external energy source is available, whereas discharging transpires when the source is unavailable. These 3 phases constitute a repeating cycle, and the efficiency of each phase is determined by the thermophysical properties of the storage medium. Recently, researchers have demonstrated a significant interest in the implementation of TES in buildings. In this context, TES enhances energy efficiency by increasing renewable energy utilization and decreasing energy consumption for heating and cooling [191].

Table 16 Differences in Thermal Storage Techniques [90,192].

TES	Principle	Advantages	Materials	Applications
Sensible Heat Storage	Increase or decrease the temperature of the storage material	Low cost, Easy operation	Water, stone, concrete, liquid metal, etc.	Solar energy storage and Building structure
Latent Heat Storage	Solid-liquid phase transition	High energy storage density, High latent heat, Maintains nearly constant temperature	Paraffin, salt hydrates, metals, etc.	Thermal energy storage, Solar power engineering, Heat pumps, Thermal control Industrial waste heat
Thermochemical Reaction Storage	Reversible chemical reactions	Highest energy storage density, Negligible heat loss	Ammonia, hydrates, metal hydrides, etc.	There is no app currently

Latent heat

The constant phase transition of a material from one physical state to another above its melting point characterizes the latent-heat-storage method. The quantity of heat stored is contingent upon the material's storage mass (kg) and enthalpy or heat of fusion (kJ/kg). Latent heat storage can utilize various phase changes, including solid-solid, solid-gas, liquid-gas, and solid-liquid changes. However, solid-liquid phase change has been extensively investigated for latent heat storage owing to its minimal volume change and cost-effectiveness. Latent heat storage using phase change materials (PCM) offers a higher energy storage density (350 MJ/m^3) compared to sensible heat storage, rendering it a promising approach for enhancing building energy efficiency [193].

Thermochemical systems use the energy absorbed and released during the breaking and reforming of molecular bonds in fully reversible chemical reactions. The capacity to provide high energy storage density and store heat at a constant temperature corresponding to the phase transition temperature of the PCM makes latent heat thermal energy storage advantageous. Consequently, any latent heat energy storage system requires a PCM with a melting point in the appropriate temperature range, a suitable heat exchange surface, an adequate container, and compatibility with the PCM. Latent heat storage (LHS) operates based on the principle of thermal absorption or release during the phase change of the storage material, whether from solid to liquid, liquid to gas, or vice versa. The storage capacity of an LHS system employing a PCM medium is determined using the following Eqs. (2) and (3):

$$Q = \int_{T_i}^{T_m} mC_p dT + ma_m \Delta h_m + \int_{T_m}^{T_f} mC_p dT \quad (2)$$

$$Q = m\left[C_{sp}(T_m - T_i) + a_m \Delta h_m + C_{1p}(T_f - T_m) \right] \quad (3)$$

where the mass of the material (m) is expressed in kilograms (kg), the temperature (T) is measured in kelvin (K), the specific heat capacity (Cp) is given in (kJ/kgK), the melting fraction of PCM (a_m), and the enthalpy of fusion (Δh_m) [194].

Sensible heat storage

Thermal energy storage (TES) in buildings predominantly uses sensible heat storage (SHS) as the primary methodology. This approach involves fluctuations in the temperature of the storage material over time, facilitating heat storage and release. The energy storage capacity is influenced by multiple factors, including mass (kg) and specific heat (J/kg.K), and temperature differential (°C) of the storage material. Additional properties affecting the SHS capacity include operational temperature, thermal conductivity, stability, vapor pressure, compatibility, and cost [195]. During SHS, the system stores thermal energy by increasing the temperature of the material in an endothermic process and releases it during an exothermic process without any phase transition. Construction materials, such as cement mortar, concrete, limestone, wood, stone, planks, and ceramic tiles, are frequently employed for sensible heat storage. The quantity of heat stored in the SHS was calculated using the heat capacity of the medium, temperature change, and quantity of storage material, as represented by a specific equation [194], as shown in Eqs. (4) and (5):

$$Q = \int_{T_i}^{T_m} mC_p dT \quad (4)$$

$$Q = mC_{ap}(T_f - T_i) \quad (5)$$

Concrete thermal energy storage system

Energy use continues to increase, resulting in an energy crisis and environmental problems, with the building sector being one of the largest contributors to energy use. Various strategies have been carried out by many researchers to reduce energy consumption [196,197]. The active and passive use of PCM in buildings ensures that the indoor temperature is as low as possible, thereby reducing the amount of energy required owing to the alternative use of air conditioners [198]. In **Figure 9**, which shows previous research related to the use of PCM in concrete, there are various variations of PCM encapsulation techniques in concrete.

Vicente and Silva [199], 3 comparable samples were investigated: 2 incorporating macroencapsulated PCM, one featuring an insulating XPS layer, and the other with a standard brick wall. The wall specimens were constructed using horizontally fired clay bricks (30×20×15 cm^3) with metal steel macrocapsule inserts (30×17×2.8 cm^3 format and 0.75 mm thickness) containing organic PCM (paraffin). **Figure 9(a)** shows the structure and composition of the wall specimens. This study utilized these materials as they reflect the prevalent construction of external sheathing walls in Southern Europe, which typically employ horizontal hollow clay bricks or blocks with external insulation.

Iqbal *et al.* [115], effects of PCM on heat transfer, thermal comfort, and energy efficiency in buildings. They developed insulated concrete hollow blocks (CHBs) and cellings (CILs) as PCM covers with mortar to reduce the costs. As depicted in **Figure 9(b)**, the CHBs measured 40×20×12 cm^3 and were comprised of 2 hollow rectangular blocks (16×7×17 cm^3). PCM was incorporated into the hollow sections of the CHBs. Eight CHBs were produced using cement mortar and varying PCM percentages (0, 50 and 75%) of the sand volume. Additionally, 3 CHB specimens were created to evaluate

the impact of substituting PU and PCM for a specific sand volume (100% PU + 0% PCM, 50% PU + 50% PCM, and 25% PU + 75% PCM) with PCM ratios of 0, 50 and 75% of the PU volume. All mixtures were maintained at a water/cement ratio of 0.5. The 8th CHB specimen contained a pure PCM. The preparation of (PCM+NS) and (PCM+PU) mixtures were prepared in a laboratory at room temperature. The process involved dry mixing of sand, aggregates, pumice, and PCM for 3 min, followed by the addition of cement and mixing for 2 min. Subsequently, 60% cold water was introduced into the dry mixture and mixed for 3 min to ensure the stability of the PCM powder. Finally, the remaining cold water was added and mixed for 4 - 5 min.

Saxena *et al.* [203], depicts modified bricks with single and double slots, as shown in **Figure 9(c)**. These bricks feature galvanised steel encapsulation with and without fins, with outer dimensions of 22.5×12×10 cm^3. The slots have dimensions of 1.7 cm (thickness) and 16 cm (length), and ASTM A525 (galvanized) steel, 0.4 mm thick, with dimensions of 15.5×9×1.5 cm^3, is used for PCM encapsulation. On the other hand, Zhang and Deng [200]. Conducted PCM experiments in concrete, as shown in **Figure 9(d)**. The figure shows 3 types of experimental hollow blocks (Block a, Block b, and Block c) containing "Capric Acid" PCM. The hollow blocks were supplemented with PCM. Compared with Laaouatni *et al.* [201]. Presented commercial hollow concrete blocks with dimensions of length × height × width: 50×20×9.5 cm^3) (as shown in **Figure 9(e)**, the blocks used in the experiments had different dimensions. The concrete block consisted of 3 parallelepiped cavities, and PVC tubes with a diameter of 2 cm and thickness of 1 mm were used. The PCM was introduced directly into the cavity in the liquid state (at a temperature higher than the solid gel temperature). The PCM used was a mixture of paraffin and styrene-type polymers. **Figure 9(f)** represents the study conducted by Tetuko *et al.* [26], where they experimented with creating concrete using a mix of lightweight aggregate, cement, sand, and water (in a ratio of 2:1:1.5:0.7). The resulting concrete had dimensions of 50×50×50 mm^3. The researchers installed copper tubes (measuring 12.7 mm in diameter and 50 mm in length) in the concrete in various arrangements, including 4 square, 4 cross and 6 rectangular formations. The concrete was then cured for 28 days at room temperature. Subsequently, the researchers filled the copper tubes with several types of PCM, including paraffin-magnetite, paraffin, and PEG composites.

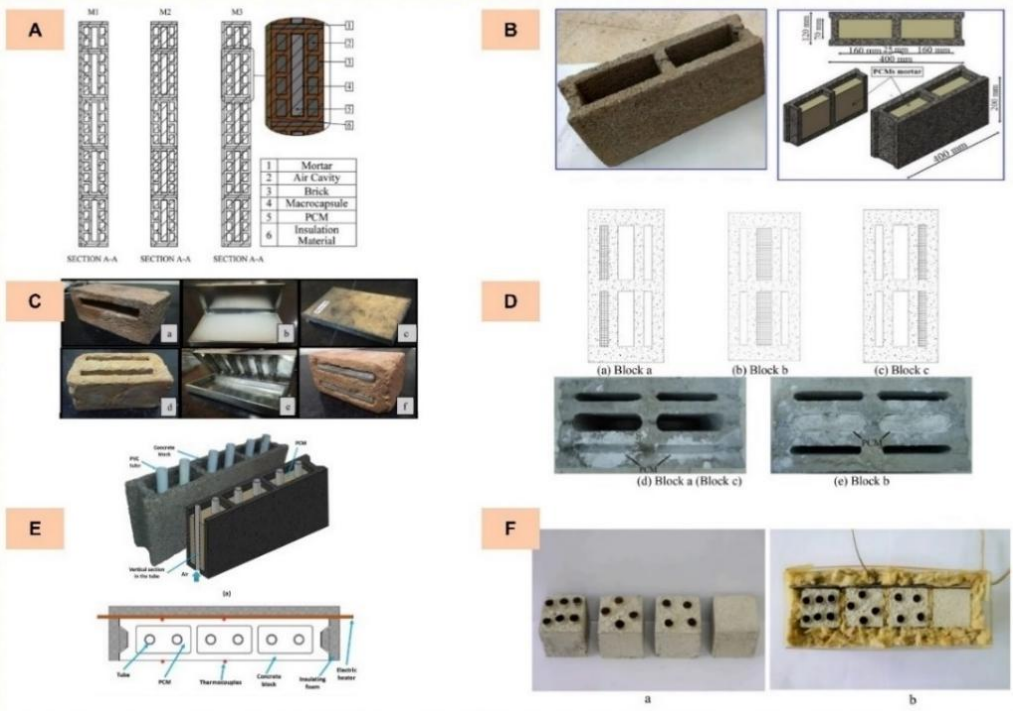

Figure 9 Thermal Energy Storage in Concrete, (a) reprinted with permission from Elsevier [199], (b) reprinted with permission from Elsevier [202], (c) reprinted with permission from Elsevier [203], (d) reprinted with permission from Elsevier [200], (e) reprinted with permission from Elsevier [201], (f) reprinted with permission from Elsevier [26].

The incorporation of PCM into concrete formulations has been shown to enhance the mechanical strength of materials. This enhancement is attributed to the high additive density of PCM and the influence of encapsulating materials, such as copper and aluminum, within the concrete matrix. Several studies have investigated the mechanical properties of concrete containing PCM. For instance, Florez *et al.* [204] reported the impact of mix content on the mechanical properties of concrete, noting that a maximum compressive strength of 60 MPa was achieved with composites containing 10 wt% magnetite, representing a 50% increase in the compressive strength of conventional concrete. However, at magnetite concentrations exceeding 20 wt.%, a notable reduction in compressive strength was observed, likely due to van der Waals forces leading to particle agglomeration. Conversely, Chang *et al.* [205] highlighted the application of microcapsule PCM in construction and demonstrated their integration into concrete mixes, wallboards, cement mortars, gypsum plasters, sandwich panels, and floor slabs to address the cooling, heating, and energy requirements of buildings [206]. The incorporation of microcapsules into concrete has been shown to enhance the fire resistance, thermal insulation, and acoustic properties of the walls. Kazanci *et al.* [207] utilized polystyrene-coated paraffin to synthesize flame-retardant microcapsule PCM, which were then incorporated into concrete blocks and evaluated using standard testing methods. The cast model, with a thickness of 12.5 mm, was subjected to a single flame source, and no dripping or flaming was observed, achieving the safety level “d0” as per the test standard “EN 1350-1”. Aguayo *et al.* [208] demonstrated that the addition of microcapsule PCM to concrete significantly improves its overall mechanical resistance and stiffness.

Hu *et al.* [209] reported that the addition of 2 wt% carbon nanotubes (CNTs) resulted in an increase in mechanical strength by 1.47 MPa. To enhance the utilization of steel slag solid waste and achieve objectives related to pollution reduction, carbon reduction, and synergistic efficiency, this study prepared a paraffin/SSMPC composite phase-change material (CPCM) using a spontaneous infiltration method, with paraffin serving as the phase change material (PCM). The achieved mechanical strength ranged from 0.53 to 4.22 MPa. Afgan *et al.* [210] demonstrated that concrete developed with 100% macro-encapsulated aggregates exhibited a compressive strength exceeding 15 MPa and has the potential to conserve energy by reducing the internal temperature by 6.4°C, while maintaining stability under high temperature fluctuations within a narrow range (22 - 30.2°C). Shen *et al.* [211] reported that the 7-day strength of high-strength concrete (HSC) increased to 8.6 MPa with the addition of multi-walled carbon nanotubes (MWCNT) to 30 wt% modified CMPCM, meeting standard requirements. Based on these research findings, the use of PCM and PCM encapsulation techniques has been confirmed to enhance the mechanical strength and durability of concrete.

PCM analysis

PCM analysis can be conducted through various measurements and characterizations, which are intended to evaluate the effectiveness of using PCM as a thermal energy storage medium, particularly in the context of concrete and buildings. The analysis techniques for PCM are classified into 4 distinct categories based on their nature and purpose: thermal properties, physical stability, chemical stability, and numerical/simulation.

Characterization of thermal properties

The characterization and measurement analysis of PCM based on thermal properties can be achieved by measuring various parameters such as thermal conductivity, thermal distribution, Differential Scanning Calorimetry (DSC), and Thermogravimetric Analysis (TGA). These measurements are critical for assessing the stability and efficiency of PCM as thermal energy storage media.

Analysis of thermal conductivity PCM

The thermal conductivity of the PCM is a crucial factor to understand, as it determines the mobility and phase change of the medium due to thermal agitation. Numerous studies have been conducted to measure the thermal conductivities of PCM, as illustrated in **Figure 10**.

According to He *et al.* [23]. As shown in **Figure 10(a)**, the addition of Fe_3O_4 nanoparticles to paraffin for thermal energy storage PCM resulted in an increase in thermal conductivity by adding Fe_3O_4 of 1, 2 and 3 wt.%

respectively to paraffin. The results obtained were 0.298, 0.315 and 0.331 W/mK, respectively, which were higher than the pristine paraffin value of 0.251 W/mK. When compared to the research of Singh *et al.* [20]. In which SiO_2, Al_2O_3, and MgO each by 0.1 vol% to paraffin, the addition of SiO_2 resulted in a significant increase in the thermal conductivity compared to Al_2O_3 and MgO, as shown in **Figure 10(b)**.

Cao *et al*. [212]. Demonstrated an increase in thermal conductivity of PCM with the addition of CNTs, as shown in **Figure 10(c)**. The thermal conductivity of the PCM without CNTs has the lowest value of 0.1816 W/mK, and on the other hand, by adding CNTs, the thermal conductivity increased to a maximum of 0.3075 W/mK, which was 1.7 times higher than that before. Laghari *et al.* [213]. Showed the thermal conductivity of paraffin wax (PW), PW/TiO_2, and PW/TiO_2Grcomposites. The results indicated that the PCM values for the PW, PW/TiO_2-0.1, PW/TiO_2-0.5, PW/TiO_2-1.0 and PW/TiO_2-2.0 composites were 0.1958, 0.3247, 0.3632, 0.4304 and 0.3655 W/m.K, respectively. All samples displayed higher thermal conductivity values than pristine PW. This is because the thermal conductivity of TiO_2 was significantly higher than that of PW. Thus, the thermal conductivity of the composite increased as the mass ratio of TiO_2 nanoparticles increased. SDBS was added as a surfactant to enhance the thermal conductivity of the composite. thermal conductivity plays a crucial role in the enhancement of energy storage. However, it should be noted that the addition of TiO_2 at 2% decreased the thermal conductivity of PW/TiO_2-2.0, as shown in **Figure 10(d)**. This suggests that the sample is unstable owing to the agglomeration of nanoparticles, which changes the measurement region of composition and properties, and results in significantly lower thermal conductivity near the base PCM.

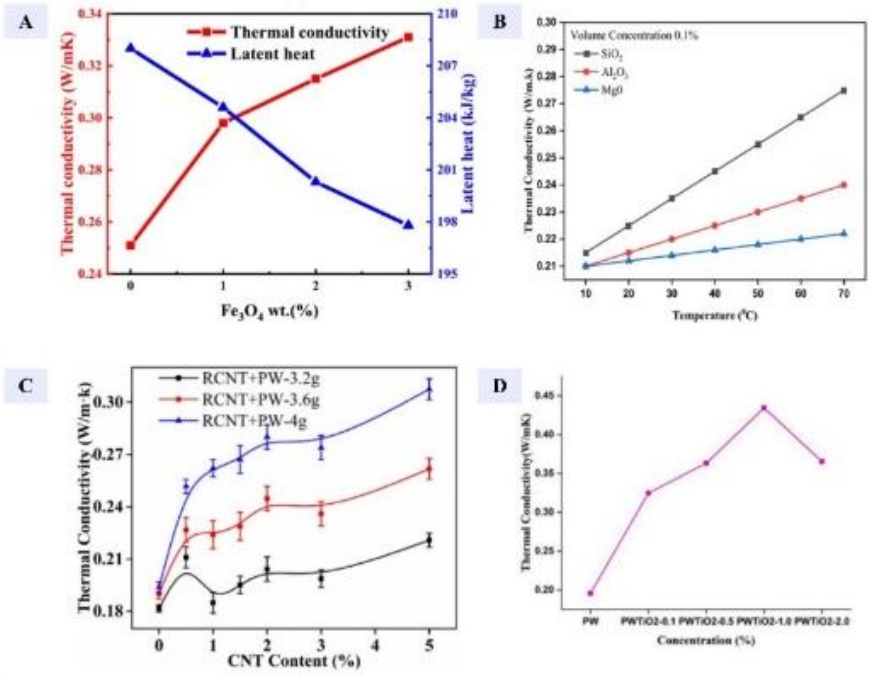

Figure 10 Thermal Conductivity Characterization Results, (a) PCM Paraffin-Fe_3O_4, reprinted with permission from Elsevier [23], (b) PCM Paraffin-SiO_2, Al_2O_3, MgO reprinted with permission from Elsevier [20], (c) PCM Paraffin Wax-CNT reprinted with permission from John Wiley and Sons [212], (d) PCM Paraffin-TiO_2 reprinted with permission from Elsevier [213].

Analysis of thermal distribution PCM

PCM for thermal energy storage in concrete require thermal distribution analysis to determine their ability to absorb and release thermal energy. Therefore, it is necessary to understand the experimental techniques for thermal distribution measurements. Several studies have been conducted using different experimental variations, as shown in **Figure 11**.

A study by Al-Yasiri and Szabó [4], investigated the thermal distribution of bricks incorporating phase change material (PCM). The researchers utilized bricks measuring 23×12×7 cm^3, with one serving as a control (A) and 7 others containing PCM capsules of various shapes and sizes (labeled B through H). The test chamber was constructed using an 80 mm thick high-density cork and covered with fiberglass for enhanced insulation. Each brick was placed in a separate compartment with thermocouples on both sides to monitor temperature differences throughout the experiment. To prevent air leakage and ensure that heat transfer occurred solely through the bricks, they were sealed with high-quality insulation foam during the installation. The experiment was conducted over 4 consecutive hot days in September, from 6:00 am on 16.09.2020 to 6:00 am on 20.09.2020. September is typically one of the hottest months in Iraq, along with July and August, and is characterized by peak solar radiation and ambient temperature levels. In addition, Qudama and Marta [25], conducted an additional investigation. They utilized an Arduino multichannel-based data logger (Mega 2560 type) for thermal distribution tests, employing T-type thermocouples to measure the temperatures of the exterior and interior surfaces of the bricks. Each brick was instrumented with 2 thermocouples, one on the outer surface and the other on the center of the inner surface. The inner sensors were inserted through small apertures in the cork frame and insulation blanket, which were subsequently sealed with foam to prevent air infiltration. The outer sensor readings were averaged to determine the outer brick surface temperature (To), whereas the inner sensors provided individual measurements for each brick (Ti). The data logger was programmed to record temperature fluctuations at 10-min intervals, continuously storing measurements throughout the diurnal cycle. Furthermore, solar radiation (SR) was manually measured at 30-min intervals during daylight hours using a solar meter.

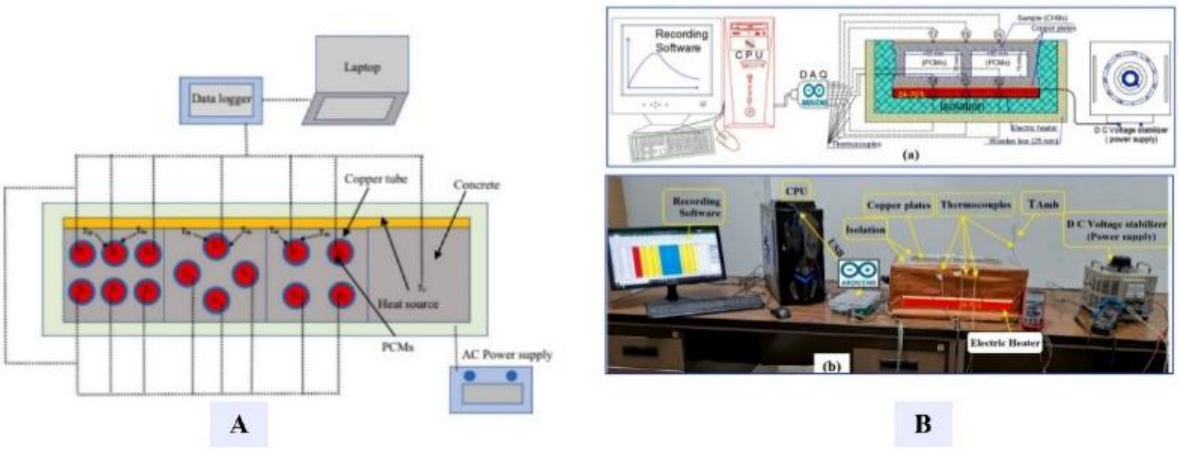

Figure 11 Experimental Thermal Distribution Testing of PCM Concrete, (a) reprinted with permission from Elsevier [26], (b) reprinted with permission from Elsevier [202].

Tetuko *et al.* [26], conducted an experimental investigation that deviated from previous research findings. They examined the temperature distribution in concrete containing Phase Change Materials (PCM) using thermocouples and data loggers. The experiment involved positioning a heater on the concrete surface connected to an AC power supply to generate a temperature of 80°C. Rockwool was used as thermal insulation to minimize heat loss. **Figure 14(c)** illustrates the experimental setup, including the configuration of concrete and copper tube formations filled with various PCM composites: paraffin-magnetite, paraffin, and PEG. Therefore, thermal distribution experiments were conducted by Heniegal *et al.* [202], using electric heaters, as depicted in **Figure 11(b)**. The experimental apparatus incorporated a heating system with a thermal electric heater, enabling heat control on the bottom surface of a 5 mm thick copper plate. This configuration

ensured heat transfer perpendicular to the specimen. The test cycle persisted for 24 h, with the initial thermal stress established to determine the appropriate heating power, not exceeding 70°C on the heated surface after approximately 6 h. Subsequently, the heating source was deactivated, and the equipment was cooled in ambient laboratory air at 24 ± 1.5°C. To minimize heat loss, the test device was enclosed in a 50 mm thick insulating thermoplastic and wooden enclosure. Temperature measurements were obtained using 9 K-type thermocouples, featuring 0.5 mm diameter welds and 1 s response times. These thermocouples were connected to a data acquisition system equipped with an Arduino Mega 2526 microcontroller, which was interfaced with a CPU to record the temperatures at the 9 points. Measurements were recorded every 0.5 s on a memory card using the Arduino Mega 2526. The acceptable error margin for experimental accuracy was ±1.5°C (±2.15%). The K value of the copper plate was subsequently utilized to calculate the heat-transfer rate and K value of the specimen.

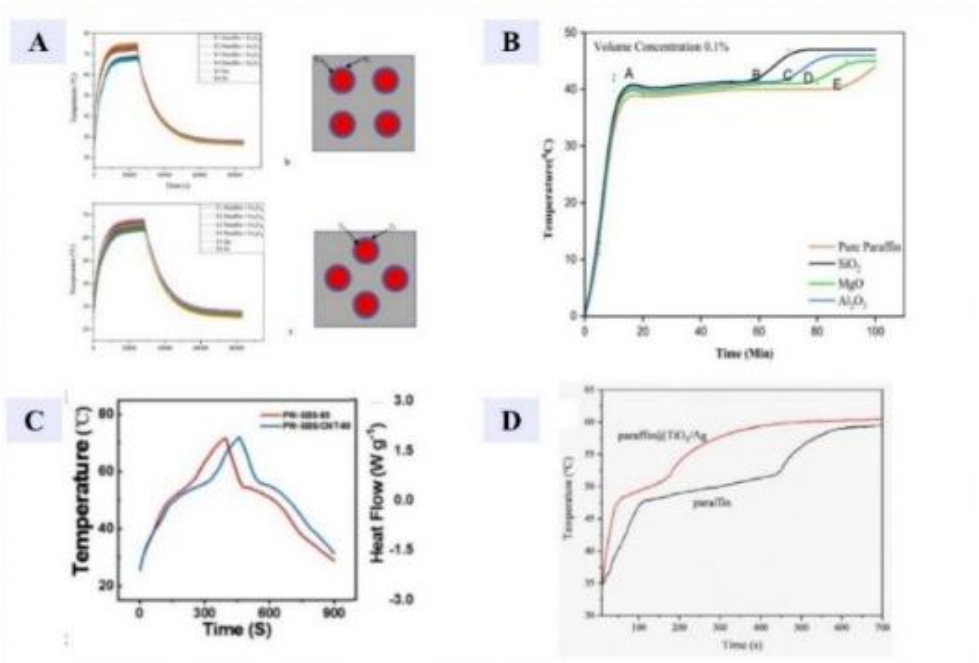

Figure 12 PCM Thermal Distribution (a) PCM Paraffin-Fe_3O_4, reprinted with permission from Elsevier [26], (b) PCM Paraffin-SiO_2, Al_2O_3, MgO, reprinted with permission from Elsevier [20], (c) PCM Paraffin Wax-CNT, reprinted with permission from Elsevier [21] (d) PCM Paraffin-TiO_2, reprinted with permission from Elsevier [214].

Figure 12 illustrates the results of the thermal distribution analysis conducted on the PCM, as reported by Tetuko *et al.* [26]. The investigation examined the temperature variations over time in concrete containing encapsulated PCM, specifically paraffin-magnetite, paraffin, and polyethylene glycol composites, as depicted in **Figure 12(a)**. This study used 4 square and 4 cross concrete designs. The graph shows the duration required for the PCM to accumulate heat during the warming phase and subsequently release it during the cooling phase. The temperature initially increased until it reached a steady state at various levels, contingent on the type of PCM. Subsequently, the heater was deactivated, causing the temperature to decrease until it matched ambient conditions. During the heating process, heat is transferred from the heater to the concrete and copper tubes via conduction, and is classified as sensible heat owing to the temperature change. Conversely, PCM undergoes a phase transition from solid to liquid (melting) without temperature alteration and is categorized as latent heat. In the cooling phase, following heater deactivation, the PCM begins to release latent heat, thereby initiating another phase change (solidification). The sample responses differed based on the capacity of the PCM to store and release heat. The heat storage ability is influenced by the heat capacitance and thermal conductivity. The low thermal conductivity of the PCM can result in high thermal

resistance, impeding heat penetration and the initiation of the melting process.

A study by Singh *et al.* [20], examined the thermal characteristics of pure paraffin under various inlet conditions, including the temperature and volume flow rate. The research demonstrated that the melting duration of paraffin is significantly influenced by the temperature, as illustrated in **Figure 12(b)**. The investigators utilized inlet temperatures of 48, 53 and 58°C, along with heat transfer fluid (HTF) flow rates of 1, 3, and 5 LMP. The findings revealed that the melting temperature of paraffin increases linearly up to 40°C with rapid sensible heat storage owing to its low specific heat capacity. As melting progressed, the temperature of the paraffin gradually increased, indicating a latent heat transfer. During this phase, the temperature increased from 41 to 44°C, with paraffin transitioning from solid to mushy solid and finally to liquid. The subsequent rapid temperature increase was attributed to the sensible heat. Melting occurred more rapidly at the top of the heat exchanger than at the bottom because conduction initially dominated the heat transfer. However, natural convection became the primary heat transfer mechanism when paraffin reached the mushy phase, causing it to rise and accumulate at the top of the heat exchanger owing to its decreased density. Increasing the HTF temperature accelerated the paraffin-filling rate, while increasing the HTF flow had a minimal impact on the filling rate because of the small cylinder size of the heat exchanger. The study found that increasing the inlet temperature from 48 to 53°C increased the melting rate by 76.1%, while a further increase from 53 to 58°C resulted in an 85.5% increase. They concluded that the HTF inlet temperature significantly affected the thermal performance of the base paraffin.

Hu *et al.* [21], investigated the temperature-time curves during heating and cooling of PW-SBS/CNT-85 and PW-SBS-85 samples, as illustrated in **Figure 12(c)**. Two temperature plateaus are observed, corresponding to PW melting and crystal transitions. The flexible phase change composites containing CNTs exhibited an accelerated heating rate and a prolonged melting process as the ambient temperature increased. PW-SBS/CNT-85 reached 48°C in 135 s, followed by a gradual increase to 56°C at 320 s. The phase transition plateau persisted for approximately 185 s, which is 1.5 times longer than that of PW-SBS-85. This phenomenon can be partially attributed to the presence of highly thermally conductive CNTs in the composite matrix, which enhanced the overall thermal conductivity and phase-change performance.

Su *et al.* [214], presented the time-temperature relationship curves for pure paraffin and paraffin@TiO_2/Ag microcapsules in **Figure 12(d)**. Both samples demonstrated a rapid temperature increase to approximately 48°C upon light exposure, with paraffin@TiO_2/Ag microcapsules exhibiting a faster heating rate owing to their higher thermal conductivities. At 48 °C, both samples displayed a slow temperature increase for a certain period, indicating that paraffin@TiO_2/Ag exhibited a latent thermal effect similar to that of paraffin. After 700 s of light exposure under identical conditions, the final temperature of the paraffin@TiO_2/Ag microcapsules exceeded that of the paraffin. These findings demonstrate the superior temperature regulation and photothermal conversion capabilities of paraffin@TiO_2/Ag microcapsules. TiO_2 is frequently employed in architectural coating materials because of its versatility, particularly its exceptional photocatalytic properties. Therefore, based on some explanations of previous research, it can be concluded that the PCM encapsulation method with concrete media has a wide enough variation, from the results of the concrete damal thermal energy storage test as shown in **Figure 12**. PCM is able to absorb heat and release heat.

Analysis of differential scanning calorimetry (DSC)

DSC characterisation was conducted to assess the heat-flow performance of the PCM. This involves examining the phase changes within the PCM, specifically during endothermic and exothermic processes, as well as determining the peak temperature of the melting and solidification process, the latent heat value required, and the glassy-rubbery transition temperature of the PCM material.

Extensive research has been conducted on the DSC characterization of PCM, with studies such as those by Lu *et al.* [73]. being frequently cited. **Figure 13(a)** illustrates the DSC curves for pure paraffin, paraffin/nano-Fe_3O_4, and PCM composite stability cycles during melting and solidification. The composite PCM exhibited 2 distinct phase-change peaks in its melting and solidification curves. The initial, less

prominent peak represents the solid-solid phase change of the composite PCM with a lower latent heat, whereas the subsequent, more pronounced peak corresponds to the liquid-solid phase change with a higher latent heat. The DSC curves for both pure paraffin and the composite PCM demonstrated minimal differences after 200 cycles, with any slight variations potentially attributable to experimental and crucible errors. Furthermore, **Figure 13** indicates that as the percentage of F Fe_3O_4 by weight increases, the required latent heat decreases. This observation suggests that incorporating a higher proportion of Fe_3O_4 into the PCM enhances the phase-change mobility by reducing the energy required for the process.

Hu *et al.* [21], conducted a study that revealed the melting temperature (Tm) of pure PW to be 61.55°C, with a melting enthalpy (ΔHm) of 200.01 kJ/kg. They also determined the crystallization temperature (Tc) of pristine PW to be 51.72°C, with a freezing enthalpy (ΔHc) of 192.88 kJ/kg, as shown in **Figure 13(b)**. Differential scanning calorimetry (DSC) curves for PW-SBS composites and PW-SBS/CNT composites with various PW concentrations exhibit 2 transitions similar to those of pure PW, indicating that the PW crystallization process remains unaltered. This suggests that no chemical reactions occurred during the incorporation of PW into the 3-dimensional SBS/CNT network. In the DSC images, as PW loading decreased, the melting and crystallization peak positions shifted to higher and lower temperatures, respectively. This phenomenon can be attributed to the crystallization mechanism of the charged PW within the SBS/CNT network, where narrower peaks indicate higher crystalline compound purity. It is noteworthy that the peak appears broad and low owing to the extended melting range and wider peak of the polymer material, resulting in a more expansive peak overall.

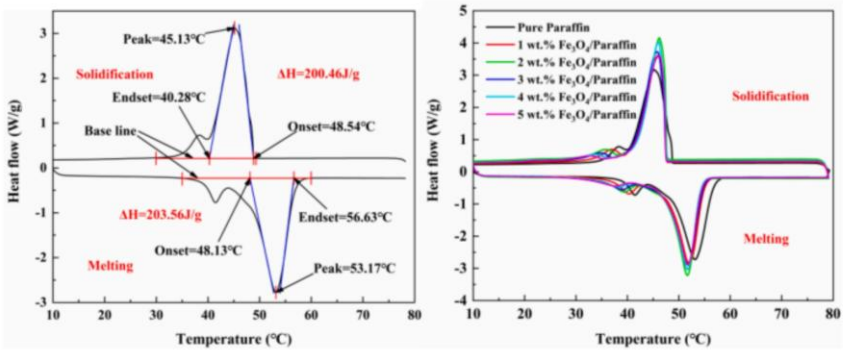

A

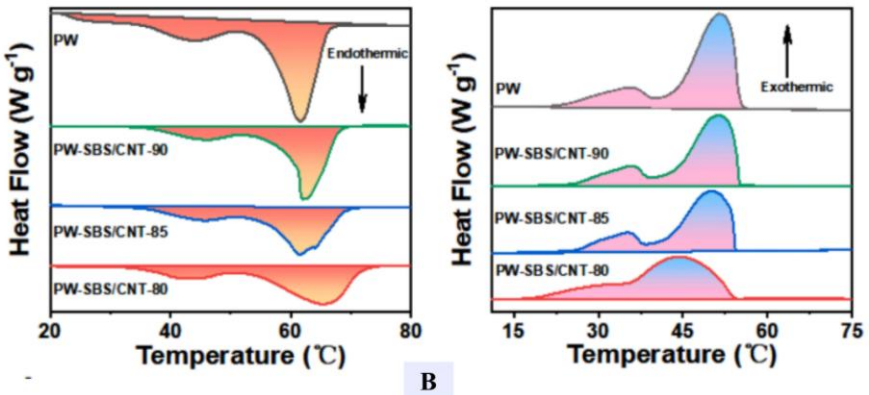

B

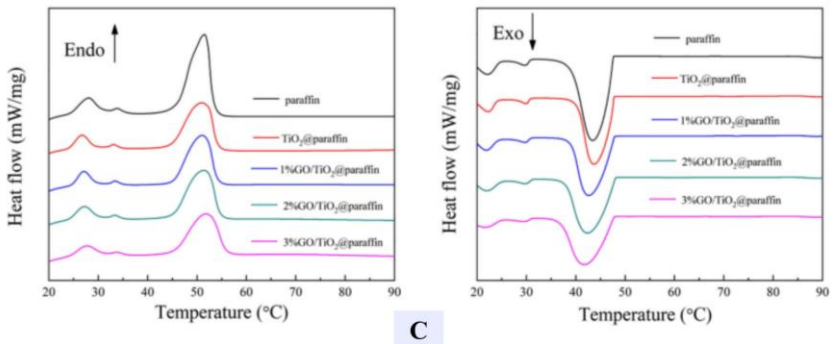

C

Figure 13 DSC Characterization Results (a) reprinted with permission from Elsevier [73], (b) reprinted with permission from Elsevier [21], (c) reprinted with permission from Elsevier [215].

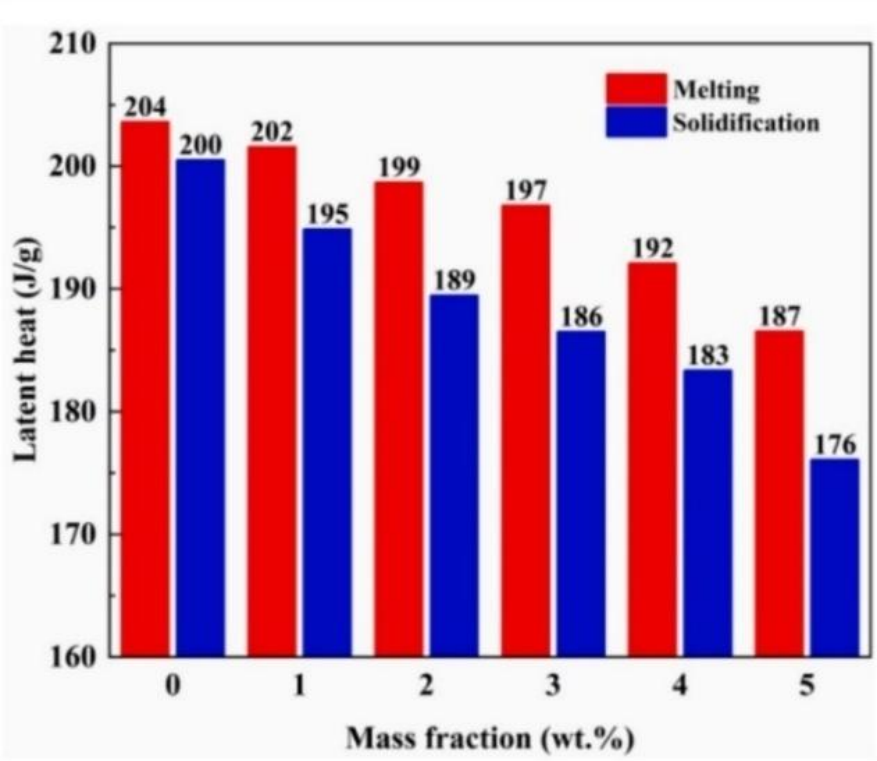

Figure 14 Paraffin-Fe_3O_4 latent heat test results, reprinted with permission from Elsevier [73].

Ji *et al.* [215], examined the Differential Scanning Calorimetry (DSC) curves of paraffin, TiO_2@paraffin, and GO/TiO_2@paraffin microcapsule phase transition materials. **Figure 13(c)** demonstrates that the thermal characteristics of these substances, including the phase transition temperature during melting and crystallization, latent heat, and encapsulation efficiency (R and E) of microencapsulated Phase Change Materials (PCM), are critical factors in determining their application and efficacy. Encapsulation rate (R) and efficiency (E) are 2 key technical indicators that quantify the effectiveness of the shell material in encapsulating the PCM core and its potential heat storage/release efficiency. The investigation revealed that the TiO_2@paraffin and GO/TiO_2@paraffin microcapsules predominantly retained the thermal behavior of paraffin during melting and crystallization. The DSC curves exhibited 2 distinct exothermic/endothermic peaks, which can be attributed to the solid-liquid phase transition heat absorption/release of straight-chain alkanes and a minor portion of branched alkanes or monocyclic cycloalkanes. The primary mechanism for PCM materials is the solid-liquid phase transition behavior of paraffin. **Table 17** indicates that paraffin's melting and crystallization temperatures are 51.53 and 43.24°C, respectively, with corresponding phase change enthalpies of 196.16 and 190.25 kJ/kg. GO/TiO_2@paraffin microcapsules exhibit a phase transition temperature comparable to that of paraffin, thus preserving the physical properties of paraffin. The phase change enthalpies for melting and crystallization are 159.62 and 156.35 kJ/kg, respectively, with an encapsulation rate of 81.37%, ensuring the practical applicability of these phase-transition heat-storage material microcapsules. For the GO/TiO_2@paraffin microcapsules, while the phase transition temperature remained close to that of paraffin, both the melting and crystallization enthalpies were reduced to varying degrees. The phase change enthalpy rates for the GO/TiO_2@paraffin microcapsules can be enhanced to 78.32, 81.95 and 75.69% with the addition of 1, 2 and 3% GO, respectively.

Table 17 DSC Characterization results of GO/TiO_2@paraffin [215].

Sample	Tm (°C)	Tc (°C)	ΔHm (kJ/kg)	ΔHc (kJ/kg)
Paraffin	51.53	43.24	196.16	190.25
TiO_2@paraffin	50.97	43.54	159.62	156.35
1%GO/TiO_2@paraffin	51.06	42.68	153.66	149.76
2%GO/TiO_2@paraffin	51.30	41.91	160.75	146.86
3%GO/TiO_2@paraffin	51.70	41.52	148.46	145.32

Analysis of thermogravimetric analysis (TGA)

Thermogravimetric analysis (TGA), a widely employed technique in mass thermal decomposition studies, allows the investigation of substance pyrolysis under diverse heating conditions and rates. As a method of thermal analysis, TGA enables the simultaneous measurement of temperature, time, and sample mass in a controlled environment [216]. The measurement of the sample weight change resulting from the thermal treatment forms the basis of these measurements. TGA allows the determination of the temperature at which the PCM material decomposes through the measurement of volatiles or decomposition-related weight loss, which is crucial for assessing the compatibility of the PCM material [216]. The outcome of the TGA research on PCM is illustrated in **Figure 15**.

Almousa *et al.* [217], conducted research on the addition of nanoparticles to paraffin wax (PW) with varying concentrations: 0.5% (PW1-CNT), 0.75% (PW-2CNT), and 1% (PW-3CNT) mass units. The study utilized Thermogravimetric analysis (TGA) was performed using a Discovery SDT 650 thermobalance from TA Instruments with an alumina crucible under nitrogen flow (100 mL/min) and a heating rate of 10 °C/min. TGA results revealed a significant mass reduction due to paraffin degradation, while also demonstrating paraffin impregnation and the high thermal stability of carbon nanotubes (CNT). The observed mass loss curve confirmed the effective dispersion of CNT within paraffin wax. CNT exhibit resistance to thermal degradation during the decomposition of paraffin wax nanocomposites. The introduction of CNT particles resulted in a gradual shift in the thermal decomposition of the Paraffin Wax nanocomposites towards slightly higher temperatures as the CNT concentration increased. Nevertheless, all nanocomposites underwent rapid degradation at approximately 210°C owing to PW breakdown, with each composite experiencing varying degrees of weight loss upon CNT addition.

Tian *et al.* [218], conducted thermogravimetric analysis (TGA) to investigate the thermal stability of n-eicosan@Fe_3O_4/$CaCO_3$ composite microcapsules, utilizing pure n-eicosan as a control. **Figure 15(a)** illustrates the resulting TGA thermogram. The analysis revealed that pure n-eicosan exhibited a characteristic single-step thermal degradation process between 130 and 265°C, resulting in no residual char owing to complete thermal evaporation. Similarly, all the microcapsule samples demonstrated one-step degradation. Upon heating to 500°C, microcapsules prepared with 0.0, 5.0, 10.0, 15.0, 20.0 and 25.0 mL of Fe_3O_4 suspension produced char residues of 52.1, 55.0, 50.3, 48.2, 47.2 and 49.4 wt.%, respectively. These residues, comprising a non-degradable $CaCO_3$ shell material and Fe_3O_4/$CaCO_3$ composite shell material, appear to correlate with the phase change enthalpy. The composite microcapsules exhibited a slight increase in the characteristic temperature at the maximum mass loss rate (Tmax), which was associated with the rapid evaporation of n-eicosan upon reaching a specific temperature. While pure n-eicosan demonstrated a Tmax of 245.3°C, the composite microcapsules produced with 0.0, 5.0, 10.0, 15.0, 20.0 and 25.0 mL of Fe_3O_4 suspension exhibited Tmax values of 250.9, 253.6, 250.8, 252.3, 255.5 and 259.4°C, respectively. The observed increase in Tmax can be attributed to the presence of $CaCO_3$ or Fe_3O_4/$CaCO_3$ shells.

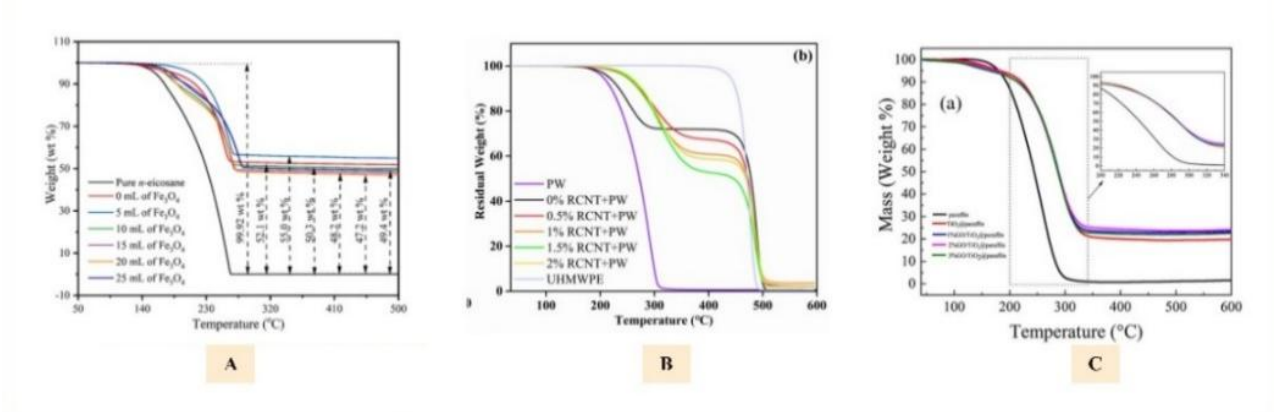

Figure 15 TGA Characterization Results (a) reprinted with permission from Elsevier [218], (b) reprinted with permission from Elsevier [212], (c) reprinted with permission from Elsevier [215].

According to Cao *et al.* [212], the Thermogravimetric Analysis (TGA) curve results for paraffin wax (PW) and composite phase-change material (CPCM) exhibited 2 distinct degradation phases. The initial degradation stage occurred between 200 and 360°C, which was attributed to PW's thermal decomposition of PW, as illustrated in **Figure 15(b)**. The subsequent degradation phase transpired between 460 and 510°C, resulting from the thermal decomposition of ultra high molecular weight polyethylene (UHMWPE). The CPCM only experienced mass loss at temperatures exceeding 200°C, demonstrating its superior thermal stability within its operational temperature range.

Ji *et al.* [215], investigated the thermal stability of TiO_2@paraffin microcapsules combined with GO. They examined the impact of high thermal conductivity on the thermal stability of PCM microcapsules using TGA, as illustrated in **Figure 15(c)**. This study demonstrated that paraffin underwent a single-step decomposition, with its peak decomposition rate occurring at 260.2°C and a mass loss of 99.38% at 400°C post-decomposition. In contrast, the TiO_2@paraffin microcapsules underwent a 2-stage decomposition process. The 1st stage's maximum decomposition rate was observed at 173.6°C, while the 2nd stage peaked at 289.2°C. Compared with pure paraffin, the TiO_2@paraffin microcapsules exhibited a 29°C increase in the temperature of the maximum decomposition rate and a mass loss of 74.92% at 400°C post-decomposition. This indicates that the TiO_2 shell enhances the decomposition temperature of paraffin and the operating temperature of the microcapsules. GO-modified microcapsules exhibited characteristics similar to those of TiO_2@paraffin microcapsules. The 2nd-stage decomposition rates for the GO/TiO_2@paraffin microcapsules with 1, 2, and 3% GO loadings were comparable, occurring at 289.1, 284.9 and 286.8°C, respectively. These temperatures represent increases of 28.9, 24.7 and 26.6°C compared to pure paraffin. The mass losses after decomposition at 400 °C were 71.76, 74.60 and 73.12%, respectively. This suggests that while the TiO_2 shell and GO remained intact after heating, paraffin was almost entirely degraded. The higher maximum degradation temperature of the microcapsule samples compared to pure paraffin indicates that the TiO_2 shell modified with GO enhances the thermal stability by inhibiting the thermal degradation of the encapsulated paraffin. Moreover, as the GO content in the microcapsules increased, the residual carbon in the TiO_2 shell also increased at the conclusion of the measurement.

Characterization of physical stability

One of the indicators to determine the ability of a PCM is to examine its physical stability, for which Scanning Electron Microscopy (SEM) and X-Ray Diffraction (XRD) characterisation can be carried out.

Analysis of scanning electron microscopy (SEM)

SEM can be used to obtain information regarding the visual appearance of the morphology and particle size of a specimen. Therefore, it is important to apply this analysis to PCM to determine their physical stability. Many previous studies have been conducted related to the SEM analysis of PCM, as presented in

Figure 19. SEM Characterization Results (a) Paraffin/SBS-CNT, (b) Paraffin-Fe_3O_4, (c) GO/TiO_2@Paraffin.

Hu *et al.* [21]. Investigated the synthetic route of the flexible phase-change composite material with a cross-linking network (PW-SBS/CNT) is shown in **Figure 16(a)**. The SBS flexible polymer matrix was combined with PW, followed by the incorporation of CNT to establish a durable and pliable 3-dimensional structure. The π-bond configuration of SBS and CNT facilitates the creation of a cross-linked network through the addition of chemical cross-linking agents. Sulfur, a commonly used cross-linking agent for SBS, was introduced into the mixture to facilitate the construction of a 3-dimensional network. Functioning as a bridge, sulfur connects the SBS molecules and links CNT with SBS. The extensive π-bond structure of CNT and the unsaturated nature of SBS provide numerous active sites for these connecting bridges. This chemical cross-linking process, which establishes chemical bonds between carbon nanotubes and the SBS matrix, enhances the interface contact between the matrix and PW while reducing the interfacial resistance of CNT, thereby improving CNT dispersion uniformity. This effectively addresses the issue of uneven CNT distribution and allows CNT to fully contribute to the toughness and heat conduction. Compared to conventional SBS networks, our SBS/CNT-reinforced network enhanced the PW encapsulation efficiency and significantly improved the heat storage performance of the composite phase change. Notably, the π–π interactions between CNT and SBS also play a crucial role in constructing flexible 3D toughened networks. The uniform distribution of PW within the CNT and the flexible SBS network contributed to the high PW encapsulation rate and elevated latent heat value of the composite material. Furthermore, as the PW ratio increased, the fibrous network structure at the fracture surface of the composite decreased, consistent with the mechanical strength observations of PW-SBS/CNT.

He *et al.* [23], revealed that the SEM characterization images of solid CTAB, PW, and phase-change nanocomposites in **Figure 16(b)** demonstrate a granular distribution of the CTAB surfactant. The PW microstructure exhibited an irregular block-like overlap, whereas the Fe_3O_4 nanoparticles were uniformly distributed throughout the PW. Notably, the nanoparticles were homogeneously embedded within the PW inner layer, which positively influenced the thermal performance. Ji *et al.* [215], examined the surface morphology and microstructure of microcapsules, as shown in **Figure 16(c)**. The micrographs clearly illustrate that the GO/TiO_2@paraffin microcapsules possess a compact core-shell structure with uniform spherical particles, averaging 2 - 4 μm in size, and featuring a smooth shell surface. This structure effectively prevents molten paraffin leakage during the phase transitions and can withstand the volume changes caused by these transitions. Notably, an inorganic TiO_2 shell can significantly enhance the low thermal conductivity of paraffin. Upon the addition of varying proportions of GO, the nanosheets were incorporated onto the surface of the microcapsules. TiO_2 flakes produced during hydrolysis and condensation were adsorbed onto the surface of the microcapsules, leading to aggregation of the microspheres. The self-assembled GO nanosheets on the microcapsules exhibited a transparent ultrathin layered structure with visible wrinkles and ripples. This ultrathin flake structure may enhance the thermodynamic stability of the 2-dimensional GO nanosheets. SEM images reveal that the core-shell microstructure of GO/TiO_2@paraffin microcapsules has a thickness of approximately 0.2 μm. Although the wall thickness of the microcapsules with different components varied slightly, the overall shell thickness remained uniform. The higher GO content in the microcapsules corresponds to a thicker TiO_2 shell, with increases of up to 50 nm. The core-shell structure is evident, with the darker TiO_2 shell encapsulating the lighter-colored paraffin core. The regular geometry observed represents a small portion of the unencapsulated paraffin crystal, confirming the typical core-shell structure of the synthesized microcapsules. The microcapsules appeared as spherical particles with diameters ranging from to 2 - 4 μm.

Analysis of X-ray diffraction (XRD)

X-Ray Diffraction (XRD) is a technique employed to elucidate the atomic and molecular arrangements of crystals by scattering X-rays in various directions. The primary purpose of XRD is to identify and examine material phases, whether in powder or solid form, in inorganic samples that are polycrystalline or

amorphous. XRD can be used for both qualitative and quantitative assessment. Quantitative analysis yielded data in the form of 2 diffractograms, showing peak intensity and lattice constant magnitude. Qualitative analysis provides phase analysis information, including phase type identification, phase composition percentages, crystallite dimensions, and orientation.

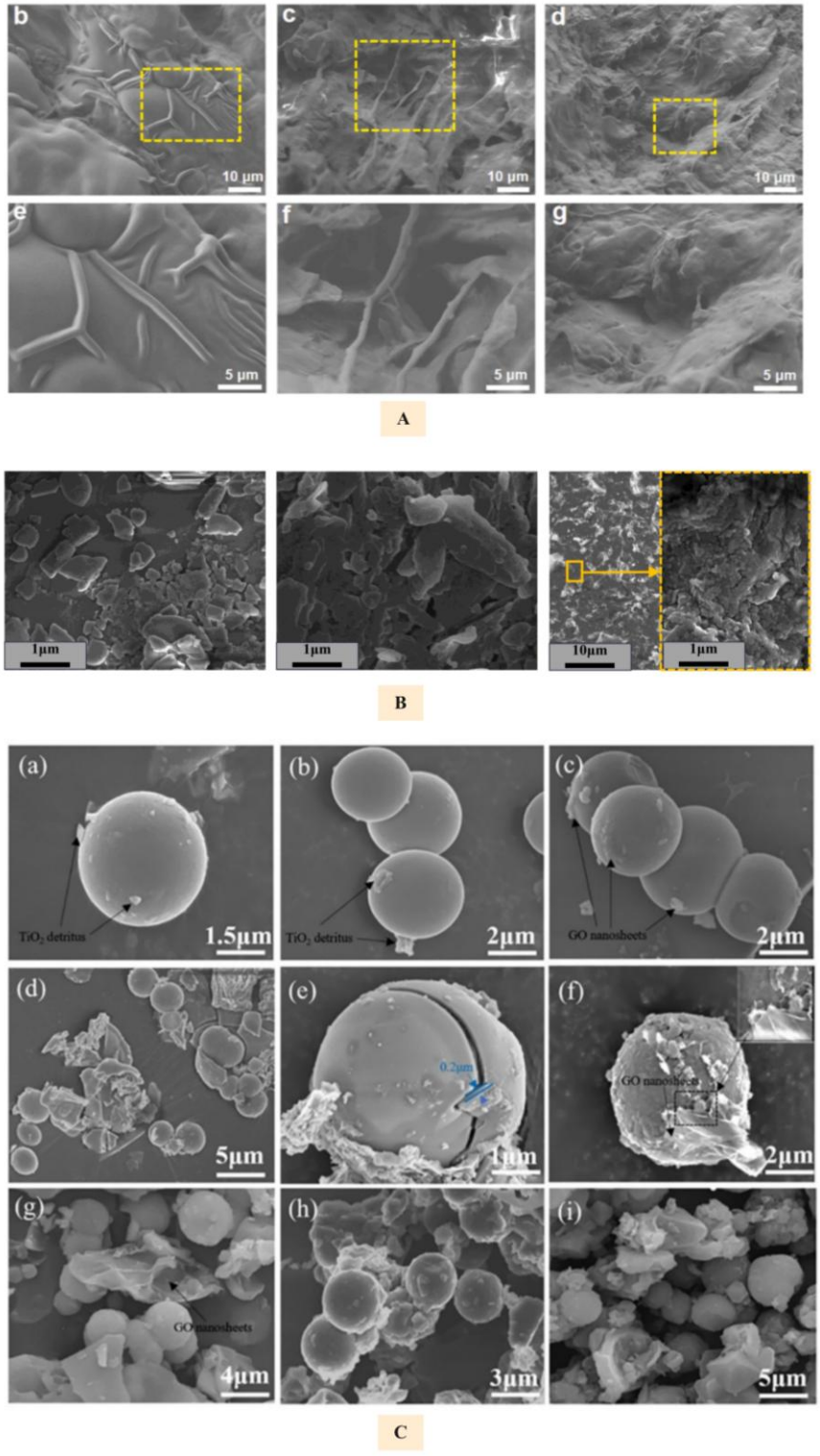

Figure 16 SEM Characterization Results (a) Paraffin/SBS-CNT, reprinted with permission from Elsevier [21], (b) Paraffin-Fe_3O_4, reprinted with permission from Elsevier [23], (c) GO/TiO_2@Paraffin, reprinted with permission from Elsevier [215].

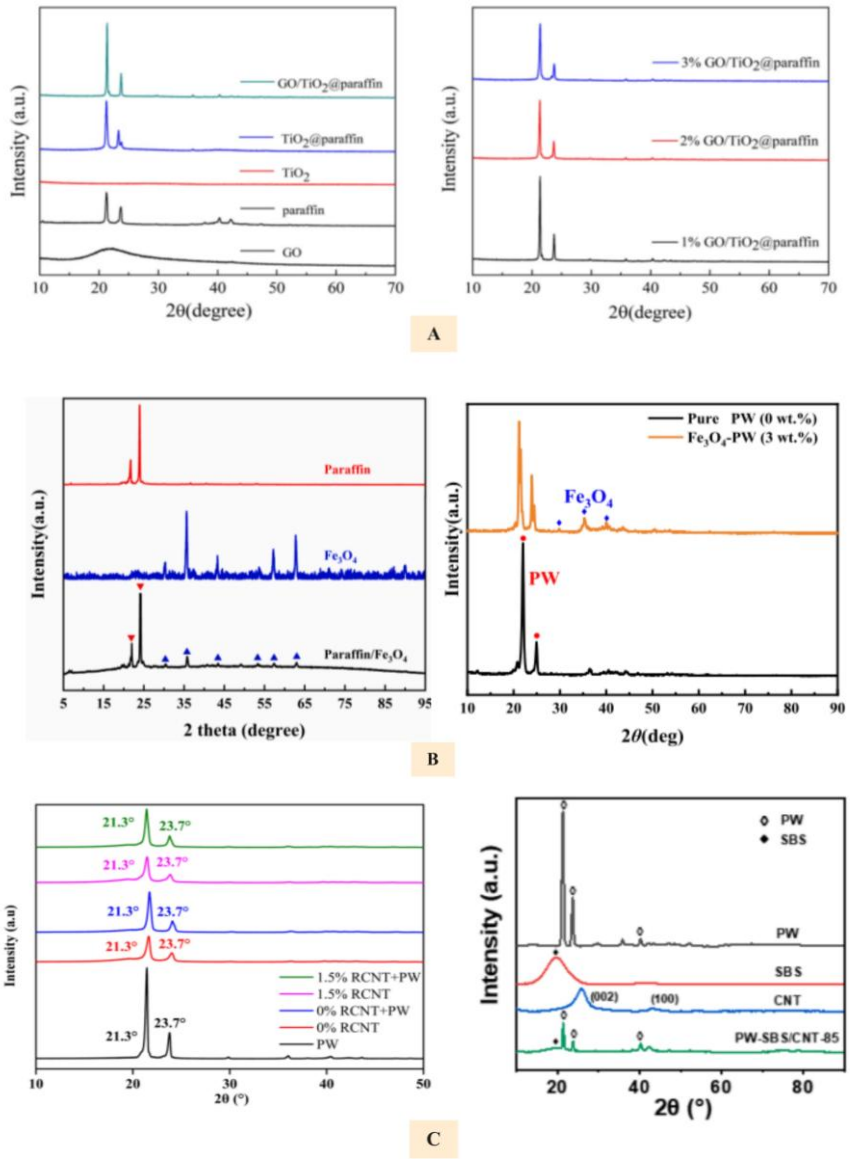

Figure 17 XRD Characterization Results (a) reprinted with permission from Elsevier [215], (b) reprinted with permission from Elsevier [23,73], (c) reprinted with permission from John Wiley and Sons [212].

XRD characterization is crucial for PCM composites. Numerous previous studies have conducted XRD analysis, as shown in **Figure 17**. Ji *et al*. [215], characterized the phase and crystal structures of paraffin, TiO_2@paraffin, and GO/TiO_2@paraffin microcapsules using XRD spectra, as depicted in **Figure 17(a)**. The XRD curve exhibited 2 prominent diffraction peaks at 21.48° and 23.86°, corresponding to the (110) and (200) planes, respectively, indicating that the microcapsules maintained the peak absorption of paraffin. A single non-typical absorption peak of TiO_2 appears at approximately 25.52°, demonstrating amorphous properties, whereas a small peak at approximately 21.76° represents a characteristic GO peak. The absorption peaks of GO/Microcapsule TiO_2@paraffin aligned with those of paraffin, suggesting that the GO-modified microcapsule sample retained the main features of paraffin. The primary absorption peaks of the modified microcapsules decreased slightly with increasing GO content. The absence of a sharp GO absorption peak in the XRD spectrum may be attributed to its low content, which makes it difficult to clearly observe. From a structural perspective, the XRD images demonstrated that TiO_2, paraffin, and GO were mechanically mixed without any new substances being synthesized during microencapsulation and self-assembly.

In a separate study by Lu *et al.* [73], XRD was employed to characterize the crystal structures of the pristine paraffin, nano-Fe_3O_4, and PCM composites, and the results are shown in **Figure 17(b)**. The diffraction peaks of the composite PCM align well with those of pristine paraffin and nano-Fe_3O_4, indicating that the composite PCM preparation is a physical process without the formation of new substances. Additionally, the Scherrer equation was used to estimate the average nano-Fe_3O_4 particle size at 26.53 nm. He *et al.* [23] presented X-ray diffraction results in **Figure 17(b)**. The diffraction peaks resulting from the Fe_3O_4 addition correspond to those of PW and Fe_3O_4, with no peak shifts observed. The emergence of new peaks confirms that only physical interactions occur between PW and Fe_3O_4.

Cao *et al.* [212], presented X-ray diffraction (XRD) patterns for paraffin wax (PW), a porous matrix, and a composite phase change material (CPCM), as illustrated in **Figure 17(c)**. The patterns demonstrate that PW, porous matrix, and CPCM exhibit 2 distinct reflection peaks at $2\theta = 21.3°$ and 23.7°, which are indicative of the orthonormal crystal structures in the (110) and (200) base planes of ultra-high molecular weight polyethylene (UHMWPE) and PW.12,35 The CPCM and porous matrix exhibit broader diffraction peaks than PW. This phenomenon can be attributed to 2 factors: Firstly, carbon nanotubes (CNT) function as effective nucleation sites, facilitating UHMWPE crystallization 36 and the combined crystallization of PW with UHMWPE in CPCM.37 Secondly, CNTs influence crystallization through the formation of "C H...π" bonding interactions with PW.38 The peaks of both PW and CPCM are more pronounced than those of the porous matrix, due to PW's higher crystalline content compared to UHMWPE and its more organized structure. In a related study, He *et al.* [23] examined the XRD patterns of PW, styrene-butadiene-styrene (SBS), CNT, and their composites. Their findings indicated that PW exhibited 2 strong, sharp diffraction peaks at 21.3° and 23.6°. SBS displayed a broad peak at 19.6°, corresponding to its polycrystalline structure. The CNT exhibited diffraction peaks at 25.8° and 43.2°, originating from the (002) and (100) lattice planes, respectively. In the PW-SBS/CNT composite material, all the individual component peaks were present without significant positional shifts, although their intensities were notably reduced. This observation suggests that the compounding process does not alter the properties of each component. As anticipated, the sample containing 90 wt.% PW exhibited the highest diffraction peak because the peak intensity was largely dependent on the PW content. The 3 samples demonstrated similar diffraction peaks with varying intensities, indicating that composites with different PW loadings maintained the same chemical structure, and increased PW loading did not affect the integration of the SBS/CNT and PW flexible networks.

Characterization of chemical stability

Another analysis of PCM can be done by measuring chemical stability to determine the performance of PCM materials in order to obtain optimum data in the form of Fourier Transform Infrared Spectroscopy (FTIR) characterisation.

Analysis of Fourier transform infrared spectroscopy (FTIR)

FTIR was performed to analyse and measure the absorbed IR and to identify the surface molecular composition, structural and geometric isomers, orientation in polymers and solutions, and measurement of impurities. Therefore, this characterisation is important for PCM analysis. **Figure 18** summarises previous research on the FTIR characterisation results. George *et al.* [219], performed FTIR analysis on PW. The FTIR spectra for each cycle are shown in **Figure 18** (a). A comparison between the initial and 3,000th thermal cycles of the PW is plotted. From the FTIR analysis, it is clear that the peak at 1,740 cm^{-1} started to appear at 500 cycles and above. In the case of sample, the peak at 1,740 cm^{-1} starts to appear at 1,000 cycles. This can be attributed to the scorching of the sample due to prolonged heating and freezing cycles and the formation of C=C or the presence of impurities. In contrast, Ting [220], performed FTIR analysis of Fe_3O_4 which shows the FTIR spectrum of iron oxide displays a strong characteristic peak in the low frequency region (1,000 - 500 cm^{-1}). This occurs due to the presence of a metal-oxygen framework (Fe-O bond in the Fe_3O_4 crystal lattice). This finding is consistent with the spectrum of magnetite (Fe_3O_4) (band between 570 and 580 cm^{-1}), and the characteristic Fe-O band at 580 cm^{-1} as indicative of Fe_3O_4.

Hu *et al.* [21], reported FTIR findings for Paraffin Wax (PW) and CNT materials. The absorbance peaks around 2,921, 2,847 and 721 cm^{-1} were attributed to the asymmetric stretching vibration-CH_2, symmetric stretching vibration-CH_2, and vibrational vibration-CH_2, respectively. The 1,470 cm^{-1} peak in the PW spectrum corresponds to the -CH_2 bond. The composite exhibited peaks from SBS, PW, and CNT, confirming the successful combination without altering PW's chemical structure of PW. Moreover, the consistent infrared peaks of PW indicated its structural stability within the composite, as shown in **Figure 18(b)**. Ji *et al.* [215], findings are presented in **Figure 18(c)** show the FTIR spectra of the composite materials prepared from the TiO paraffin and GO/TiO_2@ paraffin microcapsules. The peak at 2,957 cm^{-1} can be attributed to C\\H stretching vibrations in methyl paraffin, while the 2 strong absorption peaks at 2,917 and 2,849 cm^{-1} are attributed to alkyl C\\H pull sub vibrations of methylene.

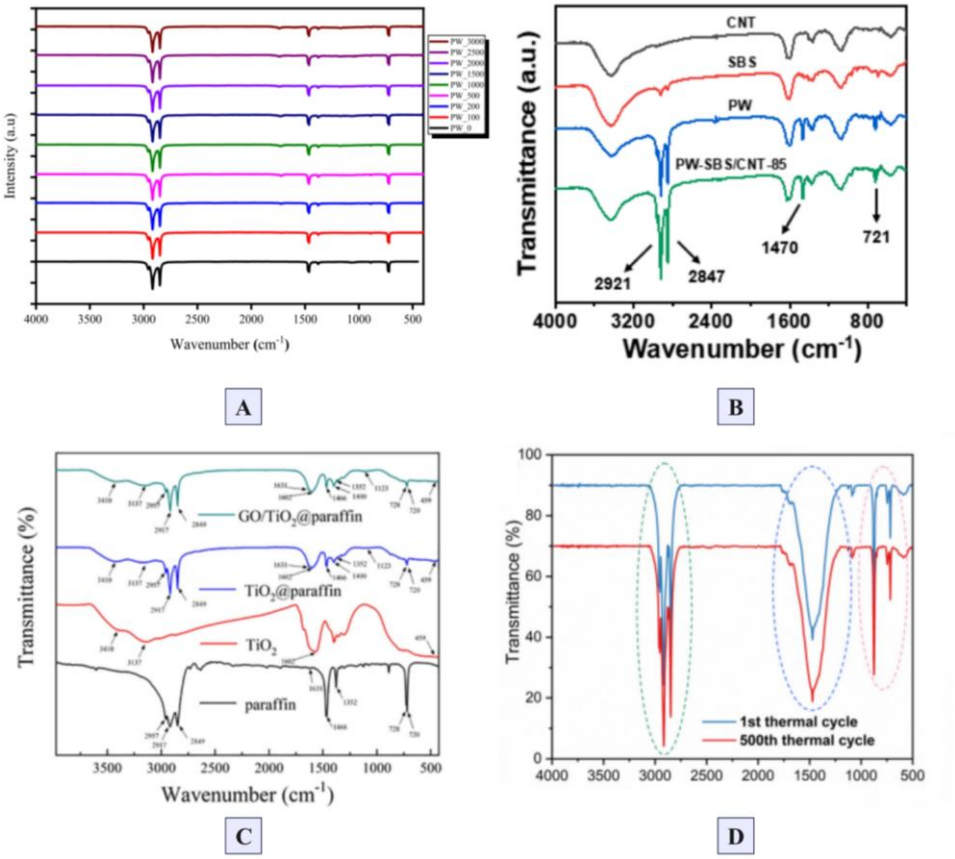

Figure 18 FTIR Characterization Results (a) PW, reprinted with permission from Elsevier [219], (b) PW-CNT/SBS, reprinted with permission from Elsevier [21] (c) GO/TiO_2@paraffin, reprinted with permission from Elsevier [215], (d) $CaCO_3$/Fe_3O_4@n-docosane, reprinted with permission from Elsevier [221].

The FTIR spectra depicted in **Figure 18(c)** reveal several significant peaks. The vibrations at 1,631, 1,466 and 1,352 cm^{-1} correspond to -CH_3 and -CH_2 deformations, respectively, while those at 728 and 720 cm^{-1} represent in-plane methylene vibrations. Amorphous TiO_2 exhibited primary stretching absorptions at 3,137 and 459 cm^{-1}. Both the regular and modified microcapsules displayed these major peaks, indicating the presence of TiO_2. The broad band near 3,410 cm^{-1} in the far-infrared region and the absorption around 1,602 cm^{-1} in the near-infrared region were attributed to -OH stretching vibrations in H_2O, which is the hydrolysis condensation precursor of TBT. TiO_2 formation occurred via precursor condensation. These peaks confirmed the presence of TiO_2 in the microcapsules and aligned with the theoretical reaction characteristics. The GO-modified microcapsules primarily exhibited overlapping paraffin and TiO_2

absorption peaks, maintaining peak consistency. This suggests that the microcapsule composite material comprised paraffin, TiO_2, and GO, with no additional impurities detected. Increasing graphene oxide content did not significantly alter the main absorption peaks of the modified microcapsules, indicating the high stability of the microencapsulation process. The absorption peaks at 1,400 and 1,123 cm^{-1} likely resulted from C=O stretching vibrations in formamide. From a structural perspective, the FTIR results demonstrated that TiO_2, paraffin, and GO were mechanically mixed without the formation of any new compounds [215].

Liu *et al.* [221], evaluated the chemical structure and morphology stability of $CaCO_3$/Fe_3O_4@n-docosane microcapsules after 500 thermal cycles using FTIR spectroscopy. The resulting spectra, presented in **Figure 18(d)**, reveal nearly identical thermal degradation profiles before and after cycling. This consistency indicated that the chemical structure of the microcapsules remained unchanged throughout the thermal cycling experiment. These findings demonstrate that the developed $CaCO_3$/Fe_3O_4@n-docosane microcapsules possess excellent phase change reliability and thermal cycling stability, rendering them suitable for practical solar photothermal energy storage applications.

Conclusions

Phase change materials (PCM) have been widely explored for thermal energy storage (TES), particularly in building applications through their integration with concrete. This is primarily due to their ability to absorb and release significant amounts of thermal energy within a specific phase-change temperature range, thus contributing to thermal load management, indoor temperature stabilization, and reduction of peak energy demand in buildings. This review presents a comprehensive analysis encompassing PCM classifications, strategies for enhancing thermal conductivity, TES applications, and detailed material characterizations including thermal properties, physical stability, and chemical stability. The key findings of this review are summarized as follows:

Classification of PCM: PCM are broadly categorized into 3 types based on their chemical composition: organic, inorganic, and eutectic. According to Scopus-indexed data, organic PCM dominate the market, comprising approximately 81% of usage, while inorganic and eutectic PCM account for 15 and 14%, respectively. PCM performance is typically evaluated based on 5 key criteria: physical, kinetic, chemical, economic, and environmental properties.

Organic PCM: Organic PCM are subdivided into paraffin-based and non-paraffin-based types. Paraffin-based PCM exhibit a latent heat range of 142 - 374 kJ/kg, a thermal conductivity between 0.2 - 0.8 W/m.K, and a melting temperature range of 7.8 - 154 °C. In contrast, non-paraffin organic PCM possess a latent heat range of 146 - 242 kJ/kg and a melting temperature range of 16.7 - 102 °C. The variation in thermophysical properties between the two is attributed to differences in atomic bonding structures.

Paraffin-based PCM Performance: Several studies indicate that paraffin-based PCM meet the required thermophysical parameters for TES applications, with latent heat values ranging from 132 - 189 kJ/kg, melting temperatures between 27 - 59 °C, and thermal conductivity ranging from 0.29 - 4.9 W/m.K.

Inorganic and Eutectic PCM: Inorganic PCM are primarily classified into salt hydrate- and metal-based types. Salt hydrate-based PCM have latent heat values ranging from 87 - 227 kJ/kg, melting points between 25 - 116 °C, and supercooling degrees of approximately 0.64 - 19.5 °C. Metal-based inorganic PCM are characterized by superior thermal conductivity and high latent heat. Eutectic PCM, composed of a combination of organic and inorganic compounds, offer latent heat values between 80.5 - 160 kJ/kg and melting temperatures ranging from 13.4 - 81.6 °C.

Thermal Conductivity Enhancement Techniques: Efficient TES requires high thermal conductivity due to the necessity for rapid heat transfer during the phase transition process. Enhancement strategies include the incorporation of high-thermal-conductivity additives (e.g., carbon-based or metal-based particles) and encapsulation techniques.

Additive-Based Enhancements: Carbon-based materials such as multi-walled carbon nanotubes (MWCNT), carbon nanotubes (CNT), graphene oxide (GO), expanded graphite (EG), and carbon fiber have been used to increase PCM thermal conductivity, achieving values from 0.2 to 2.04 W/m·K. Similarly, metal-based additives including Al_2O_3, MgO, Fe_3O_4,

TiO_2, ZnO, CuO, and SiO_2 have demonstrated enhancements within the range of 0.26 - 3 W/m·K.

Encapsulation Methods: Encapsulation techniques isolate PCM from surrounding environments, improving stability and preventing leakage. These techniques are categorized based on particle size: nano-encapsulation (1 - 1,000 nm), microencapsulation (up to 1,000 μm), and macro-encapsulation (greater than 1 mm).

Encapsulation Performance: Nano and microencapsulation can be achieved via polymerization, coacervation, and sol-gel methods. Latent heat values for nano-encapsulated PCM range from 49.03 - 145 kJ/kg, whereas microencapsulated PCM exhibit ranges of 92.5 - 202.8 kJ/kg.

Macro-Encapsulation Applications: Macro-encapsulation is particularly relevant for large-scale building and concrete applications, offering structural compatibility and improved durability by preventing direct interaction between PCM and construction materials.

TES Integration in Building Systems: Thermal energy in buildings can be stored using mechanical, electrical, thermochemical, or thermal approaches. Among these, thermal energy storage is commonly implemented through sensible heat, latent heat (via PCM), and thermochemical storage mechanisms.

Acknowledgements

The authors gratefully acknowledge the Research Center for Advanced Materials, National Research and Innovation Agency (BRIN), Indonesia for providing the necessary facilities. Furthermore, the authors express their gratitude to BRIN for awarding Muhammad Fauzi the Degree by Research Scholarship, designated by "Nomor 27/II/HK/2024".

Declaration of Generative AI in Scientific Writing

The authors acknowledge the use of generative AI tools (e.g., Paperpal AI) in the preparation of this manuscript, specifically for language editing and grammar correction. No content generation or data interpretation was performed by AI. The authors take full responsibility for the content and conclusions of this work.

CRediT Author Statement

Muhammad Fauzi: Conceptualization, Data curation, Formal analysis, Visualization, Validation, and Writing – original draft.

Budhy Kurniawan: Conceptualization, Supervision, Validation, and Writing – review & editing.

Amdy Fachredzy: Data curation, Project administration.

Muhammad Alif Hamzah Nabawi: Data curation, Visualization.

Anggito Pringgo Tetuko: Formal analysis, Supervision, Validation, and Writing – review & editing.

References

[1] SS Magendran, FSA Khan, MN Mujawar, M Vaka, W Rashmi, M Khalid, EC Abdullah, N Sabzoi and RR Karri. Synthesis of organic phase change materials (PCM) for energy storage applications: A review. *Nano-Structures & Nano-Objects* 2019; **20(1)**, 100399.

[2] SW Sharshir, NM El-Shafai, MM Ibrahim, AW Kandeal, HS El-Sheshtawy, MS Ramadan, M Rashad and IM El-Mehasseb. *Journal of Energy Storage* 2021; **38**, 102526.

[3] SS Prabhu, P Selvakumar and JS Heric. Thermal stability and behaviour of paraffin nano Al_2O_3, graphene and surfactant sodium oleate composite as phase change material. *Materials Research Express* 2022; **9(11)**, 115504.

[4] Q Al-Yasiri and M Szabó. Thermal performance of concrete bricks based phase change material encapsulated by various aluminium containers: An experimental study under Iraqi hot climate conditions. *Journal of Energy Storage* 2021; **40(2021)**, 102710.

[5] T Qian, B Dang, Y Chen, C Jin, J Qian and Q Sun. Fabrication of magnetic phase change n-eicosane@Fe_3O_4/SiO_2 microcapsules on wood surface via sol-gel method. *Journal of Alloys and Compounds* 2019; **772**, 871-876.

[6] R Bharathiraja, T Ramkumar and M Selvakumar. Studies on the thermal characteristics of nano-enhanced paraffin wax phase change material (PCM) for thermal storage applications. *Journal of Energy Storage* 2023; **73(C)**, 109216.

[7] MAM Irwan, CSN Azwadi, Y Asako and J Ghaderian. Review on numerical simulations for nano-enhanced phase change material (NEPCM) phase change process. *Journal of Thermal Analysis and Calorimetry* 2020; **141**, 669-684.

[8] K Yu, Y Liu and Y Yang. Review on form-stable inorganic hydrated salt phase change materials: Preparation, characterization and effect on the thermophysical properties. *Applied Energy* 2021; **292**, 116845.

[9] G Alva, Y Lin and G Fang. An overview of thermal energy storage systems. *Energy* 2018; **144**, 341-378.

[10] MA Fikri, AK Pandey, M Samykano, K Kadirgama, M George, R Saidur, J Selvaraj, NA Rahim, K Sharma and VV Tyagi. Thermal conductivity, reliability, and stability assessment of phase change material (PCM) doped with functionalized multi-wall carbon nanotubes (FMWCNTs). *Journal of Energy Storage* 2022; **50**, 104676.

[11] PKS Rathore, KK Gupta, B Patel, RK Sharma and NK Gupta. Beeswax as a potential replacement of paraffin wax as shape stabilized solar thermal energy storage material: An experimental study. *Journal of Energy Storage* 2023; **68**, 107714.

[12] Z Chang, K Wang, XH Wu, G Lei, Q Wang, H Liu, Y Wang and Q Zhang. Review on the preparation and performance of paraffin-based phase change microcapsules for heat storage. *Journal of Energy Storage* 2022; **46(2)**, 103840.

[13] P Gadhave, F Pathan, S Kore and C Prabhune. Comprehensive review of phase change material based latent heat thermal energy storage system. *International Journal of Ambient Energy* 2022; **43(9)**, 4181-4206.

[14] Y Huang, A Stonehouse and C Abeykoon. Encapsulation methods for phase change materials - A critical review. *International Journal of Heat and Mass Transfer* 2023; **200(8)**, 123458.

[15] V Pethurajan and S Sivan. Fabrication, characterisation and heat transfer study on microencapsulation of nano-enhanced phase change material. *Chemical Engineering and Processing - Process Intensification* 2018; **133**, 12-23.

[16] JY Do, N Son, J Shin, RK Chava, SW Joo and M Kang. n-Eicosane-Fe_3O_4@SiO_2@Cu microcapsule phase change material and its improved thermal conductivity and heat transfer performance. *Materials & Design* 2021; **198(1)**, 109357.

[17] M Samykano. Role of phase change materials in thermal energy storage: Potential, recent progress and technical challenges. *Sustainable Energy Technologies and Assessments* 2022; **52(C)**, 102234.

[18] Y Lin, Y Jia, G Alva and G Fang. Review on thermal conductivity enhancement, thermal properties and applications of phase change materials in thermal energy storage. *Renewable and Sustainable Energy Reviews* 2018; **82(3)**, 2730-2742.

[19] F Hassan, F Jamil, A Hussain, HM Ali, MM Janjua, S Khushnood, M Farhan, K Altaf, Z Said and C Li. Recent advancements in latent heat phase change materials and their applications for thermal energy storage and buildings: A state of the art review. *Sustainable Energy Technologies and Assessments* 2022; **49(SI)**, 101646.

[20] SK Singh, SK Verma and R Kumar. Thermal performance and behavior analysis of SiO_2, Al_2O_3 and MgO based nano-enhanced phase-changing materials, latent heat thermal energy storage system. *Journal of Energy Storage* 2022; **48**, 103977.

[21] D Hu, L Han, W Zhou, P Li, Y Huang, Z Yang and X Jia. Flexible phase change composite based on loading paraffin into cross-linked CNT/SBS network for thermal management and thermal storage. *Chemical Engineering Journal* 2022; **437(P1)**, 135056.

[22] SW Sharshir, NM El-Shafai, MM Ibrahim, AW Kandeal, HS El-Sheshtawy, MS Ramadan, M Rashad and IM El-Mehasseb. Effect of copper oxide/cobalt oxide nanocomposite on phase change material for direct/indirect solar energy applications: Experimental investigation. *Journal of Energy Storage* 2021; **38**, 102526.

[23] W He, Y Zhuang, Y Chen and C Wang. Thermo-magnetic convection regulating the solidification behavior and energy storage of Fe_3O_4 nanoparticles composited paraffin wax under the

magnetic-field. *Applied Thermal Engineering* 2022; **214(3)**, 118617.

[24] W He, Y Zhuang, Y Chen and C Wang. Experimental and numerical investigations on the melting behavior of Fe3O4 nanoparticles composited paraffin wax in a cubic cavity under a magnetic-field. *International Journal of Thermal Sciences* 2023; **184(11)**, 107961.

[25] Q Al-Yasiri and M Szabó. Effect of encapsulation area on the thermal performance of PCM incorporated concrete bricks: A case study under Iraq summer conditions. *Case Studies in Construction Materials* 2021; **15**, e00686.

[26] AP Tetuko, AMS Sebayang, A Fachredzy, EA Setiadi, NS Asri, AY Sari, F Purnomo, C Muslih, MA Fajrin and P Sebayang. Encapsulation of paraffin-magnetite, paraffin, and polyethylene glycol in concretes as thermal energy storage. *Journal of Energy Storage* 2023; **68(PB)**, 107684.

[27] J Vadhera, A Sura, G Nandan and G Dwivedi. Study of Phase Change materials and its domestic application. *Materials Today: Proceedings* 2018; **5(2)**, 3411-3417.

[28] PKS Rathore, NK Gupta, D Yadav, SK Shukla and S Kaul. Thermal performance of the building envelope integrated with phase change material for thermal energy storage: An updated review. *Sustainable Cities and Society* 2022; **79(6)**, 103690.

[29] R Aridi and A Yehya. Review on the sustainability of phase-change materials used in buildings. *Energy Conversion and Management: X* 2022; **15**, 100237.

[30] K Faraj, M Khaled, J Faraj, F Hachem and C Castelain. A review on phase change materials for thermal energy storage in buildings: Heating and hybrid applications. *Journal of Energy Storage* 2021; **33**, 101913.

[31] KMK Faraj, M Khaled, J Faraj, F Hachem and C Castelain. Phase change material thermal energy storage systems for cooling applications in buildings: A review. *Renewable and Sustainable Energy Reviews* 2020; **119**, 109579.

[32] AK Pandey, MS Hossain, VV Tyagi, NA Rahim, JAL Selvaraj and A Sari. Novel approaches and recent developments on potential applications of phase change materials in solar energy. *Renewable and Sustainable Energy Reviews* 2018; **82(P1)**, 281-323.

[33] SM Wang, P Matiašovský, P Mihálka and CM Lai. Experimental investigation of the daily thermal performance of a mPCM honeycomb wallboard. *Energy and Buildings* 2018; **159**, 419-425.

[34] S Motahar. Experimental study and ANN-based prediction of melting heat transfer in a uniform heat flux PCM enclosure. *Journal of Energy Storage* 2020; **30(2)**, 101535.

[35] Y Zhang, S Zheng, S Zhu, J Ma, Z Sun and M Farid. Evaluation of paraffin infiltrated in various porous silica matrices as shape-stabilized phase change materials for thermal energy storage. *Energy Conversion and Management* 2018; **171**, 361-70.

[36] MW Chang, E Stride and M Edirisinghe. A novel process for drug encapsulation using a liquid to vapour phase change material. *Soft Matter* 2009; **5**, 5029.

[37] C Liu, L Wang, Y Li, X Diao, C Dong, A Li and X Chen. Fe_3O_4/carbon-decorated graphene boosts photothermal conversion and storage of phase change materials. *Journal of Colloid and Interface Science* 2024; **657(11)**, 590-597.

[38] C Zeng, S Liu and A Shukla. Adaptability research on phase change materials based technologies in China. *Renewable and Sustainable Energy Reviews* 2017; **73**, 145-158.

[39] G Duttaluru, P Singh, AK Ansu, RK Sharma, A Kumar and S Mishra. Methods to enhance the thermal properties of organic phase change materials: A review. *Materials Today Proceedings* 2022; **63(3)**, 685-691.

[40] MM Kenisarin, K Mahkamov, SC Costa and I Makhkamova. Melting and solidification of PCMs inside a spherical capsule: A critical review. *Journal of Energy Storage* 2020; **27(2)**, 101082.

[41] L Navarro, AD Gracia, S Colclough, M Browne, SJ McCormack, P Griffiths and LF Cabeza. Thermal energy storage in building integrated thermal systems: A review. Part 1. active storage systems. *Renewable Energy* 2016; **88**, 526-547.

[42] BP Jelle and SE Kalnæs. *Phase change materials for application in energy-efficient buildings*. *In:* F Pacheco-Torgal, CG Granqvist, BP Jelle, GP Vanoli, N Bianco and J Kurnitski (Eds.). Cost-

effective energy efficient building retrofitting. Woodhead Publishing, Sawston, United Kingdom, 2017, p. 57-118.

[43] C Liu, L Wang, Y Li, X Diao, C Dong, A Li and X Chen. Fe_3O_4/carbon-decorated graphene boosts photothermal conversion and storage of phase change materials. *Journal of Colloid and Interface Science* 2024; **657(11)**, 590-597.

[44] G Duttaluru, P Singh, AK Ansu, RK Sharma, A Kumar and S Mishra. Methods to enhance the thermal properties of organic phase change materials: A review. *Materials Today Proceedings* 2022; **63(3)**, 685-691.

[45] R Pichandi, KM Kulandaivelu, K Alagar, HK Dhevaguru and S Ganesamoorthy. Performance enhancement of photovoltaic module by integrating eutectic inorganic phase change material. *Energy Sources, Part A: Recovery, Utilization, and Environmental Effects* 2020: **46(1)**, 16360-16377.

[46] RA Lawag and HM Ali. Phase change materials for thermal management and energy storage: A review. *Journal of Energy Storage* 2022; **55(C)**, 105602.

[47] S Xie, J Sun, Z Wang, S Liu, L Han, G Ma, Y Jing and Y Jia. A thermally stable phase change material with high latent heat based on an oxalic acid dihydrate/boric acid binary eutectic system. *Solar Energy Materials and Solar Cells* 2017; **168**, 38-44.

[48] H Peng, J Wang, X Zhang, J Ma, T Shen, S Li and B Dong. A review on synthesis, characterization and application of nanoencapsulated phase change materials for thermal energy storage systems. *Applied Thermal Engineering* 2021; **185**, 116326.

[49] X Huang, G Alva, Y Jia and G Fang. Morphological characterization and applications of phase change materials in thermal energy storage: A review. *Renewable and Sustainable Energy Reviews* 2017; **72(3)**, 128-145.

[50] R Naveenkumar, M Ravichandran, V Mohanavel, A Karthick, LSRL Aswin, SSH Priyanka, SK Kumar and S Pradeep Kumar. Review on phase change materials for solar energy storage applications. *Environmental Science and Pollution Research* 2022; **29(7)**, 9491-9532.

[51] J Jaguemont, N Omar, PVD Bossche and J Mierlo. Phase-change materials (PCM) for automotive applications: A review. *Applied Thermal Engineering* 2018; **132**, 308-320.

[52] P Bose and VA Amirtham. A review on thermal conductivity enhancement of paraffinwax as latent heat energy storage material. *Renewable and Sustainable Energy Reviews* 2016; **65**, 81-100.

[53] Harish S, Orejon D, Takata Y, Kohno M. Thermal conductivity enhancement of lauric acid phase change nanocomposite with graphene nanoplatelets. *Applied Thermal Engineering* 2015; **80**, 205-211.

[54] H Fatahi, K Daoust, A Akbarzadeh, S Mancin, JP Claverie and S Poncet. Thermal conductivity improvement of adipic acid by the addition of AlO(OH) and AlO(OH)@SiO_2 core-shell nanoparticles. *International Journal of Thermofluids* 2024; **22**, 100617.

[55] MM Kenisarin. Thermophysical properties of some organic phase change materials for latent heat storage. A review. *Solar Energy* 2014; **107**, 553-575.

[56] D Haillot, T Bauer, U Kröner and R Tamme. Thermal analysis of phase change materials in the temperature range 120 - 150 °C. *Thermochim Acta* 2011; **513(1-2)**, 49-59.

[57] S Faraji, H Shekaari, MT Zafarani-Moattar, M Mokhtarpour and E Asghari. Thermal properties of phase change materials ionic liquid/fatty acids for thermal energy storage applications. *Journal of Energy Storage* 2023; **67**, 107464.

[58] C Ma, J Wang, Y Wu, Y Wang, Z Ji and S Xie. Characterization and thermophysical properties of erythritol/expanded graphite as phase change material for thermal energy storage. *Journal of Energy Storage* 2022; **46**, 103864.

[59] M Zandie, A Moghaddas, A Kazemi, M Ahmadi, HN Feshkache, MH Ahmadi and M Sharifpur. The impact of employing a magnetic field as well as Fe_3O_4 nanoparticles on the performance of phase change materials. *Engineering Applications of Computational Fluid Mechanics* 2022; **16(1)**, 196-214.

[60] Q Al-Yasiri and M Szabó. Thermal performance of concrete bricks based phase change material encapsulated by various aluminium containers: An

experimental study under Iraqi hot climate conditions. *Journal of Energy Storage* 2021; **40**, 102710.

[61] S Wu, T Yan, Z Kuai and W Pan. Thermal conductivity enhancement on phase change materials for thermal energy storage: A review. *Energy Storage Materials* 2020; **25**, 251-295.

[62] Z Chang, K Wang, X Wu, G Lei, Q Wang, H Liu, Y Wang and Q Zhang. Review on the preparation and performance of paraffin-based phase change microcapsules for heat storage. *Journal of Energy Storage* 2022; **46(2)**, 103840.

[63] Xu B, Wang B, Zhang C, Zhou J. Synthesis and light-heat conversion performance of hybrid particles decorated MWCNTs/paraffin phase change materials. *Thermochim Acta* 2017; **652**, 77-84.

[64] SS Chandel and T Agarwal. Review of current state of research on energy storage, toxicity, health hazards and commercialization of phase changing materials. *Renewable and Sustainable Energy Reviews* 2017; **67(C)**, 581-596.

[65] J Paul, M Samykano, AK Pandey, K Kadirgama and VV Tyagi. Nano Engineered paraffin-based phase change material for building thermal management. *Buildings* 2023; **13(4)**, 900.

[66] R Bharathiraja, T Ramkumar, M Selvakumar and N Radhika. Thermal characteristics enhancement of paraffin wax phase change material (PCM) for thermal storage applications. *Renew Energy* 2024; **222(C)**, 119986.

[67] D Hu, L Han, W Zhou, P Li, Y Huang, Z Yang and X Jia. Flexible phase change composite based on loading paraffin into cross-linked CNT/SBS network for thermal management and thermal storage. *Chemical Engineering Journal* 2022; **437(P1)**, 135056.

[68] HG Lorsch, KW Kauffman and JC Denton. Thermal energy storage for solar heating and off-peak air conditioning. *Energy Conversion* 1975; **15(1-2)**, 1-8.

[69] A Abhat. Low temperature latent heat thermal energy storage: Heat storage materials. *Solar Energy* 1983; **30(4)**, 313-332.

[70] MK Rathod and J Banerjee. Thermal stability of phase change materials used in latent heat energy storage systems: A review. *Renewable and Sustainable Energy Reviews* 2013; **18(C)**, 246-258.

[71] R Bharathiraja, T Ramkumar and M Selvakumar. Studies on the thermal characteristics of nano-enhanced paraffin wax phase change material (PCM) for thermal storage applications. *Journal of Energy Storage* 2023; **73(C)**, 109216.

[72] A Babapoor, AR Haghighi, SM Jokar and MA Mezjin. The performance enhancement of paraffin as a PCM during the solidification process: Utilization of graphene and metal oxide nanoparticles. *Iranian Journal of Chemistry and Chemical Engineering* 2022; **41(1)**, 37-48.

[73] B Lu, Y Zhang, J Zhang, J Zhu, H Zhao and Z Wang. Preparation, optimization and thermal characterization of paraffin/nano-Fe_3O_4 composite phase change material for solar thermal energy storage. *Journal of Energy Storage* 2022; **46(8)**, 103928.

[74] W He, Y Zhuang, Y Chen and C Wang. Thermo-magnetic convection regulating the solidification behavior and energy storage of Fe_3O_4 nanoparticles composited paraffin wax under the magnetic-field. *Applied Thermal Engineering* 2022; **214(3)**, 118617.

[75] A Hussain, IH Abidi, CY Tso, KC Chan, Z Luo and CYH Chao. Thermal management of lithium ion batteries using graphene coated nickel foam saturated with phase change materials. *International Journal of Thermal Sciences* 2018; **124**, 23-35.

[76] F Souayfane, F Fardoun and PH Biwole. Phase change materials (PCM) for cooling applications in buildings: A review. *Energy and Buildings* 2016; **129**, 396-431.

[77] B Lu, Y Zhang, J Xiao, M Hu, Y Niu, M Luo, J Zhu and J Zhang. Experimental investigation of the effect of rotating magnetic field on the melting performance enhancement of paraffin/nano-Fe_3O_4 composite phase change material. *Journal of Energy Storage* 2024; **83**, 110751.

[78] S Paneliya, S Khanna, Utsav, AP Singh, YK Patel, A Vanpariya, NH Makani, R Banerjee and I Mukhopadhyay. Core shell paraffin/silica nanocomposite: A promising phase change material for thermal energy storage. *Renewable Energy* 2021; **167(2)**, 591-599.

[79] X Sun, L Liu, Y Mo, J Li and C Li. Enhanced thermal energy storage of a paraffin-based phase change material (PCM) using nano carbons. *Applied Thermal Engineering* 2020; **181**, 115992.

[80] M Ghalambaz, M Aljaghtham, M Fteiti, AJ Chamkha, A Abdullah and M Ghalambaz. Thermal energy storage optimization using composite foam-nano enhanced phase change materials. *Journal of Energy Storage* 2023; **63(5)**, 107001.

[81] FS Javadi, HSC Metselaar and P Ganesan. Performance improvement of solar thermal systems integrated with phase change materials (PCM), a review. *Solar Energy* 2020; **206(3)**, 330-352.

[82] PKS Rathore and SK Shukla. Enhanced thermophysical properties of organic PCM through shape stabilization for thermal energy storage in buildings: A state of the art review. *Energy and Buildings* 2021; **236(1)**, 110799.

[83] Y Huang, A Stonehouse and C Abeykoon. Encapsulation methods for phase change materials - A critical review. *International Journal of Heat and Mass Transfer* 2023; **200(8)**, 123458.

[84] C Cárdenas-Ramírez, MA Gómez, F Jaramillo, AG Fernández and LF Cabeza. Thermal reliability of organic-organic phase change materials and their shape-stabilized composites. *Journal of Energy Storage* 2021; **40**, 102661.

[85] DG Atinafu, W Dong, X Huang, H Gao and G Wang. Introduction of organic-organic eutectic PCM in mesoporous N-doped carbons for enhanced thermal conductivity and energy storage capacity. *Applied Energy* 2018; **211**, 1203-1215.

[86] FS Javadi, HSC Metselaar and P Ganesan. Performance improvement of solar thermal systems integrated with phase change materials (PCM), a review. *Solar Energy* 2020; **206(3)**, 330-352.

[87] F Peng, X Zhu, R Lin, R Lub and F Lu. Advances in erythritol-based composite phase change materials. *Sustainable Energy & Fuels* 2024; **8(4)**, 1389-1404.

[88] J Zhou, X Lai, J Hu, H Qi, S Liu and Z Zhang. Design of a graphene oxide@melamine foam/polyaniline@erythritol composite phase change material for thermal energy storage. *Chinese Journal of Chemical Engineering* 2023; **58(7)**, 282-290.

[89] Y Krishna, N Aslfattahi, R Saidur, M Faizal and KC Ng. Fatty acid/metal ion composite as thermal energy storage materials. *SN Applied Sciences* 2020; **2(5)**, 798.

[90] A Sharma, VV Tyagi, CR Chen and D Buddhi. Review on thermal energy storage with phase change materials and applications. *Renewable and Sustainable Energy Reviews* 2009; **13(2)**, 318-345.

[91] G Fang, M Zhao and P Sun. Experimental study of the thermal properties of a fatty acid-modified graphite composite phase change material dispersion system. *Journal of Energy Storage* 2022; **53(1)**, 105108.

[92] J Jaguemont, N Omar, PVD Bossche and J Mierlo. Phase-change materials (PCM) for automotive applications: A review. *Applied Thermal Engineering* 2018; **132**, 308-320.

[93] SKR Kanchipuram, R Dinesh, AR Arulandhusamy and S Kalaiselvam. Performance analysis of heat pipe aided NEPCM heat sink for transient electronic cooling. *Microelectronics Reliability* 2017; **73**, 1-13.

[94] D Zou, X Ma, X Liu, P Zheng and Y Hu. Thermal performance enhancement of composite phase change materials (PCM) using graphene and carbon nanotubes as additives for the potential application in lithium-ion power battery. *International Journal of Heat and Mass Transfer* 2018; **120**, 33-41.

[95] A Sharma, VV Tyagi, CR Chen and D Buddhi. Review on thermal energy storage with phase change materials and applications. *Renewable and Sustainable Energy Reviews* 2009; **13(2)**, 318-345.

[96] P Dixit, VJ Reddy, S Parvate, A Balwani, J Singh, TK Maiti, A Dasari and S Chattopadhyay. Salt hydrate phase change materials: Current state of art and the road ahead. *Journal of Energy Storage* 2022; **51**, 104360.

[97] PJ Shamberger and NM Bruno. Review of metallic phase change materials for high heat flux transient thermal management applications. *Applied Energy* 2020; **258(15)**, 113955.

[98] M Guo, M Liang, Y Jiao, W Zhao, Y Duan and H Liu. A review of phase change materials in asphalt

binder and asphalt mixture. *Construction and Building Materials* 2020; **258(11)**, 119565.

[99] Z He, H Ma and S Lu. Preparation and thermal performance study of a novel hydrated salt composite PCM for space heating. *Journal of Energy Storage* 2024; **90(A)**, 111906.

[100] Q Xiao, J Fan, Y Fang, L Li, T Xu and W Yuan. The shape-stabilized light-to-thermal conversion phase change material based on $CH_3COONa \cdot {}_3H_2O$ as thermal energy storage media. *Applied Thermal Engineering* 2018; **136**, 701-707.

[101] S Zhou, Y Zhou, Z Ling, Z Zhang and X Fang. Modification of expanded graphite and its adsorption for hydrated salt to prepare composite PCMs. *Applied Thermal Engineering* 2018; **133**, 446-451.

[102] J Liu, C Zhu, W Liang, Y Li, H Bai, Q Guo and C Wang. Experimental investigation on micro-scale phase change material based on sodium acetate trihydrate for thermal storage. *Solar Energy* 2019; **193(9)**, 413-421.

[103] L Fu, Q Wang, R Ye, X Fang and Z Zhang. A calcium chloride hexahydrate/expanded perlite composite with good heat storage and insulation properties for building energy conservation. *Renewable Energy* 2017; **114(B)**, 733-743.

[104] C Shen, X Li, G Yang, Y Wang, L Zhao, Z Mao, B Wang, X Feng and X Sui. Shape-stabilized hydrated salt/paraffin composite phase change materials for advanced thermal energy storage and management. *Chemical Engineering Journal* 2020; **385**, 123958.

[105] L Liu, B Peng, C Yue, M Guo and M Zhang. Low-cost, shape-stabilized fly ash composite phase change material synthesized by using a facile process for building energy efficiency. *Materials Chemistry and Physics* 2019; **222**, 87-95.

[106] N Xie, J Luo, Z Li, Z Huang, X Gao, Y Fang and Z Zhang. Salt hydrate/expanded vermiculite composite as a form-stable phase change material for building energy storage. *Solar Energy Materials and Solar Cells* 2019; **189**, 33-42.

[107] Y Li, N Kumar, J Hirschey, DO Akamo, K Li, T Tugba, M Goswami, R Orlando, TJ LaClair, S Graham and KR Gluesenkamp. Stable salt hydrate-based thermal energy storage materials. *Composites Part B: Engineering* 2022; **233**, 109621.

[108] MI Lone and R Jilte. A review on phase change materials for different applications. *Materials Today: Proceedings* 2021; **46(20)**, 10980-10986.

[109] W Kraft, V Stahl and P Vetter. Thermal storage using metallic phase change materials for bus heating-state of the art of electric buses and requirements for the storage system. *Energies* 2020; **13(11)**, 3023.

[110] AE Gheribi, AD Pelton and JP Harvey. Determination of optimal compositions and properties for phase change materials in a solar electric generating station. *Solar Energy Materials and Solar Cells* 2020; **210(14-15)**, 110506.

[111] S Koohi-Fayegh and MA Rosen. A review of energy storage types, applications and recent developments. *Journal of Energy Storage* 2020; **27(2)**, 101047.

[112] M Al-Jethelah, S Ebadi, K Venkateshwar, SH Tasnim, S Mahmud and A Dutta. Charging nanoparticle enhanced bio-based PCM in open cell metallic foams: An experimental investigation. *Applied Thermal Engineering* 2019; **148**, 1029-1042.

[113] M Promsen, K Selvam, Y Komatsu, A Sciazko, S Kaneko and N Shikazono. Metallic PCM-integrated solid oxide fuel cell stack for operating range extension. *Energy Conversion and Management* 2022; **255(59)**, 115309.

[114] N Şahan and H Paksoy. Determining influences of SiO_2 encapsulation on thermal energy storage properties of different phase change materials. *Solar Energy Materials and Solar Cells* 2017; **159**, 1-7.

[115] K Iqbal, A Khan, D Sun, M Ashraf, A Rehman, F Safdar, A Rehman and F Safdar. Phase change materials, their synthesis and application in textiles-a review. *The Journal of The Textile Institute* 2019; **110(4)**, 625-638.

[116] H Lu, N Liu, T Sun, Z Liu, X Luo, Q Zhao and S Wang. Release kinetics study of fatty acids eutectic mixture gated mesoporous carbon nanoparticles for chemo-photothermal therapy. *Colloids and Surfaces A: Physicochemical and Engineering Aspects* 2023; **669**, 131450.

[117] E Alehosseini and SM Jafari. Micro/nano-encapsulated phase change materials (PCMs) as emerging materials for the food industry. *Trends in Food Science & Technology* 2019; **91**, 116-128.

[118] S Kahwaji and MA White. Prediction of the properties of eutectic fatty acid phase change materials. *Thermochim Acta* 2018; **660**, 94-100.

[119] Z Fan, Y Zhao, X Liu, Y Shi and D Jiang. Thermal properties and reliabilities of lauric acid-based binary eutectic fatty acid as a phase change material for building energy conservation. *ACS Omega* 2022; **7(18)**, 16097-16108.

[120] TM Tritt. *Thermal conductivity: Theory, properties, and applications.* Springer, New York, 2003, p. 290.

[121] S Stankovich, DA Dikin, GHB Dommett, KM Kohlhaas, EJ Zimney, EA Stach, RD Piner, SBT Nguyen and RS Ruoff. Graphene-based composite materials. *Nature* 2006; **442(7100)**, 282-286.

[122] SK Srivastav, MR Sahu, K Watanabe, T Taniguchi, S Banerjee and A Das. Universal quantized thermal conductance in graphene. *Science Advances* 2019; **5(7)**, eaaw5798.

[123] R Wen, X Zhang, Z Huang, M Fang, Y Liu, X Wu, X Min, W Gao and S Huang. Preparation and thermal properties of fatty acid/diatomite form-stable composite phase change material for thermal energy storage. *Solar Energy Materials and Solar Cells* 2018; **178**, 273-279.

[124] X Huang, X Chen, A Li, D Atinafu, H Gao, W Dong and G Wang. Shape-stabilized phase change materials based on porous supports for thermal energy storage applications. *Chemical Engineering Journal* 2019; **356**, 641-661.

[125] S Pei and HM Cheng. The reduction of graphene oxide. *Carbon* 2012; **50(9)**, 3210-3228.

[126] PK Boruah, DJ Borah, J Handique, P Sharma, P Sengupta and MR Das. Facile synthesis and characterization of Fe_3O_4 nanopowder and Fe3O4/reduced graphene oxide nanocomposite for methyl blue adsorption: A comparative study. *Journal of Environmental Chemical Engineering* 2015; **3(3)**, 1974-1985.

[127] W Cui, X Li, X Li, T Si, L Lu, T Ma and Q Wang. Thermal performance of modified melamine foam/graphene/paraffin wax composite phase change materials for solar-thermal energy conversion and storage. *Journal of Cleaner Production* 2022; **367**, 133031.

[128] Z Jiang, T Ouyang, L Ding, W Li, W Li, MS(JT) Balogun. 3D self-bonded porous graphite fiber monolith for phase change material composite with high thermal conductivity. *Chemical Engineering Journal* 2022; **438(2007)**, 135496.

[129] D Hu, L Han, W Zhou, P Li, Y Huang, Z Yang and X Jia. Flexible phase change composite based on loading paraffin into cross-linked CNT/SBS network for thermal management and thermal storage. *Chemical Engineering Journal* 2022; **437(1)**, 135056.

[130] AR Akhiani, M Mehrali, ST Latibari, M Mehrali, TMI Mahlia, E Sadeghinezhad, HSC Metselaar. One-step preparation of form-stable phase change material through self-assembly of fatty acid and graphene. *The Journal of Physical Chemistry C* 2015; **119(40)**, 22787-22796.

[131] NH Abu-Hamdeh, A Khoshaim, MA Alzahrani and RI Hatamleh. Study of the flat plate solar collector's efficiency for sustainable and renewable energy management in a building by a phase change material: Containing paraffin-wax/Graphene and Paraffin-wax/graphene oxide carbon-based fluids. *Journal of Building Engineering* 2022; **57(6)**, 104804.

[132] M Shaker, Q Qin, DW Zhaxi, X Chen, K Chen, S Yang, H Tian and W Cao. Improving the cold thermal energy storage performance of paraffin phase change material by compositing with graphite, expanded graphite, and graphene. *Journal of Materials Engineering and Performance* 2023; **32(1)**, 10275-10284.

[133] Y Zhou, C Li, H Wu and S Guo. Construction of hybrid graphene oxide/graphene nanoplates shell in paraffin microencapsulated phase change materials to improve thermal conductivity for thermal energy storage. *Colloids and Surfaces A: Physicochemical and Engineering Aspects* 2020; **597**, 124780.

[134] A Karaipekli, A Biçer, A Sarı and VV Tyagi. Thermal characteristics of expanded perlite/paraffin composite phase change material with enhanced thermal conductivity using carbon nanotubes. *Energy Conversion and Management* 2017; **134**, 373-381.

[135] TH Wang, TF Yang, CH Kao, WM Yan and M Ghalambaz. Paraffin core-polymer shell micro-encapsulated phase change materials and expanded graphite particles as an enhanced energy storage medium in heat exchangers. *Advanced Powder Technology* 2020; **31(6)**, 2421-2429.

[136] X Zhu, L Han, F Yang, J Jiang and X Jia. Lightweight mesoporous carbon fibers with interconnected graphitic walls for supports of form-stable phase change materials with enhanced thermal conductivity. *Solar Energy Materials and Solar Cells* 2020; **208**, 110361.

[137] N Sheng, Z Rao, C Zhu and H Habazaki. Honeycomb carbon fibers strengthened composite phase change materials for superior thermal energy storage. *Applied Thermal Engineering* 2020; **164**, 114493.

[138] F Cheng, X Zhang, R Wen, Z Huang, M Fang, Y Liu, X Wu and X Min. Thermal conductivity enhancement of form-stable tetradecanol/expanded perlite composite phase change materials by adding Cu powder and carbon fiber for thermal energy storage. *Applied Thermal Engineering* 2019; **156**, 653-659.

[139] Z Shen, S Kwon, HL Lee, M Toivakka and K Oh. Cellulose nanofibril/carbon nanotube composite foam-stabilized paraffin phase change material for thermal energy storage and conversion. *Carbohydrate Polymers* 2021; **273(8)**, 118585.

[140] X Cao, C Li, G He, Y Tong and Z Yang. Composite phase change materials of ultra-high molecular weight polyethylene/paraffin wax/carbon nanotubes with high performance and excellent shape stability for energy storage. *Journal of Energy Storage* 2021; **44(B)**, 103460.

[141] RK Mande, SR Raju and KPVK Varma. Thermophysical properties of TiO_2/CuO hybrid nanofluids for heat transfer applications. *Materials Research Innovations* 2024; **28(2)**, 83-93.

[142] Y Hu, L Shi, Z Zhang, Y He and J Zhu. Magnetic regulating the phase change process of Fe_3O_4-paraffin wax nanocomposites in a square cavity. *Energy Conversion and Management* 2020; **213(1)**, 112829.

[143] Kumar K. S, Muniamuthu S, Mohan A, Amirthalingam P, Anbu Muthuraja M. Effect of charging and discharging process of PCM with paraffin and Al_2O_3 additive subjected to three point temperature locations. *Journal of Ecological Engineering* 2022; **23(2)**, 34-42.

[144] M Gamal, MS Radwan, IG Elgizawy and MH Shedid. Thermophysical characterization on water and ethylene glycol/water-based MgO and ZnO nanofluids at elevated temperatures: An experimental investigation. *Journal of Molecular Liquids* 2023; **369(1)**, 120867.

[145] M Ma, M Xie and Q Ai. Study on photothermal properties of Zn-ZnO/paraffin binary nanofluids as a filler for double glazing unit. *International Journal of Heat and Mass Transfer* 2022; **183(A)**, 122173.

[146] B Zhao, Y Wang, C Wang, R Zhu, N Sheng, C Zhu and Z Rao. Thermal conductivity enhancement and shape stabilization of phase change thermal storage material reinforced by combustion synthesized porous Al_2O_3. *Journal of Energy Storage* 2021; **42**, 103028.

[147] X Zheng, X Gao, Z Huang, Z Li, Y Fang and Z Zhang. Form-stable paraffin/graphene aerogel/copper foam composite phase change material for solar energy conversion and storage. *Solar Energy Materials and Solar Cells* 2021; **226**, 111083.

[148] SS Prabhu, P Selvakumar and JS Heric. Thermal stability and behaviour of paraffin nano Al_2O_3 , graphene and surfactant sodium oleate composite as phase change material. *Materials Research Express* 2022; **9(11)**, 115504.

[149] I Ali, S Mahendran, AK Pandey, Z Said, K Kadirgma and V Tyagi. Thermal conductivity and Thermal properties enhancement of Paraffin/ Titanium Oxide based Nano enhanced Phase change materials for Energy storage. *In:* Proceedings of the 2022 Advances in Science and Engineering Technology International Conferences (ASET), Dubai, United Arab Emirates. 2022, p. 1-5.

[150] N Şahan, M Fois and H Paksoy. Improving thermal conductivity phase change materials-A study of paraffin nanomagnetite composites. *Solar Energy Materials and Solar Cells* 2015; **137**, 61-67.

[151] B Sivapalan, KS Suganthi, S Kiruthika, MK Saranprabhu and KS Rajan. Superior thermal conductivity and charging performance of zinc

oxide dispersed paraffin wax for thermal energy storage applications. *Korean Journal of Chemical Engineering* 2024; **41**, 2389-2404.

[152] C Xu, H Zhang and G Fang. Review on thermal conductivity improvement of phase change materials with enhanced additives for thermal energy storage. *Journal of Energy Storage* 2022; **51**, 104568.

[153] H Alrobei and RA Malik. Effect of different micelles on charging and discharging behavior of phase change material. *Journal of King Saud University - Science* 2024; **36(2)**, 103066

[154] SPH Largani, H Salimi-Kenari, SR Nabavi and AAR Darzi. Manipulation of the thermo-rheological properties of stable Fe_3O_4 nanoparticles-embedded PCM nanoemulsions. *Journal of Energy Storage* 2024; **80**, 110351.

[155] KY Leong, S Hasbi, KZK Ahmad, NM Jali, HC Ong and MFM Din. Thermal properties evaluation of paraffin wax enhanced with carbon nanotubes as latent heat thermal energy storage. *Journal of Energy Storage* 2022; **52(C)**, 105027.

[156] Y Sheikh, MF Orhan, M Kanoglu, M Umair and E Mehaisi. Effect on the thermal performance of a bio-based phase change material with the addition of graphite with surfactants. *Heat Transfer Engineering* 2024; **45(9)**, 765-778.

[157] NHM Zaimi, A Nawabjan, SFA Rahman, SM Hussin and SNNA Hamidon. Evaluating the role of sodium dodecylbenzene sulfonate as surfactant towards enhancing thermophysical properties of paraffin/graphene nanoplatelet phase change material: Synthesis and characterization in PV cooling perspective. *International Journal of Thermophysics* 2022; **43(1)**, 1-25.

[158] G Zhou, Y Liu, S Li, Y Zhang, Q Zhang, C Xu, B Sun and R Liu. Effects of SDBS and BS-12 on functional groups/wettability of multicomponent acidified lignite. *Journal of Molecular Liquids* 2023; **390(A)**, 122908.

[159] YE Milián, A Gutiérrez, M Grágeda and S Ushak. A review on encapsulation techniques for inorganic phase change materials and the influence on their thermophysical properties. *Renewable and Sustainable Energy Reviews* 2017; **73**, 983-999.

[160] Z Chen, R Zhu, N Sheng, C Zhu and Z Rao. Synchronously improved thermal conductivity and anti-leakage performance for phase change composite by SiC nanowires modified wood carbon. *Journal of Energy Storage* 2022; **47**, 103567.

[161] X Liu and Z Rao. Experimental study on the thermal performance of graphene and exfoliated graphite sheet for thermal energy storage phase change material. *Thermochim Acta* 2017; **647**, 15-21.

[162] T Khadiran, MZ Hussein, Z Zainal and R Rusli. Encapsulation techniques for organic phase change materials as thermal energy storage medium: A review. *Solar Energy Materials and Solar Cells* 2015; **143(143)**, 78-98.

[163] X Chen, H Gao, Z Tang, W Dong, A Lic and G Wang. Optimization strategies of composite phase change materials for thermal energy storage, transfer, conversion and utilization. *Energy & Environmental Science* 2020; **13(12)**, 4498-4535.

[164] C Liu, Z Rao, J Zhao, Y Huo and Y Li. Review on nanoencapsulated phase change materials: Preparation, characterization and heat transfer enhancement. *Nano Energy* 2015; **13(13)**, 814-826.

[165] A Arshad, M Jabbal, Y Yan and J Darkwa. The micro-/nano-PCMs for thermal energy storage systems: A state of art review. *International Journal of Energy Research* 2019; **43(8)**, 5572-5620.

[166] F Marske, J Dasler, C Haupt, K Bacia, T Hahn and D Enke. Influence of surfactants and organic polymers on monolithic shape-stabilized phase change materials synthesized via sol-gel route. *Journal of Energy Storage* 2022; **49**, 104127.

[167] S Park, Y Lee, YS Kim, HM Lee, JH Kim, IW Cheong and WG Koh. Magnetic nanoparticle-embedded PCM nanocapsules based on paraffin core and polyurea shell. *Colloids and Surfaces A: Physicochemical and Engineering Aspects* 2014; **450(1)**, 46-51.

[168] J Shi, X Wu, X Fu and R Sun. Synthesis and thermal properties of a novel nanoencapsulated phase change material with PMMA and SiO_2 as hybrid shell materials. *Thermochim Acta* 2015; **617**, 90-94.

[169] J Giro-Paloma, Y Konuklu and AI Fernández. Preparation and exhaustive characterization of

paraffin or palmitic acid microcapsules as novel phase change material. *Solar Energy* 2015; **112**, 300-309.

[170] MGD Cortazar and R Rodríguez. Thermal storage nanocapsules by miniemulsion polymerization. *Journal of Applied Polymer Science* 2013; **127(6)**, 5059-5064.

[171] IS Hussain, AA Roseline and S Kalaiselvam. Bifunctional nanoencapsulated eutectic phase change material core with SiO2/SnO2 nanosphere shell for thermal and electrical energy storage. *Materials & Design* 2018; **154**, 291-301.

[172] MNA Hawlader, MS Uddin and MM Khin. Microencapsulated PCM thermal-energy storage system. *Applied Energy* 2003; **74(1-2)**, 195-202.

[173] S Drissi, TC Ling, KH Mo and A Eddhahak. A review of microencapsulated and composite phase change materials: Alteration of strength and thermal properties of cement-based materials. *Renewable and Sustainable Energy Reviews* 2019; **110**, 467-484.

[174] G Peng, G Dou, Y Hu, Y Sun and Z Chen. Phase change material (PCM) microcapsules for thermal energy storage. *Advances in Polymer Technology* 2020; **2020**, 1-20.

[175] R Jacob and F Bruno. Review on shell materials used in the encapsulation of phase change materials for high temperature thermal energy storage. *Renewable and Sustainable Energy Reviews* 2015; **48(3)**, 79-87.

[176] H Nazir, M Batool, FJB Osorio, M Isaza-Ruiz, X Xu, K Vignarooban, P Phelan, Inamuddin and AM Kannan. Recent developments in phase change materials for energy storage applications: A review. *International Journal of Heat and Mass Transfer* 2019; **129**, 491-523.

[177] G Alva, Y Lin, L Liu and G Fang. Synthesis, characterization and applications of microencapsulated phase change materials in thermal energy storage: A review. *Energy and Buildings* 2017; **144**, 276-294.

[178] A Khan, P Saikia, R Saxena, D Rakshit and S Saha. Microencapsulation of phase change material in water dispersible polymeric particles for thermoregulating rubber composites-A holistic approach. *International Journal of Energy Research* 2020; **44(1)**, 1567-1579.

[179] PKS Rathore and SK Shukla. Potential of macroencapsulated PCM for thermal energy storage in buildings: A comprehensive review. *Construction and Building Materials* 2019; **225(2019)**, 723-744.

[180] L Erlbeck, P Schreiner, K Schlachter, P Dörnhofer, F Fasel, FJ Methner and M Rädle. Adjustment of thermal behavior by changing the shape of PCM inclusions in concrete blocks. *Energy Conversion and Management* 2018; **158**, 256-265.

[181] Y Gao, F He, X Meng, Z Wang, M Zhang, H Yu and W Gao. Thermal behavior analysis of hollow bricks filled with phase-change material (PCM). *Journal of Building Engineering* 2020; **31(10)**, 101447.

[182] Y Zhou, S Wu, Y Ma, H Zhang, X Zeng, FF Liu, J Ryu and Z Guo. Recent advances in organic/composite phase change materials for energy storage. *ES Energy & Environment* 2020; **9**, 28-40.

[183] D Vérez, E Borri, A Crespo, BD Mselle, ÁD Gracia, G Zsembinszki and LF Cabeza. Experimental study on two PCM Macro-encapsulation designs in a thermal energy storage tank. *Applied Sciences* 2021; **11(13)**, 6171.

[184] A Alhusseny, N Al-Zurfi, Q Al-Aabidy, A Nasser and H Al-Madhhachi. Response to the design conditions of a tube-bundle thermal energy storage unit with paraffin-copper foam composite as a storage medium. *International Journal of Heat and Mass Transfer* 2024; **228**, 125679.

[185] B Medjahed, S Dardouri, H Hammou, FZ Fellouh and M Arıcı. Paraffin/beeswax/plaster as thermal energy storage composite: Characterization and application in buildings. *Journal of Energy Storage* 2024; **88(3)**, 111344.

[186] R Andrzejczyk, T Muszynski, T Kowalczyk and M Saqib. Experimental and numerical investigation on shell and coil storage unit with biodegradable PCM for modular thermal battery applications. *International Journal of Thermal Sciences* 2023; **185**, 108076.

[187] SK Suraparaju, M Samykano, R Dhivagar, SK Natarajan and MF Ghazali. Synergizing environmental and technological advances: Discarded transmission oil and paraffin wax as a phase change material for energy storage in solar

distillation as a step towards sustainability. *Journal of Energy Storage* 2024; **85**, 111046.

[188] WQ Li, YX Li, TH Yang, TY Zhang and F Qin. Experimental investigation on passive cooling, thermal storage and thermoelectric harvest with heat pipe-assisted PCM-embedded metal foam. *International Journal of Heat and Mass Transfer* 2023; **201(P1)**, 123651.

[189] M Sheikholeslami and SM Mousavi. Numerical simulation of heat pipe solar system combined with finned thermal storage unit incorporating mixture of nanoparticles and paraffin. *International Communications in Heat and Mass Transfer* 2024; **155(6)**, 107468.

[190] LF Cabeza and E Oró. *Thermal energy storage for renewable heating and cooling systems. In:* G Stryi-Hipp (Ed.). Renewable heating and cooling: Technologies and applications. Woodhead publishing, Cambridge, United Kingdom,2016, p. 139-179.

[191] J Heier, C Bales and V Martin. Combining thermal energy storage with buildings - a review. *Renewable and Sustainable Energy Reviews* 2015; **42**, 1305-1325.

[192] Cabeza LF. Advances in thermal energy storage systems: methods and applications. *In:* LF Cabeza (Ed.). Advances in thermal energy storage systems. Woodhead Publishing, Cambridge, United Kingdom, 2021, p. 37-54.

[193] U Berardi and AA Gallardo. Properties of concretes enhanced with phase change materials for building applications. *Energy and Buildings* 2019; **199**, 402-414.

[194] KS Reddy, V Mudgal and TK Mallick. Review of latent heat thermal energy storage for improved material stability and effective load management. *Journal of Energy Storage* 2018; **15**, 205-227.

[195] A Gil, M Medrano, I Martorell, A Lázaro, P Dolado, B Zalba and LF Cabeza. State of the art on high temperature thermal energy storage for power generation. Part 1-Concepts, materials and modellization. *Renewable and Sustainable Energy Reviews* 2010; **14(1)**, 31-55.

[196] MK Nematchoua, A Yvon, SEJ Roy, CG Ralijaona, R Mamiharijaona, JN Razafinjaka and R Tefy. A review on energy consumption in the residential and commercial buildings located in tropical regions of Indian Ocean: A case of Madagascar island. *Journal of Energy Storage* 2019; **24(12)**, 1-15.

[197] R Qiao and T Liu. Impact of building greening on building energy consumption: A quantitative computational approach. *Journal of Cleaner Production* 2020; **246(S2)**, 119020.

[198] Ahangari M, Maerefat M. An innovative PCM system for thermal comfort improvement and energy demand reduction in building under different climate conditions. *Sustainable Cities and Society* 2019; **44**, 120-129.

[199] R Vicente and T Silva. Brick masonry walls with PCM macrocapsules: An experimental approach. *Applied Thermal Engineering* 2014; **67(1-2)**, 24-34.

[200] Y Zhang and M Deng. Taguchi optimization and a fast evaluation method on the transient thermal performance of phase change material outfitted walls. *Journal of Energy Storage* 2021; **43**, 103120.

[201] A Laaouatni, N Martaj, R Bennacer, M Lachi, ME Omari and ME Ganaoui. Thermal building control using active ventilated block integrating phase change material. *Energy and Buildings* 2019; **187**, 50-63.

[202] AM Heniegal, OMO Ibrahim, NB Frahat and M Amin. New techniques for the energy saving of sustainable buildings by using phase change materials. *Journal of Building Engineering* 2021; **41**, 102418.

[203] R Saxena, D Rakshit and SC Kaushik. Experimental assessment of Phase Change Material (PCM) embedded bricks for passive conditioning in buildings. *Renewable Energy* 2020; **149**, 587-599.

[204] R Florez, HA Colorado, A Alajo, CHC Giraldo. The material characterization and gamma attenuation properties of Portland cement-Fe_3O_4 composites for potential dry cask applications. *Progress in Nuclear Energy* 2019; **111(2)**, 65-73.

[205] Z Chang, K Wang, X Wu, G Lei, Q Wang, H Liu, Y Wang and Q Zhang. Review on the preparation and performance of paraffin-based phase change microcapsules for heat storage. *Journal of Energy Storage* 2022; **46(2)**, 103840.

[206] Y Shen, S Liu, C Zeng, Y Zhang, Y Li, X Han, L Yang and X Yang. Experimental thermal study of

a new PCM-concrete thermal storage block (PCM-CTSB). *Constr Build Mater* 2021; **293**, 123540.

[207] B Kazanci, K Cellat and H Paksoy. Preparation, characterization, and thermal properties of novel fire-resistant microencapsulated phase change materials based on paraffin and a polystyrene shell. *RSC Advances* 2020; **10**, 24134-24144.

[208] M Aguayo, S Das, A Maroli, N Kabay, JCE Mertens, SD Rajan, G Sant, N Chawla and N Neithalath. The influence of microencapsulated phase change material (PCM) characteristics on the microstructure and strength of cementitious composites: Experiments and finite element simulations. *Cement and Concrete Composites* 2016; **73**, 29-41.

[209] D Hu, L Han, W Zhou, P Li, Y Huang, Z Yang and X Jia. Flexible phase change composite based on loading paraffin into cross-linked CNT/SBS network for thermal management and thermal storage. *Chemical Engineering Journal* 2022; **437(P1)**, 135056.

[210] S Afgan, RA Khushnood, SA Memon and N Iqbal. Development of structural thermal energy storage concrete using paraffin intruded lightweight aggregate with nano-refined modified encapsulation paste layer. *Construction and Building Materials* 2019; **228(7)**, 116768.

[211] L Shen, H Tan, Y Yang and W He. Preparation and characteristics of paraffin/silica aerogel composite phase-change materials and their application to cement. *Construction and Building Materials* 2023; **387(139)**, 131609.

[212] X Cao, C Li, Y Li, Y Tong, G He and Z Yang. Novel paraffin wax/ultra-high molecular weight polyethylene composite phase change materials modified by carbon nanotubes with excellent combination property. *Journal of Applied Polymer Science* 2022; **139(5),** 51564.

[213] IA Laghari, M Samykano, AK Pandey, K Kadirgama and YN Mishra. Binary composite (TiO2-Gr) based nano-enhanced organic phase change material: Effect on thermophysical properties. *Journal of Energy Storage* 2022; **51**, 104526.

[214] J Su, H Zhang, Y Gong, Q Xu, M Hou and B Xu. Fabrication and properties analysis of paraffin@TiO_2/Ag phase change microcapsules for thermal energy storage and photocatalysis. *Materials Science and Engineering: B* 2024; **301(1)**, 117150.

[215] W Ji, X Cheng, S Chen, X Wang and Y Li. Self-assembly fabrication of GO/TiO_2@paraffin microcapsules for enhancement of thermal energy storage. *Powder Technology* 2021; **385**, 546-556.

[216] CD Blasio. *Fundamentals of biofuels engineering and technology.* Springer International Publishing, Cham, Germany, 2019, p. 450.

[217] NH Almousa, MR Alotaibi, M Alsohybani, D Radziszewski, SM AlNoman, BM Alotaibi and MM Khayyat. Paraffin wax [as a phase changing material (PCM)] based composites containing multi-walled carbon nanotubes for thermal energy storage (TES) development. *Crystals* 2021; **11(8)**, 951.

[218] D Tian, T Shi, X Wang, H Liu and X Wang. Magnetic field-assisted acceleration of energy storage based on microencapsulation of phase change material with $CaCO_3$/Fe_3O_4 composite shell. *Journal of Energy Storage* 2022; **47**, 103574.

[219] M George, AK Pandey, NA Rahim, VV Tyagi, S Shahabuddin and R Saidur. Long-term thermophysical behavior of paraffin wax and paraffin wax/polyaniline (PANI) composite phase change materials. *Journal of Energy Storage* 2020; **31**, 101568.

[220] TH Ting. Synthesis, characterization of Fe_3O_4/polymer composites with stealth capabilities. *Results in Physics* 2020; **16**, 102975.

[221] H Liu, X Tian, M Ouyang, X Wang, D Wu and X Wang. Microencapsulating n-docosane phase change material into $CaCO_3$/Fe_3O_4 composites for high-efficient utilization of solar photothermal energy. *Renewable Energy* 2021; **179(35)**, 47-64.